R90-15

A CHANNEL NETWORK EVOLUTION MODEL WITH SUBSURFACE SATURATION MECHANISM AND ANALYSIS OF THE CHAOTIC BEHAVIOR OF THE MODEL

by
EDE J. IJJÁSZ-VÁSQUEZ
and
RAFAEL L. BRAS

RALPH M. PARSONS LABORATORY
HYDROLOGY AND WATER RESOURCE SYSTEMS

Report Number 330

Prepared under the support of
National Science Foundation,
Army Research Office, and
National Research Council of Italy

The Ralph M. Parsons Laboratory Technical Report Series
is supported in part by a grant from the Ralph M. Parsons Foundation

September, 1990

MASTER COPY KEEP THIS COPY FOR REPRODUCTION PURPOSES

REPORT DOCUMENTATION PAGE

Form Approved
OMB No. 0704-0188

1. AGENCY USE ONLY (Leave blank)	2. REPORT DATE	3. REPORT TYPE AND DATES COVERED
	September 1990	Technical Report

4. TITLE AND SUBTITLE

A Channel Network Evolution Model with Subsurface Saturation Mechanism and Analysis of the Chaotic Behavior of the Model

5. FUNDING NUMBERS

DAAL03-89-K-0151

6. AUTHOR(S)

Ede J. Ijjasz-Vasquez and Rafael L. Bras

7. PERFORMING ORGANIZATION NAME(S) AND ADDRESS(ES)

MIT
Cambridge, Massachusetts 02139

8. PERFORMING ORGANIZATION REPORT NUMBER

9. SPONSORING / MONITORING AGENCY NAME(S) AND ADDRESS(ES)

U. S. Army Research Office
P. O. Box 12211
Research Triangle Park, NC 27709-2211

10. SPONSORING / MONITORING AGENCY REPORT NUMBER

ARO 26902.1-GS

11. SUPPLEMENTARY NOTES

The view, opinions and/or findings contained in this report are those of the author(s) and should not be construed as an official Department of the Army position, policy, or decision, unless so designated by other documentation.

12a. DISTRIBUTION / AVAILABILITY STATEMENT

Approved for public release; distribution unlimited.

12b. DISTRIBUTION CODE

13. ABSTRACT *(Maximum 200 words)*

In the first part of this work the overland flow production mechanism used in the Willgoose-Bras-Rodriguez-Iturbe channel network and catchment evolution model was modified from the Hortonian to the subsurface saturation runoff mechanism. Two important differences were found oin the behavior of the new model; one was in the evolution of the hypsometric curves of the catchment; the second was in the importance of mass movement (e.g. creep and landsliding) sediment transport in the overall behavior of the system. A new nondimensional number related to the threshold of saturation in hillslopes was added to the list of nondimensional numbers belonging to the original model. Common geomorphological statistics were measured on the simulated catchments and found to be similar to field data.

cont'd on reverse side

14. SUBJECT TERMS	15. NUMBER OF PAGES
	16. PRICE CODE

17. SECURITY CLASSIFICATION OF REPORT	18. SECURITY CLASSIFICATION OF THIS PAGE	19. SECURITY CLASSIFICATION OF ABSTRACT	20. LIMITATION OF ABSTRACT
UNCLASSIFIED	UNCLASSIFIED	UNCLASSIFIED	UL

NSN 7540-01-280-5500

Standard Form 298 (Rev 2-89)
Prescribed by ANSI Std 239-18
298-102

The second part of this work examines the sensitivity to initial conditions present in the WBR model. Using an appropiate measure between elevation fields, the evolution of different catchments was examined. Exponential separation in phase space between trajectories of the system was found in a variety of tests. This exponential separation is the reason for the apparent randomness present in the evolution of the model. The influence of different parameters of the model on this exponential separation was also examined.

R90-15

A CHANNEL NETWORK EVOLUTION MODEL WITH SUBSURFACE SATURATION MECHANISM AND ANALYSIS OF THE CHAOTIC BEHAVIOR OF THE MODEL

by

Ede J. Ijjász-Vásquez
Rafael L. Bras

RALPH M. PARSONS LABORATORY
HYDROLOGY AND WATER RESOURCES SYSTEMS

Report Number 330

Prepared under the support of the
National Science Foundation,
Army Research Office and
National Research Council of Italy

SEPTEMBER 1990

A CHANNEL NETWORK EVOLUTION MODEL WITH SUBSURFACE SATURATION MECHANISM AND ANALYSIS OF THE CHAOTIC BEHAVIOR OF THE MODEL

Abstract

In the first part of this work the overland flow production mechanism used in the Willgoose-Bras-Rodriguez-Iturbe channel network and catchment evolution model was modified from the Hortonian to the subsurface saturation runoff mechanism. Two important differences were found oin the behavior of the new model; one was in the evolution of the hypsometric curves of the catchment; the second was in the importance of mass movement (e.g. creep and landsliding) sediment transport in the overall behavior of the system. A new nondimensional number related to the threshold of saturation in hillslopes was added to the list of nondimensional numbers belonging to the original model. Common geomorphological statistics were measured on the simulated catchments and found to be similar to field data.

The second part of this work examines the sensitivity to initial conditions present in the WBR model. Using an appropiate measure between elevation fields, the evolution of different catchments was examined. Exponential separation in phase space between trajectories of the system was found in a variety of tests. This exponential separation is the reason for the apparent randomness present in the evolution of the model. The influence of different parameters of the model on this exponential separation was also examined.

Acknowledgements

This report essentially constitutes the Master of Science thesis of Ede J. Ijjasz-Vasquez.

Support for this work was provided by the National Science Foundation (Grant No. CES-8815725), Army Research Office Contract DAALO3-89-K-0151 and the National Research Council of Italy through a cooperative agreement between the University of Florence and MIT. This support is gratefully acknowledged.

Table of Contents

List of Figures

List of Tables

Chapter 1

Introduction

1.1 Scope

Hydrologists have always been interested in the geomorphologic aspects of catchments and river networks. An understanding of the relationships between basin shapes and hydrologic responses is fundamental for the purpose of hydrologic predictions, especially in ungaged basins.

Another goal is to try to understand not only the properties and the response of a catchment at a certain time but to study the evolution of the catchment over a long period of time. This approach has potential applications in the study of geomorphologic impacts produced by global climate changes. Water, as a vehicle of sediment transport, plays a fundamental role in the process. Recently a model developed by Willgoose, Bras and Rodriguez-Iturbe [47] quantified the evolution of the channel network and the catchment. This work uses that model to address two questions: what is the influence of the overland flow production mechanism in the overall behavior of the basin and why is there an apparent randomness present in the evolution process even if the system is completely deterministic.

1.2 Outline

Chapter 2 presents a general review of previous work. This chapter gives basic definitions and describes some channel network models. The problems described in the above section will be discussed in two separate chapters. Chapter 3 studies a modification to the WBR model where a subsurface saturation mechanim is used to calculate the

overland flow distribution. Several simulations are presented and the geomorphological properties of the catchment and networks are studied. Also, comparisons between the original model and its modified version are made. A non-dimensional form of the model is developed which is useful for comparisons among basins of different spatial characteristics. The influence of a probabilistic distribution of rainfall over the overland flow distribution and the behavior of the model is studied in the last section of Chapter 3.

Chapter 4 addresses the hypothesis of the existence of transient chaos in the system and its implication in the system's sensitivity to perturbations in the elevation field, a reflection of the chaotic nature of the system. The possibility of the existence of chaos would explain the apparent randomness in the resulting channel networks.

Chapter 5 summarizes this work and suggests further avenues for research. Appendix A presents the values of the non-dimensional parameters of the different simulations.

Chapter 2

Literature review

2.1 Basic Concepts

The flow of water shapes river basins but at the same time it is the form of the basin that determines in what direction water flows. These two complementary effects constitute the link between hydrology and geomorphology: hydrologic behavior of basins and evolution of catchments and river networks.

The quantitative study of channel networks began with two papers by Horton [13], [14] in which an ordering system of networks was introduced. Later, Strahler [41] modified this system and it is his ordering that is most commonly used today. In this scheme a stream that has a source as one of its extreme points is assigned order 1. Where two streams of order i join, the channel downstream is of order i+1. If two channels of unequal order join, the channel downstream has the same order as the higher order incoming stream. The order of the outlet stream is the basin order, Ω. Exterior links are those between a source and a junction and interior links are those between two junctions. Various link properties like length, area and slope are of interest to hydrologists. One of the purposes of network ordering is to find general relationships between links of different orders across the basin.

The most common geomorphological measures are the Horton/Strahler statistics which are stream based are:

$$R_b = \frac{N_\omega}{N_{\omega+1}} \tag{2.1}$$

$$R_l = \frac{L_\omega}{L_{\omega-1}} \tag{2.2}$$

$$R_a = \frac{A_\omega}{A_{\omega-1}} \tag{2.3}$$

$$R_s = \frac{S_\omega}{S_{\omega-1}} \tag{2.4}$$

where N_ω is the number of streams of order ω, L_ω is the mean length of streams of order ω, A_ω is the mean area contributing to streams of order ω, and S_ω is the mean slope of streams of order ω. R_b, R_l, R_a and R_s are the bifurcation, length, area and slope Horton's ratios. The interest of these ratios is that they are approximately constant when plotted against order, a property that is usually called Horton's law. A lot of work has been devoted to the analysis of these ratios in real networks under a variety of conditions. These catchment statistics can help to understand hydrologic properties of the basin and the work on the geomorphologic instantaneous unit hydograph GIUH by Rodriguez-Iturbe and Valdes [31] and Gupta et al. [10] has generated a renewed interest in this direction.

Another relationship has been proposed by Tokunaga [45]. Using Strahler's ordering system, he defined $\varepsilon_{i-j} = {}_i\varepsilon_j$ as the average number of streams of order j flowing laterally into a single stream of order i. These ratios are approximately constant independently of order. The ratio $K=\varepsilon_i / \varepsilon_{i-1}$ is also approximately constant.

Using elevations, another interesting relationship has been found empirically by Flint [9]. The relationship between slope and area can be expressed as $S = CA^{-\theta}$, which is, like Horton's slope law, a reflection of the fact that stream profiles are concave. Gupta and Waymire [11] and Tarboton et al. [43] have also studied this relationship. Tarboton et al. [42] has postulated a relationship of the form $R_b=R_l^2$ based on fractal arguments.

2.2 Models of Channel Network

The stability of the Horton's ratios under a variety of conditions motivated geomorphologists to develop random models that reproduce this behavior. Based on the work on topological trees by Cayley [7], Shreve [32] developed the random topology model. In this model it is assumed that in the absence of geologic controls, channel networks are topologically random, i.e. all the topologically distinct channel networks with the same number of sources are equally likely. As a consequence of this postulate, in such a population of channel networks, the most probable set of stream numbers N_ω approximately obeys Horton's law.

The random topology model was extended by Smart [36] and Shreve [33], [34] to include the hypothesis that interior and exterior link lengths as well as their associated areas are random variables with separate statistical distributions. This new postulate makes the model have very interesting properties like numerical values of the bifurcation, length, and area ratios that are similar to the values found in real networks.

Years later, Mesa [29] modelled the topologically random networks as a birth and death Markov process where at any distance there is a probability of bifurcation or death of the channel.

All the properties and all the network representations which have been shown up to this point have a common characteristic: they look at a snapshot within the time of the network history. One of the first attempts to model the process of growth of a network was made by Howard [15] (see also van der Tak [46]). In this model the network grows over a grid of points. Nodes are defined as active or inactive. Beginning at an outlet node the network extends according to a growth probability assigned at each site. Avoiding closed loops, the algorithm proceeds until it achieves a certain drainage density level.

Another model is the random walk model proposed by Leopold and Langbein

[21] where source points and source areas assigned to them are distributed as a Poisson process in space. Then, random walks proceed from the sources until they hit the boundary or find other realizations originating in other sources. In this way networks are generated.

Other works like the ones by Kirkby [18] and Smith and Bretherton [40] look at sediment transport, especially at the hillslope scale. The idea is to consider a sediment continuity equation, with flow in the steepest slope direction. The amount of sediment transported is a function of slope and flow of water. The amount of water flowing depends on the contributing area to each point. Smith and Bretherton [40] present a perturbation analysis of the 2D case around the 1D equilibrium solution. They find that small perturbations grow in concave 2D landscapes, an instability that is manifested in channel growth. Luke [22] generalizes this approach to include erosion and deposition. In this case the instabilities develop into shock discontinuities interpreted as channels.

Recently Willgoose et al. [47] have developed a catchment and channel network evolution model. This model is used in this work and will be explained in Section 2.4.

2.3 A Simulation Model of Leaf Veins Growth

Meinhardt [24], [25] developed a model that simulates the growth of leaf vein cells and their differentiation from normal leaf cells. Four variables were used in the model: an activator variable "a" that triggers the differentiation process; an inhibitor h that has a countereffect and reduces production of activator; a substrate z consumed by the differentiation process and a differentiation variable Y that determines whether a cell is a leaf vein cell or a normal cell. The model studied by Meinhardt was:

$$\frac{\partial a}{\partial t} = \frac{ca^2z}{h} - \upsilon a + D_a\frac{\partial^2 a}{\partial x^2} + \rho_0 Y \qquad (2.5)$$

$$\frac{\partial h}{\partial t} = ca^2 z - \nu h + D_h \frac{\partial^2 h}{\partial x^2} + \rho_1 Y \tag{2.6}$$

$$\frac{\partial z}{\partial t} = c_0 - \gamma c_0 z - \xi Y z + D_z \frac{\partial^2 z}{\partial x^2} \tag{2.7}$$

$$\frac{\partial Y}{\partial t} = c_1 a - 0.1Y + \frac{Y^2}{1+9Y^2} \tag{2.8}$$

In the simulation process the initial values of the activator and inhibitor fields are small and z=1 everywhere. A point is chosen as the seed and a value of Y=1 is defined at this point. A random field with a small coefficient of variation is used as input in the parameter c. Willgoose et al. [47] studied this model and showed analitically how very small differences in the c field generated completely different leaf vein network structures. The explanation was found in the chaotic nature of the system. Chapter 4 will explain in more detail the concept of chaos in a dynamical system. Willgoose et al. [47] also studied three features that made possible the generation of branched structures in the Meinhardt model: a potential growth region exists around the growing branch and moves with it; the growth potential is supressed behind the growing tip so that the branch grows as a line; a repulsion between growing branches exists so that no closed loops appear and the final network fills the entire space.

2.4 The WBR Model

Based on the conclusions derived in the study of the Meinhardt model, Willgoose, Bras and Rodriguez-Iturbe [47] constructed a model that simulates the catchment evolution and network growth in a grid. The model uses some concepts of erosion engineering to define an activator function that triggers the growth of channels; the Einstein-Brown

sediment transport equation; and the idea of preferred erosion in channels. Four variables are studied: the elevation z, the indicator Y that tells whether a node is a channel or a hillslope, and the channel formation function, a. The form of this model, henceforth called the WBR model is:

$$\frac{\partial z_j}{\partial t} = c_{0_j} + K_1 \Sigma_i Q_{s_i} I_{ij} + D_z \frac{\partial^2 z_j}{\partial x_i^2} \tag{2.9}$$

$$\frac{\partial Y_j}{\partial t} = d_t \left[K_2 a_j + \left(-0.1 Y_j + \frac{Y_j^2}{1+9Y_j^2} \right) \right] \tag{2.10}$$

$$a_j = \beta_5 Q_j^{m_5} S_j^{n_5} \tag{2.11}$$

where Q_s is the sediment transport (assumed to be equal to $\beta_1 Q_j^{m_1} S_j^{n_1}$ in channels and $O_t \beta_1 Q_j^{m_1} S_j^{n_1}$ with $O_t<1$ in hillslopes); Q_j is the overland flow which is proportional to the area that contributes to each node; S_j is the steepest slope downhill; c_{0_j} the tectonic input at node j; I_{ij} an indicator function that says whether node i drains into node j; and K_1, K_2 and d_t are constants. The physical processes on which this model is based will be explained in more detail in Section 3.3. This model is the basis for the subsurface saturation modification model described in Chapter 3. In this chapter a more detailed explanation of the different variables, the physical mechanisms behind them and details about the implementation of the simulations will be presented.

The WBR model generates realistic looking catchments and channel network with values of statistical measures similar to the networks found in nature. In this work an extension of the model to include a different way of generating overland flow and a closer look at the chaotic behavior of the system will be presented.

Chapter 3

A Catchment Evolution Model with a Subsurface Saturation Mechanism

3.1 Introduction

In this chapter a modified version of the WBR model is developed. The purpose is to modify the mechanism of overland flow production to include subsurface saturation besides the classical Hortonian infiltration excess. In the Hortonian mechanism overland flow is assumed to be generated uniformly over the whole area whereas in the subsurface saturation mechanism only saturated areas contribute to the overland flow. The modified model will permit us to understand the role of overland flow distribution in the overall behavior of the system.

The organization of this chapter is as follows. An analytical formulation of the subsurface saturation mechanism is derived. This formulation is then incorporated in the WBR model. An example of a typical simulation and the variation in time of the spatial distribution of the principal variables of the model are shown. Afterwards, four different random elevation fields are used as initial conditions for different smulations with exactly the same parameter values. The variability of common geomorphological statistics is then illustrated. The question of whether chaos is the explanation for this variability is addressed in Chapter 4.

The following section studies the influence of diffusive sediment transport processes like rainsplash and rockslide in the evolution of the networks. Then a non-dimensional formulation of the modified model is developed. In this formulation the original parameters are transformed into new non-dimensional ones that will allow comparisons between catchments with different scales.

whether a hillslope node is saturated or not. Then, various characteristics of importance that have been studied and measured in real basins are examined in the resulting networks that are generated by the modified version of the WBR model. Finally, in Section 3.11 the influence of a probabilistic distribution of rainfall on the overall behavior of the system is studied.

3.2 Overland Flow Distribution Using the Subsurface Saturation Mechanism

This section presents the analytical formulation of the procedure to assign contributing flow to each node using the subsurface saturation mechanism. The overall reasoning is as follows. Assuming an exponential profile of hydraulic conductivity with depth, the amount of water required to obtain saturation at each node can be calculated based on an average net rainfall. Then, for each node the difference between the rainfall at the mean flood event and the saturation deficit can be calculated. If the difference is positive then overland flow is produced at that node. By adding this difference along elevation gradients contributing overland flows to each node can be found.

The following derivation is based on [4], [5], [6], [8], [19], [20], [30], and [35]. First of all, assume exponential decrease of hydraulic conductivity in the soil profile [2]:

$$K(z) = K_0 e^{-\alpha_1 z} \tag{3.1}$$

where z is the depth from the soil surface, K(z) and K_0 are hydraulic conductivities at depth z and at the soil surface respectively and α_1 is a parameter.

If the water table depth is h and the maximum depth of interest is H, then the subsurface flow rate at node i is:

$$q_i = S_i \int_h^H K(z)\,dz = S_i \left(\frac{K_0}{\alpha_1}\right) \left[e^{-\alpha_1 h} - e^{\alpha_1 H}\right] \tag{3.2}$$

where S_i is the steepest downhill slope. Equation (3.2) assumes that the local hydraulic gradient is everywhere equal to the surface slope angle [30]. If H is large enough, then q_i can be approximated to:

$$q_i = S_i \left(\frac{K_0}{\alpha_1}\right) e^{-\alpha_1 h} \tag{3.3}$$

The second main assumption is to consider a moisture profile as shown in Figure 3-1

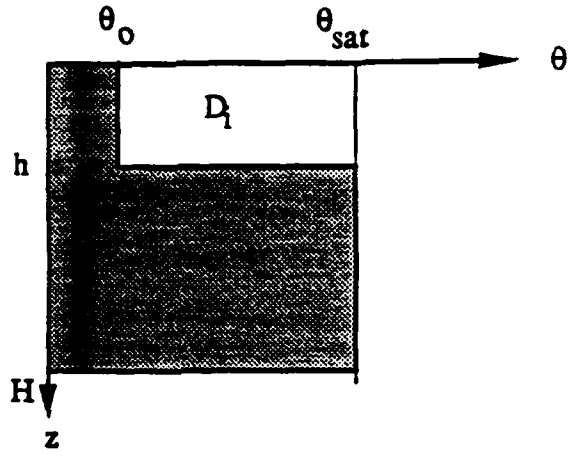

Figure 3-1: Soil Profile Assumption in Subsurface Saturation Mechanism

The saturation deficit is defined as:

$$D_i = h(\theta_{sat} - \theta_0) \tag{3.4}$$

Replacing in Equation (3.3):

$$q_i = S_i \left(\frac{K_0}{\alpha_1}\right) \exp\left[-\frac{\alpha_1 D_i}{\theta_{sat} - \theta_0}\right] \tag{3.5}$$

Define:

$$\alpha_2 = \frac{K_0}{\alpha_1} \qquad \beta_6 = \frac{\theta_{sat} - \theta_0}{\alpha_1} \tag{3.6}$$

The values of these two constants are assumed to be homogeneous over the whole basin. Then replacing (3.6) in (3.5) results in:

$$q_i = S_i \alpha_2 e^{-D_i/\beta_6} \tag{3.7}$$

from where:

$$D_i = \beta_6 \ln\left[\frac{\alpha_2 S_i}{q_i}\right] \tag{3.8}$$

Assume that subsurface flow is approximately in steady state with the net recharge rate r at any time. Then:

$$q_i = r A_i \tag{3.9}$$

where A_i is the contributing area to node i. Replacing in Equation (3.8) and defining $T_c=\alpha_2/r$ results in:

$$D_i = \beta_6 \ln\left[\frac{T_c}{A_i/S_i}\right] \tag{3.10}$$

if this quantity is positive or $D_i=0$ otherwise. A negative value of the expression (3.10) (i.e.$D_i=0$) implies that the node i is saturated. The saturation criteria for a node is then:

$$\frac{A_i}{S_i} > T_c \tag{3.11}$$

For every point the excess water is calculated as the difference between β_3 and D_i. β_3 is considered as the rainfall at the mean flood event (for a definition of this concept and its relationship with the sediment transport equation to be used in the model, see Appendix C.1.3. in [47]). The sum along the elevation gradient of the excess water at each node gives the contributing overland flow to be used in the modified model.

3.3 Model Description

This section presents the subsurface saturation mechanism modification to the WBR model. Two variables are solved on a plane grid: the elevation at each node z_i and the indicator function Y_i that identifies a node as either a channel or a hillslope. The downhill slopes S_i determine flow directions. Following these flow directions the contributing area A_i to each node is calculated. The next step is to find the deficits D_i using areas and slopes and the saturation criteria decribed in Section 3.2. The excess water is summed downhill along the flow directions giving as a result the total overland flow through each node Q_i. The flows Q_i enter the channel formation function a_i and sediment transport Q_{si} equations. These two latter variables go into the elevation and indicator function differential equations.

The resulting model is:

$$\frac{\partial z_i}{\partial t} = C_{0_i} + \frac{1}{\rho_s(1-n)L_g^{\,2}} \sum_j Q_{s_j} I_{ji} + D_z L_g \frac{\partial^2 z_i}{\partial x_j^{\,2}} \tag{3.12}$$

$$\frac{\partial Y_i}{\partial t} = d_i \left[0.0025 c_1 a_i + \left(-0.1 Y_i + \frac{Y_i^{\,2}}{1+9Y_i^{\,2}}\right)\right] \tag{3.13}$$

$$Q_{s_i} = f(Y_i)\, Q_i^{m_1}\, S_i^{n_1} \tag{3.14}$$

$$a_i = \beta_5 Q_i^{m_5}\, S_i^{n_5} \tag{3.15}$$

$$Q_i = \langle \beta_3 - D_i \rangle + \sum_j Q_j I_{ji} \tag{3.16}$$

$$f(Y_i) = \begin{cases} \beta_1 O_i & \text{if} \quad Y_i = 0 \\ \beta_1 & \text{if} \quad Y_i = 1 \end{cases} \tag{3.17}$$

$$D_i = <\beta_6 ln(\frac{T_c}{A_i / S_i})> \tag{3.18}$$

where <x> stands for max(x,0) and the subindices i and j denote grid nodes. Most of the variables have already been defined. The following is a complete list of all constants and variables involved in the equations:

z_i	=elevation
Y_i	=indicator variable for channelization (0 hillslope, 1 channel)
Q_{s_i}	=sediment transport
a_i	=channel formation function function
Q_i	=discharge
D_i	=saturation deficit
t	=time
C_{0_i}	=tectonic input
ρ_s	=density of eroded material
n	=porosity of material before erosion and after deposition
L_g	=grid spacing
I_{ji}	=indicator function for whether node j drains into or out node i -1(j=i,drainage of node i), 1(node j drains into node i), 0(node j does not drain into or out of node i)
D_z	=diffusivity constant for diffusive transport processes
x_j	=horizontal distance in direction j
d_t	=rate constant for channel growth
c_1	=1/threshold on the channel formation function of channelization
m_1,n_1	=powers of Q_i and S_i in the sediment transport equation
β_5	=multiplicative factor on channel formation function equation
m_5,n_5	=powers of Q_i and S_i in the channel formation function equation
β_3	=additive term on overland flow equation
β_6	=multiplicative factor on saturation deficit equation
T_c	=threshold value in saturation criteria

Let us explain in more detail the equations that govern the evolution of the system. There are three basic variables: elevation, channelization indicator and value of channel formation function. The first two are the variables to be solved in the grid plane. They are related to each other through the channel formation function function. Grid points are defined as channel or hillslope nodes according to the value of the indicator function Y_i (1 for channels, 0 for hillslopes). The differential equation (3.13) for Y_i is constructed in such

a way that the values 0 and 1 are attractive fixed points. Y_i depends on the values of the channel formation function function defined by Equation (3.15). The purpose of the channel formation function is to trigger the process that transforms a hillslope node into a channel node. Once the channel formation function exceeds a threshold value given by $1/c_1$, the indicator function moves from 0 to 1 at a rate determined by d_i. The specific way in which Equation (3.13) rules this transformation is not important for the overall behavior of the system: any equation with 0 and 1 as attractive fixed points and a dependence on a parameter that behaves like **a** will work as well.

The definition of the channel formation function, in Equation (3.15), is a conceptualization of erosion processes. Concepts like overland flow velocity and threshold bed shear stress, that are commonly used in sedimentation engineering, can be placed into the framework of Equation (3.15) (see [47] for details).

On the other hand, the variation in grid node elevations is produced by three factors: the tectonic input, the fluvial sediment transport and diffusive transport. The tectonic input can take a variety of forms. The expressions studied in this work correspond to a single uplift event (see [26]) or a continuous process.

The fluvial sediment transport term is simply a sediment continuity equation. The amount of sediment Q_{s_i} that is washed away from the node by fluvial transport processes is calculated using Equation (3.14). The term $f(Y_i)$ in this equation parametrizes the difference in sediment transport phenomena that occurs in hillslopes and channels. A small value of O_i in Equation (3.17) describes the fact that sediment transport in hillslopes is smaller than in channels. Details about the derivation of Equation (3.14) from the well known Einstein-Brown sediment transport equation can be found in [47].

The term Q_i in Equation (3.14) is the net overland flow contributing to node i. Equation (3.16) is the overland flow continuity equation, where flow from adjacent nodes that drain into node i and excess water from that node are equated to the flow from the

node. The excess water at each node is calculated based on the saturation deficit equation (3.18) as described in Section 3.2.

The last term in the differential equation (3.12) for the elevation field corresponds to transport processes that occur on the hillslope and can be modelled as diffusive processes. These processes are soil creep, rainsplash and rockslide.

Finally, the sediment transport is the non-linear link between the elevation and indicator variables. The sediment movement changes node elevations and this affects both slopes and contributing overland flow. Then the channel formation function changes and its new value enters the indicator differential equation, triggering the channelization process if the value surpasses the threshold $1/c_1$. The indicator function is not just an artifact to differentiate hillslope and channel nodes but it also affects the way sediment transport takes place. The preferred transport in channels creates valleys around the channels and the whole slope field behaves accordingly. The dependence cycle in the system is then closed.

In the implementation of the program, the system is solved in a rectangular grid. An initial random elevation field with a very small coefficient of variation is generated and the elevation at the bottom left-hand corner is set at a lower value. That node is defined as the outlet and its elevation is kept constant during the simulation.

3.4 A Simulation Example

In order to show the overall behavior of the system described by Equations (3.12) to (3.18), a simulation example will be presented in this section. No detailed analysis of the different network properties will be performed here. Such an analysis will be presented in subsequent sections. Rather, the variation in time of the most important properties of the catchment and the channel network for a typical simulation are going to be shown graphically.

The parameters for this simulation BR643SATU10 are shown in Appendix A. Four steps in the evolution of the network have been chosen to show the variation in time of different properties. The time interval spans over the whole network growth period. The properties to be examined are elevation, slope, contributing area, overland flow and channel formation function at each node. For a better appreciation of the properties, three things are presented in each graph: the spatial distribution of the property underneath an isometric view of the elevation field; a contour map corresponding to the values of the property under study; and the simulated channel network at that time step. The contour levels in each figure are not evenly spaced; instead, their values have been chosen to highlight certain aspects of the behavior of the system.

Figures 3-2 to 3-5 show the evolution of the elevation field. The preferential erosion at channels, determined by O_i , produces well differentiated valleys along the channel. Figure 3-6 to 3-9 correspond to the steepest slope S_i in the downhill direction at each node. Notice that the steepest slopes in the field occur not on the channel heads but on the lateral hills along the channel. The zone outside the region captured by the network has slopes that are very small. Figures 3-10 to 3-13 present the contributing area A_i. As expected, channel nodes have the larger areas as a result of the organization of flow directions in the catchment. Figures 3-14 to 3-17 show which nodes are saturated (in black) and which nodes are unsaturated (in white). Equation (3.11) was the criteria for selecting the saturation status of each node. At the beginning, every node was saturated; with time, only channel nodes and nodes around them remain saturated. Figures 3-18 to 3-21 correspond to the channel formation function distribution. The contours show how the higher values of the channel formation function are located in those zones of active network growing at the channel heads. In the original WBR model the areas and contributing flow were directly proportional. In the subsurface saturation mechanism modification the overland flow is not directly proportional to areas anymore, even though strong links exist between both

variables. In the modified model overland flows are calculated according to the derivation presented in Section 3.2. Finally, Figure 3-22 shows the variation in time of the hypsometric curve for the catchment. Detailed analysis of this curve under different parameter values will be presented in a later section.

Table 3-I presents the values of commonly studied statistics for the final network. Notice that all the values of the statistics are within reasonable limits.

The overall behavior of the system variables have been shown in a typical simulation. The final result is a realistic catchment and geomorphologic network with characteristics similar to real networks. An analysis of the dependence of the system's behavior on the parameters and a comparison between the original WBR model with its subsurface satuation modification will be presented in the following sections.

3.5 Variability in Final Channel Networks

This section will illustrate the high variability present in the final results of the catchment evolution model. This variability is the reason for an apparent randomness in the final channel network. The differential equations of the model have two important characteristics: they are non-linear and they are coupled in space. This is the reason why even if two different simulations have the same parameter values, small differences in the elevation field generate completely different networks.

Four simulations are shown in this section. All of them have the same parameter values. The difference between simulations lies in the initial elevation field. Different realizations of random elevation fields with identical statistical properties were used. Final networks are shown in Figure 3-23.

For each of the four catchment evolutions common geomorphological measures were examined: Strahler's bifurcation, length, slope and area ratios. The evolution in time of

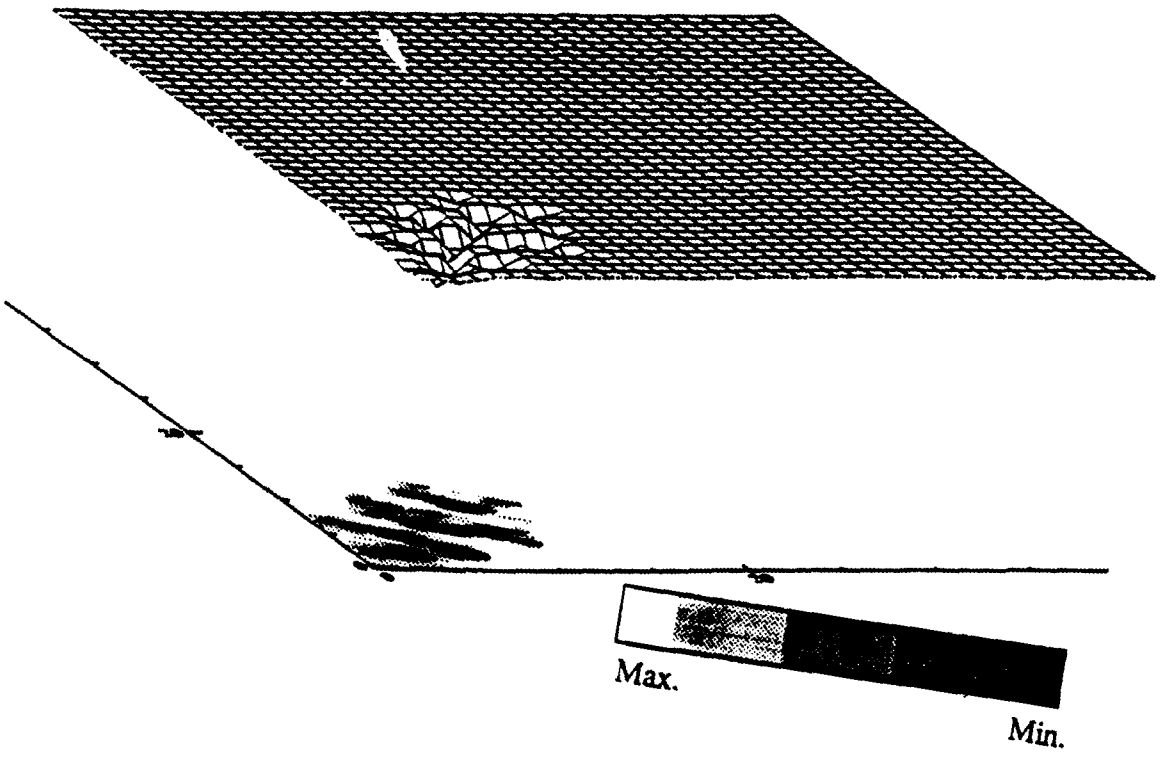

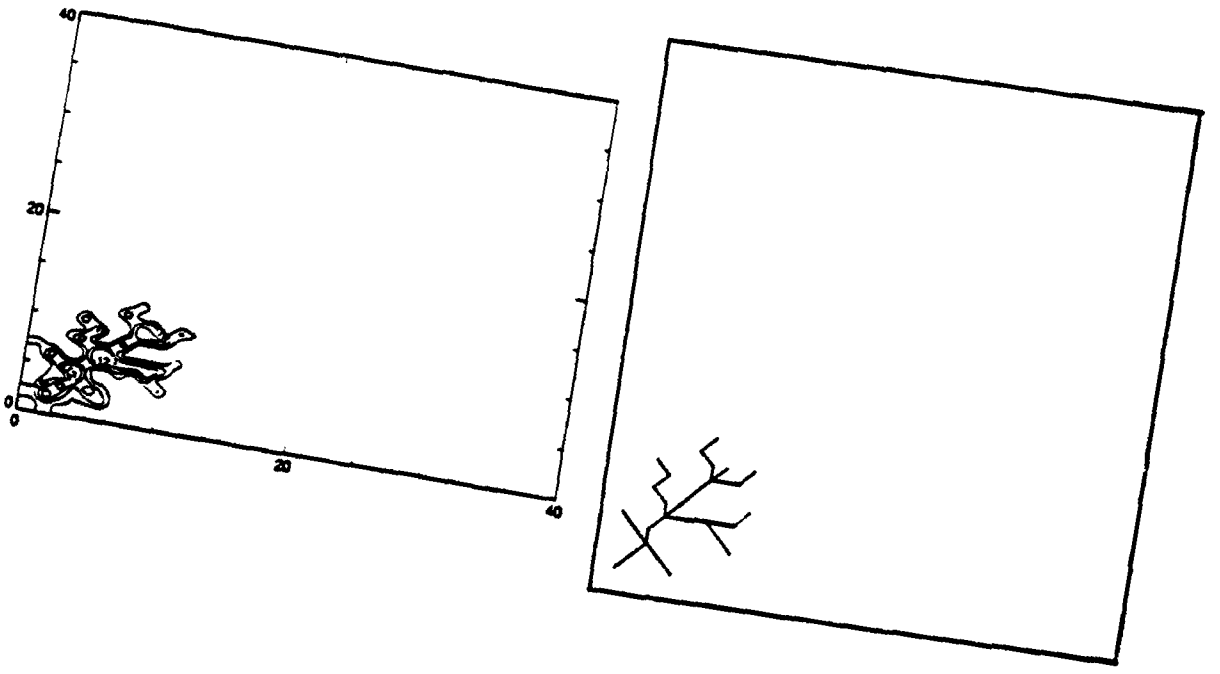

Figure 3-2: Elevation Spatial Distribution Timestep *1000*

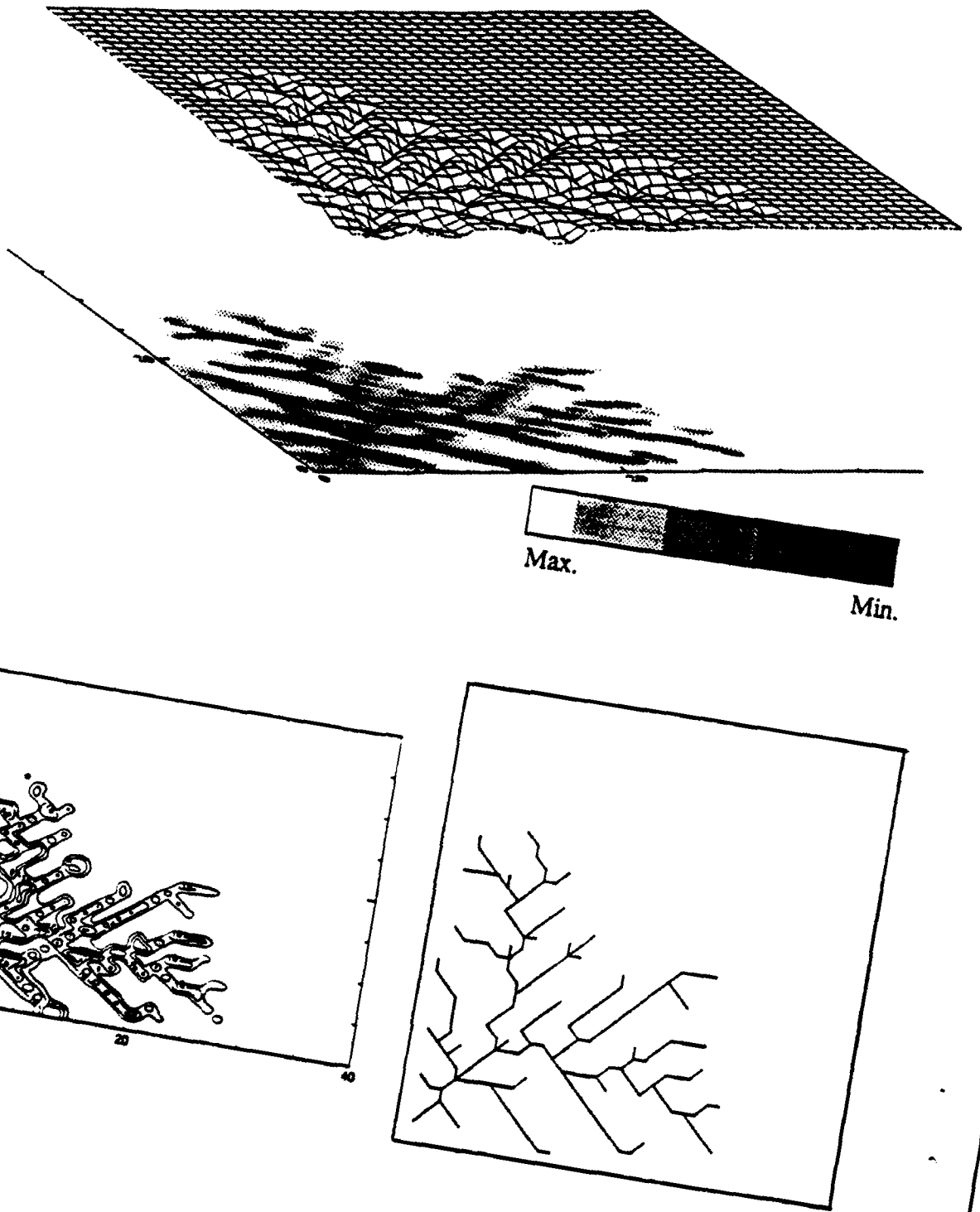

Figure 3-3: Elevation Spatial Distribution Timestep 3000

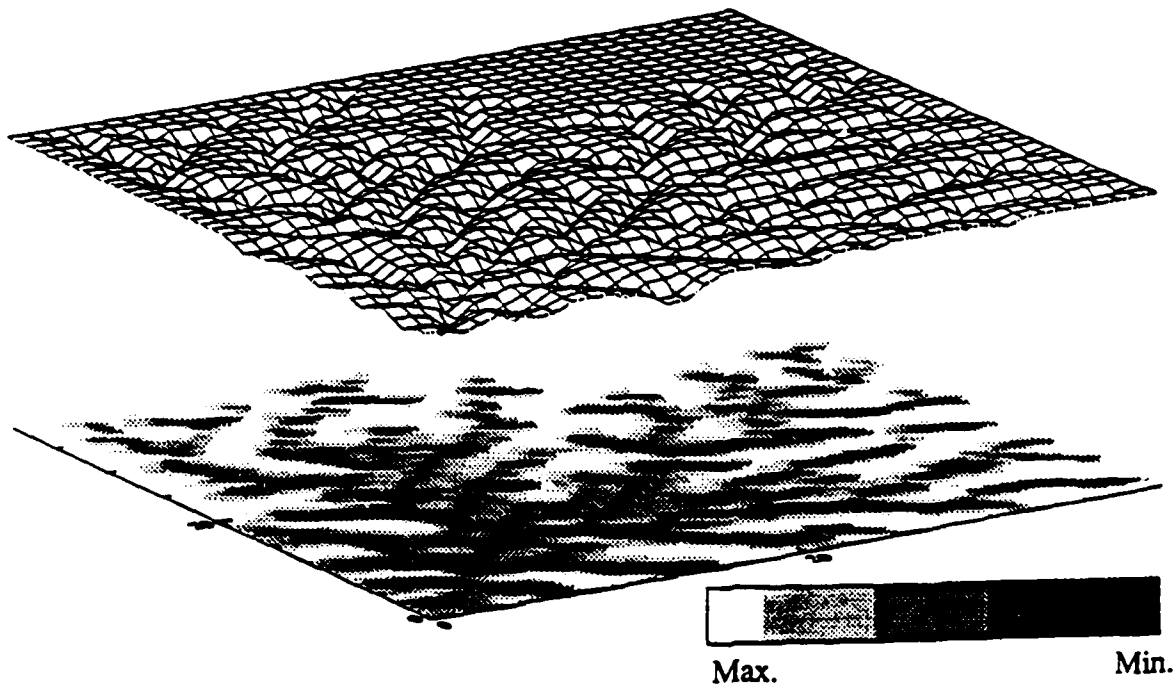

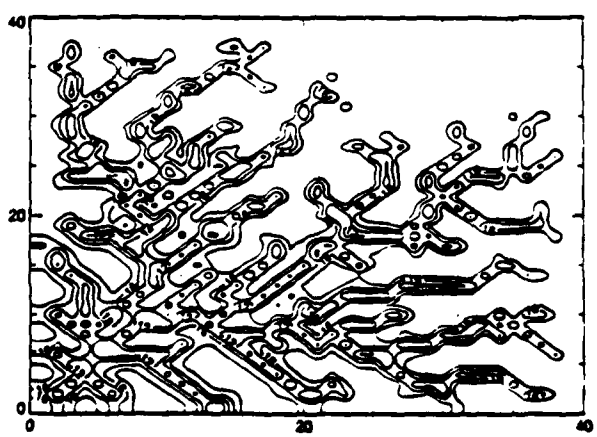

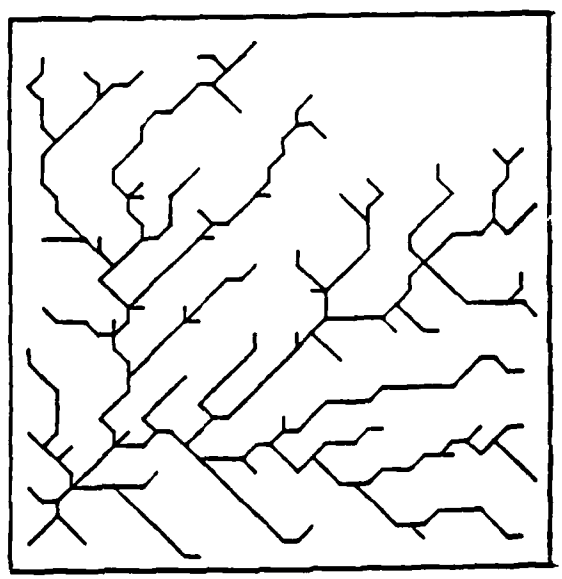

Figure 3-4: Elevation Spatial Distribution Timestep 5000

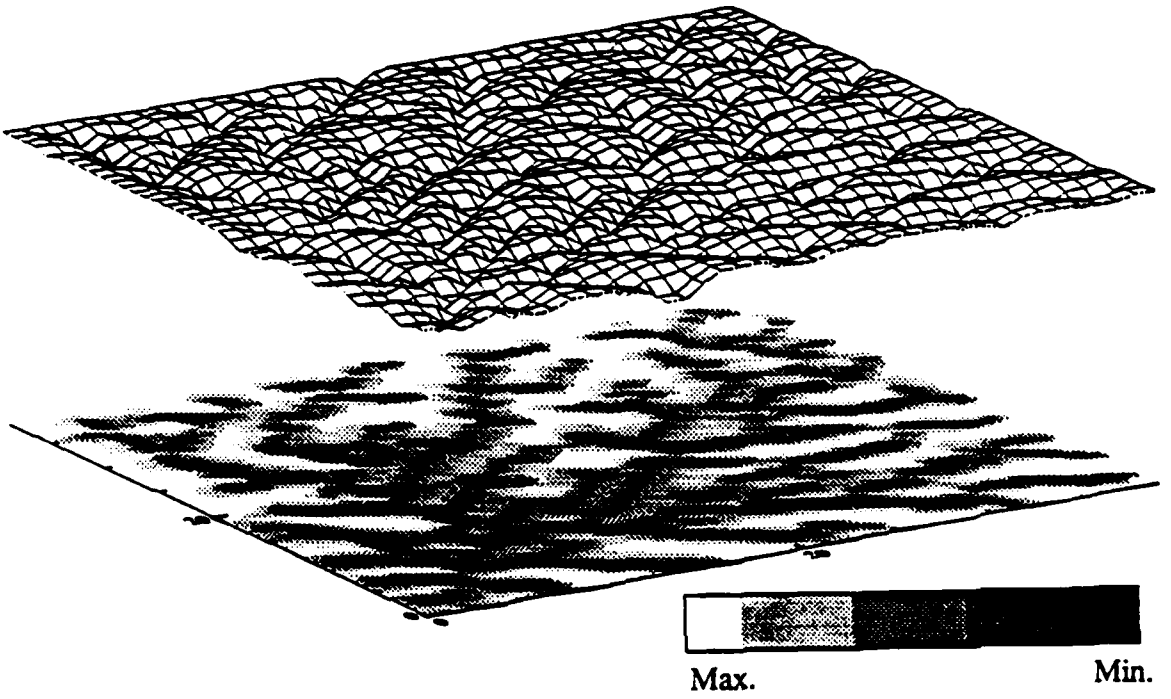

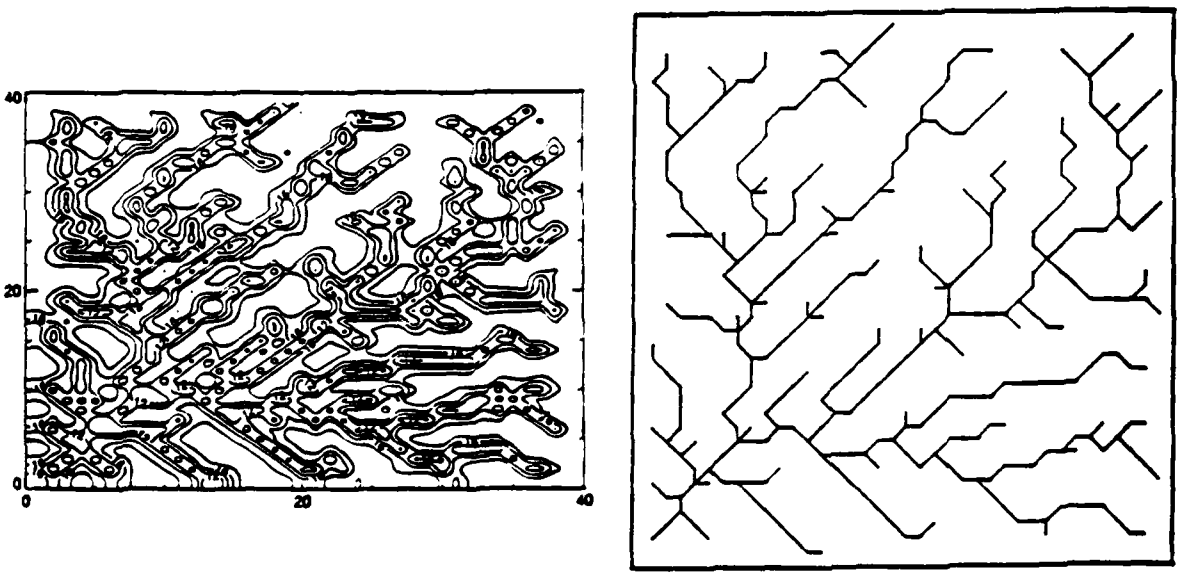

Figure 3-5: Elevation Spatial Distribution Timestep 7000

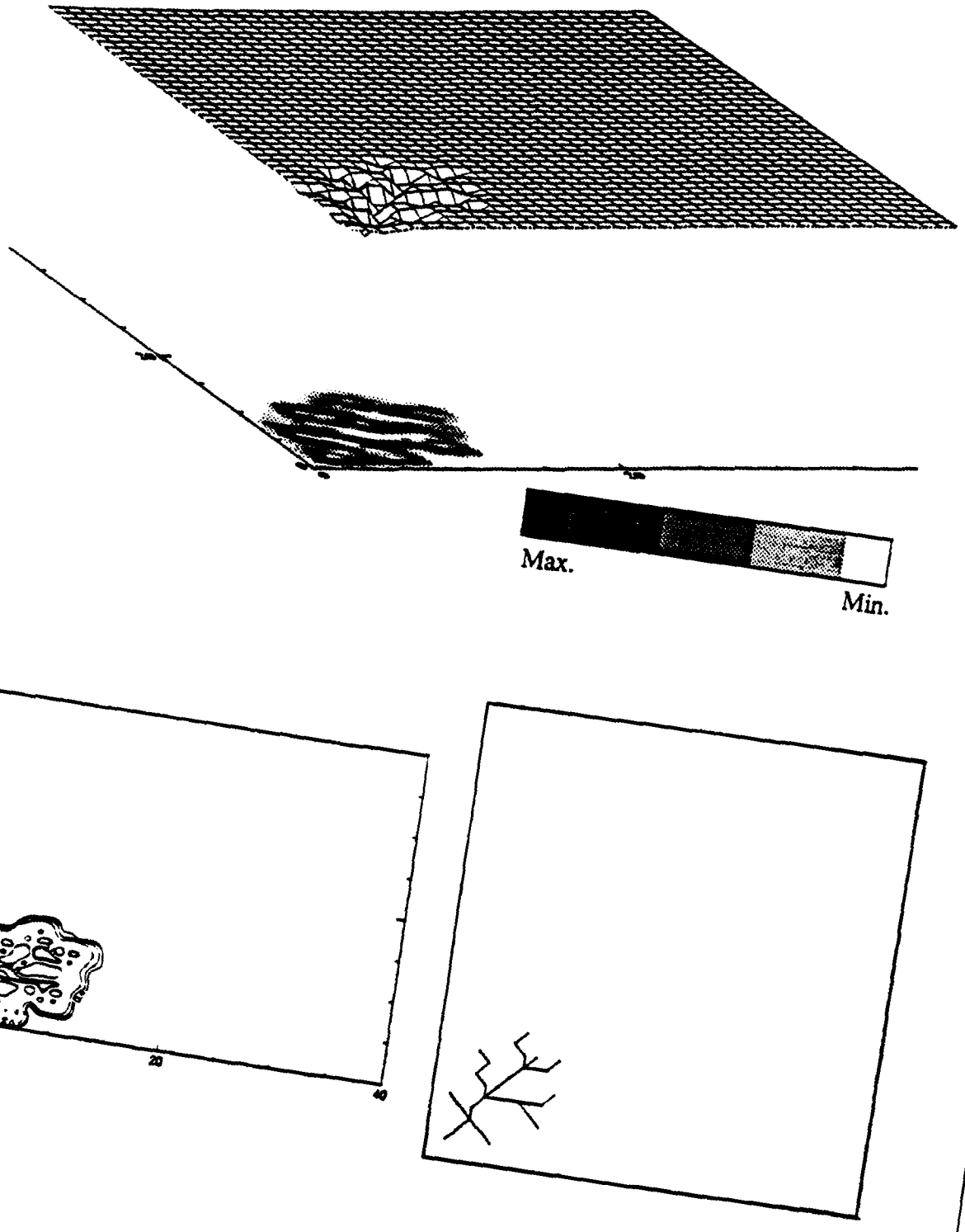

Figure 3-6: Slopes Spatial Distribution Timestep 1000

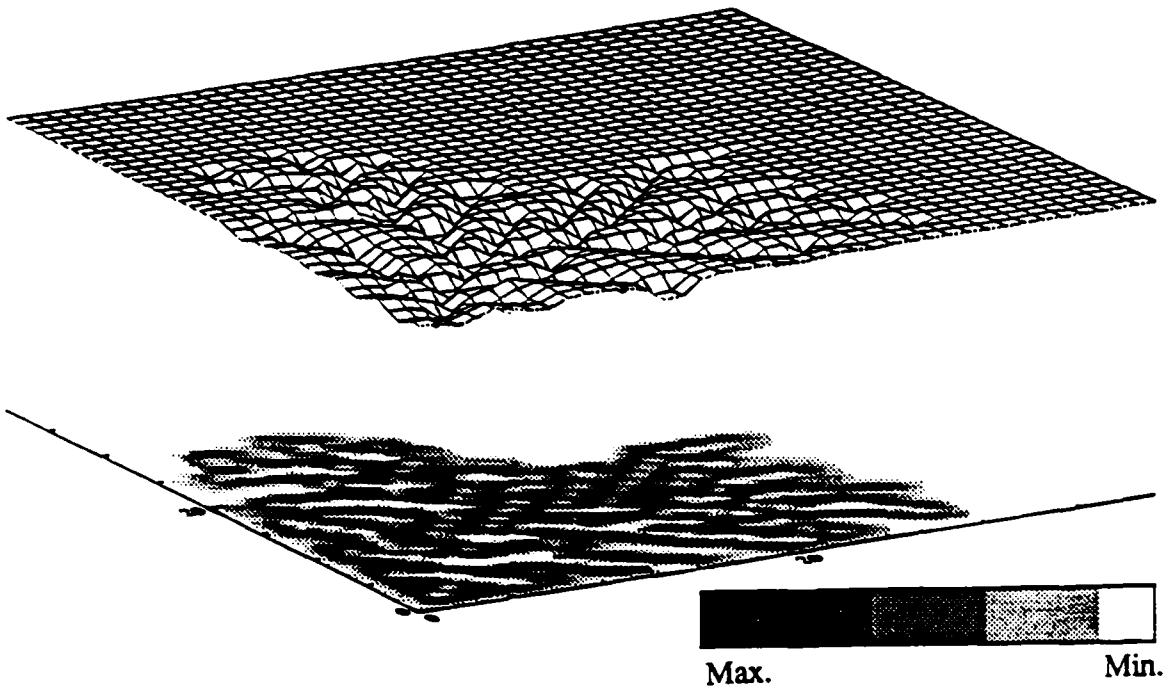

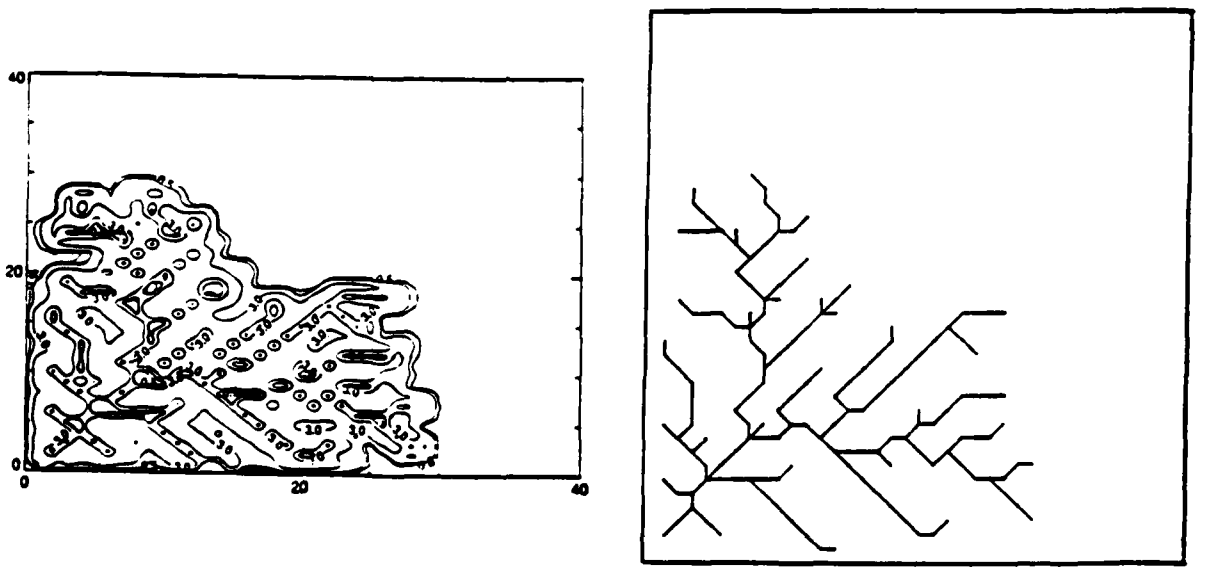

Figure 3-7: Slopes Spatial Distribution Timestep 3000

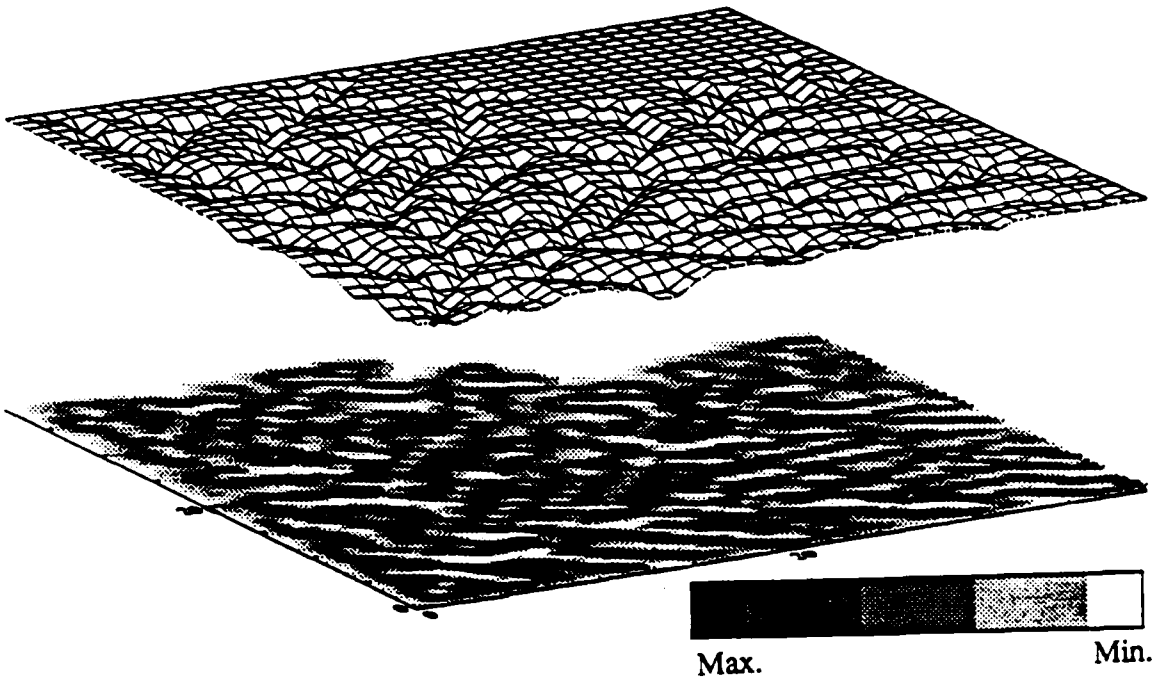

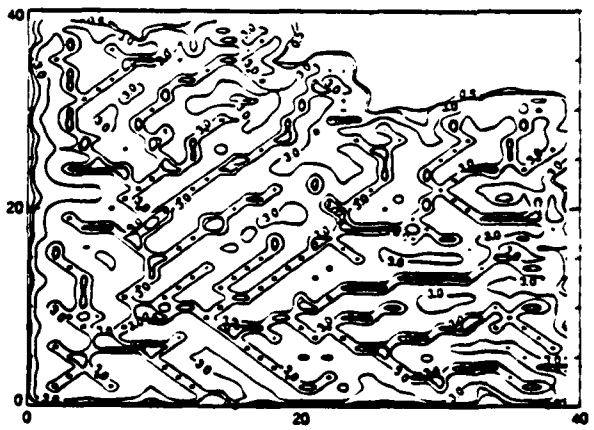

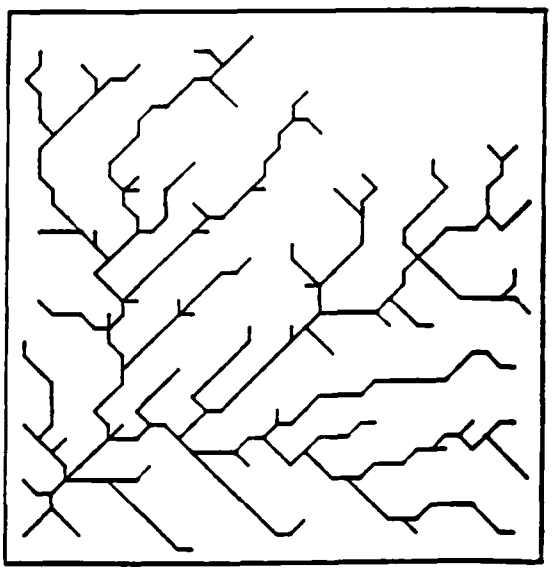

Figure 3-8: Slopes Spatial Distribution Timestep 5000

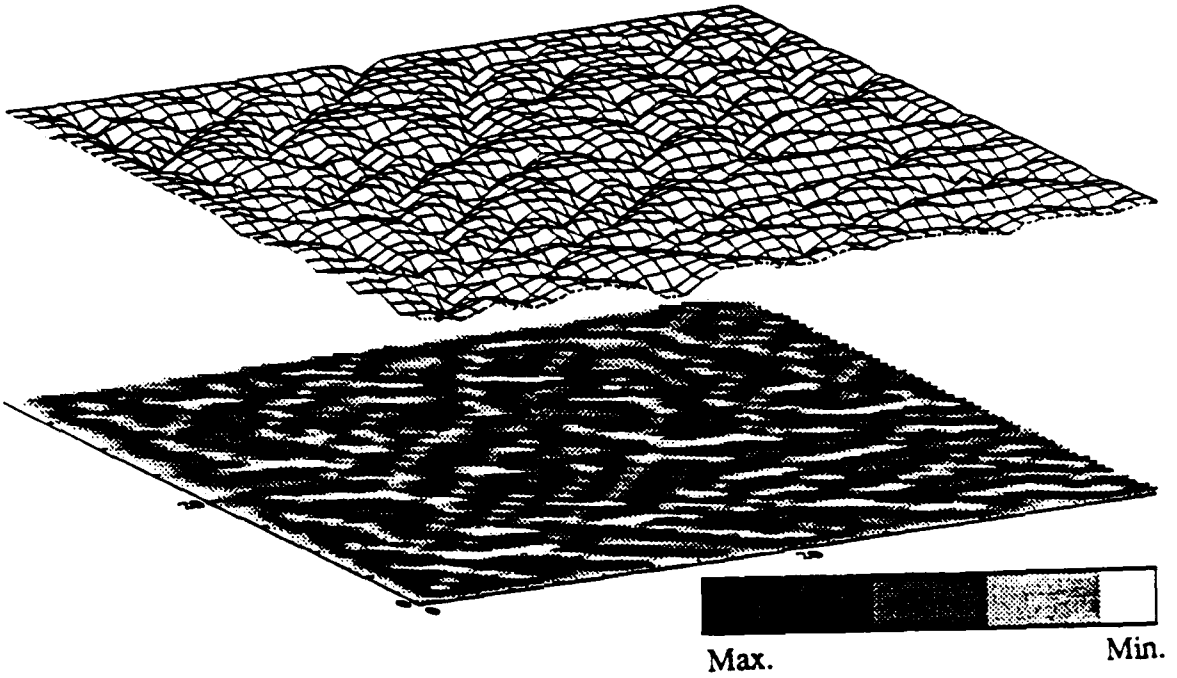

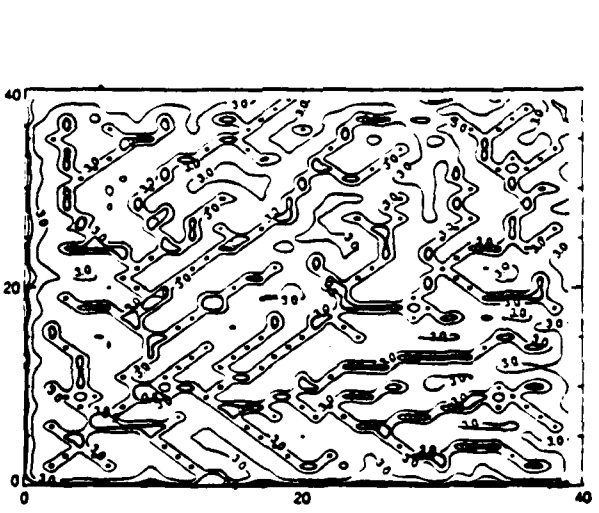

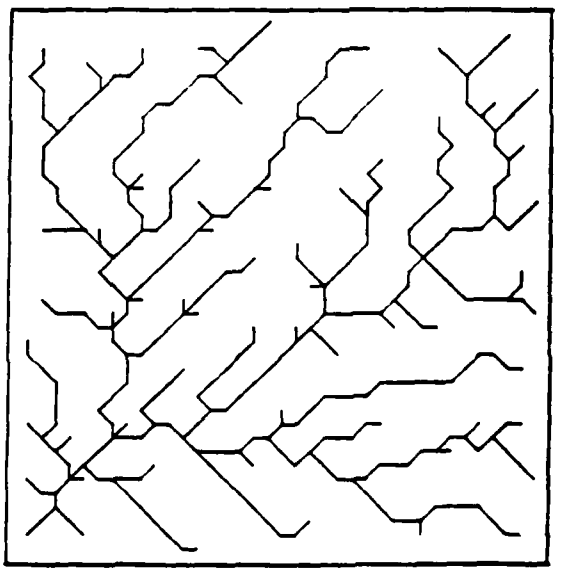

Figure 3-9: Slopes Spatial Distribution Timestep 7000

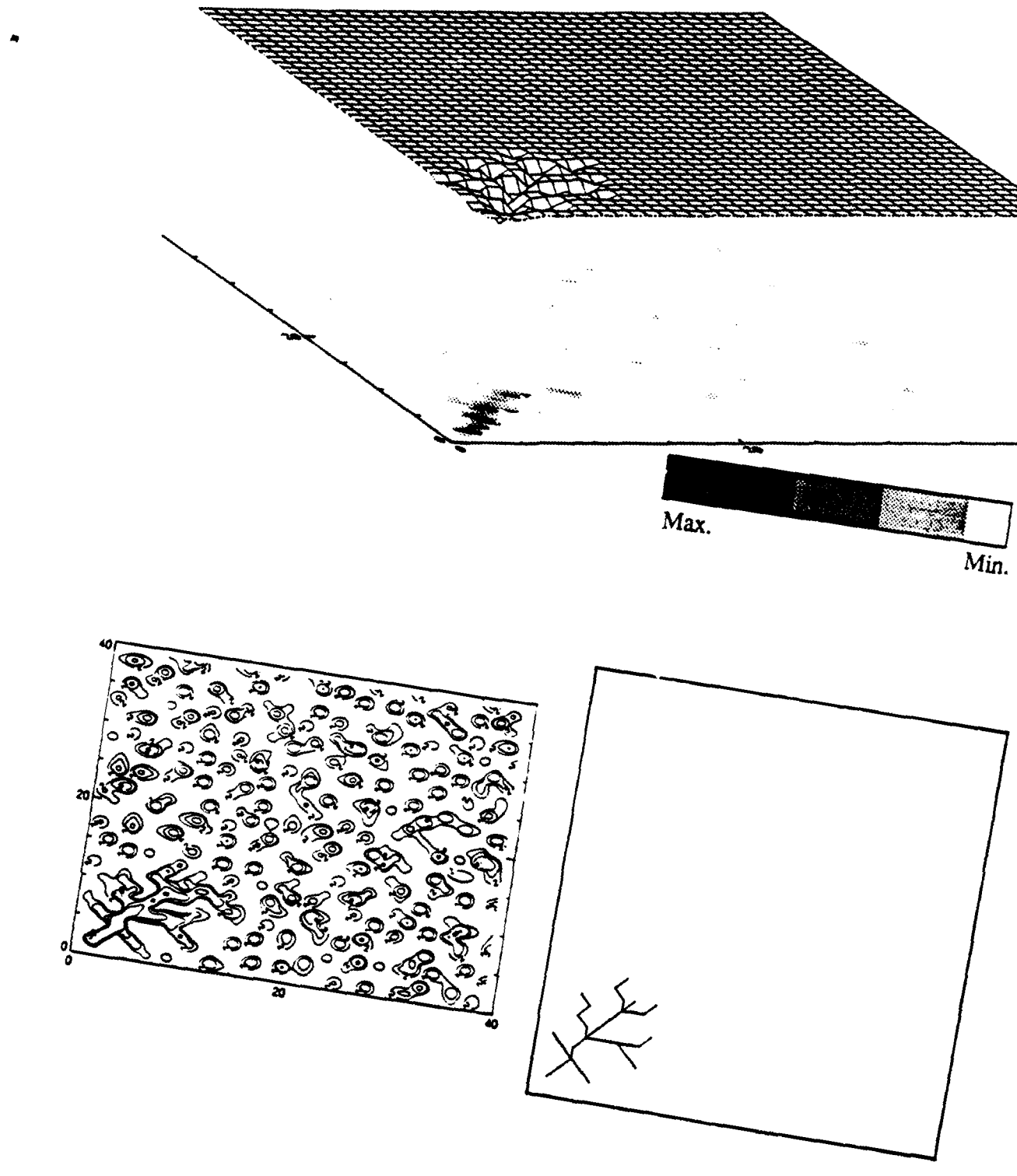

Figure 3-10: Contributing Area Spatial Distribution Timestep 1000

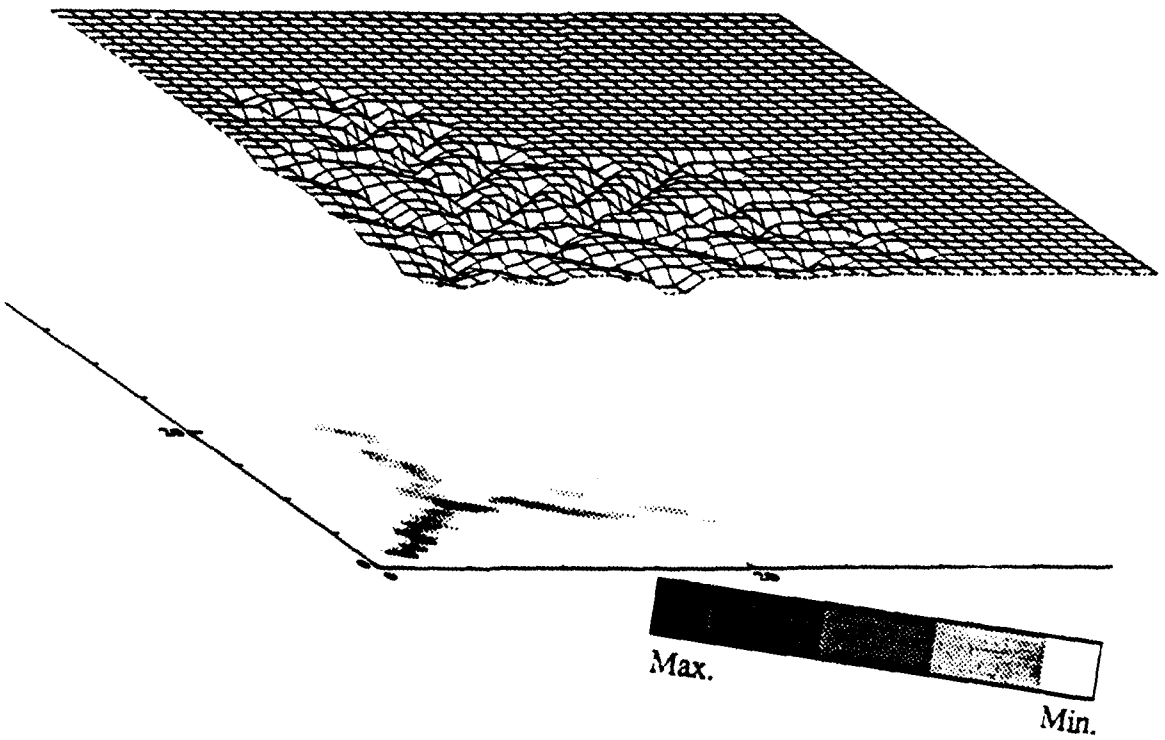

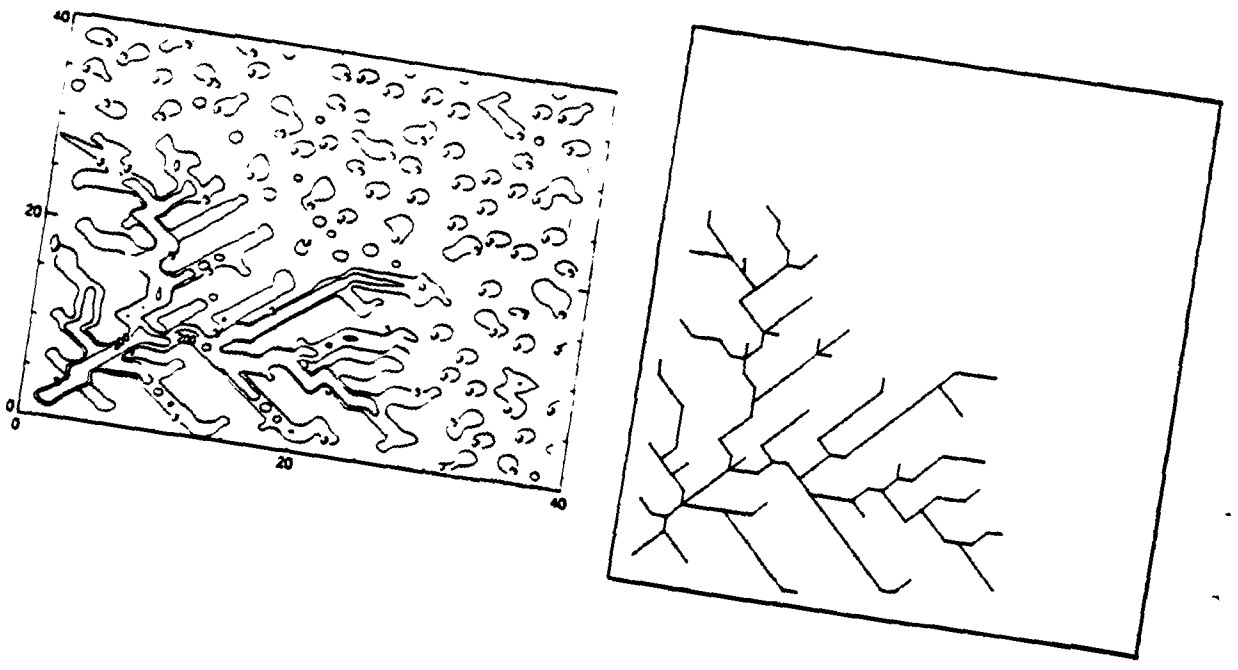

Figure 3-11: Contributing Area Spatial Distribution Timestep *3000*

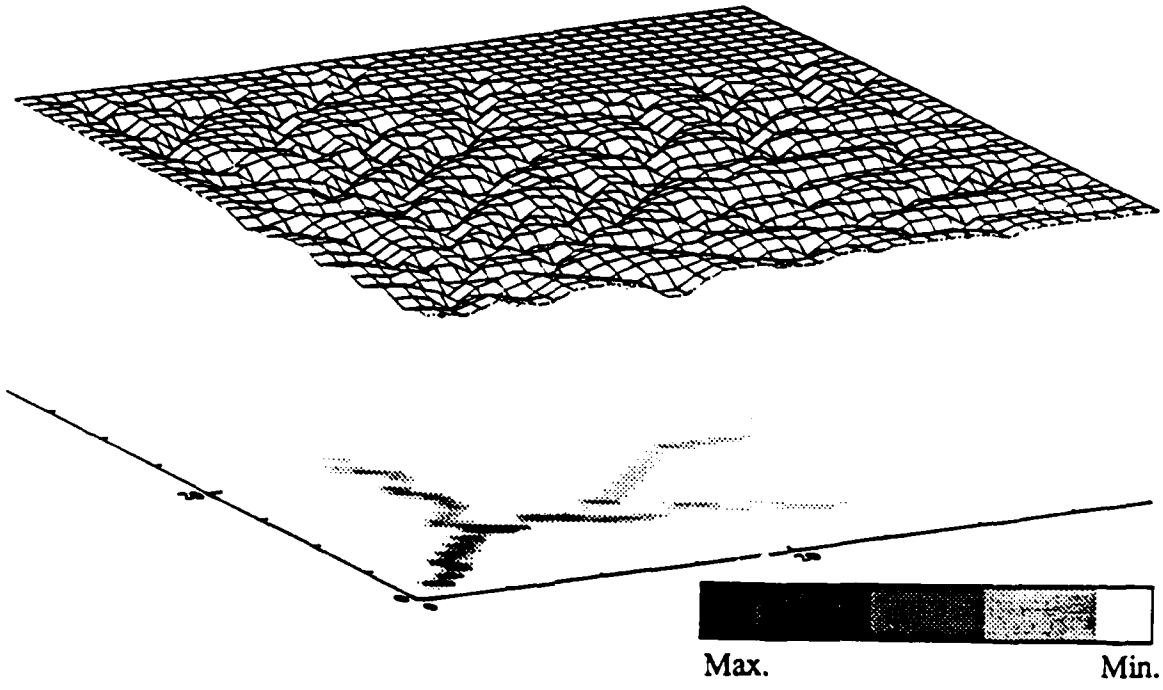

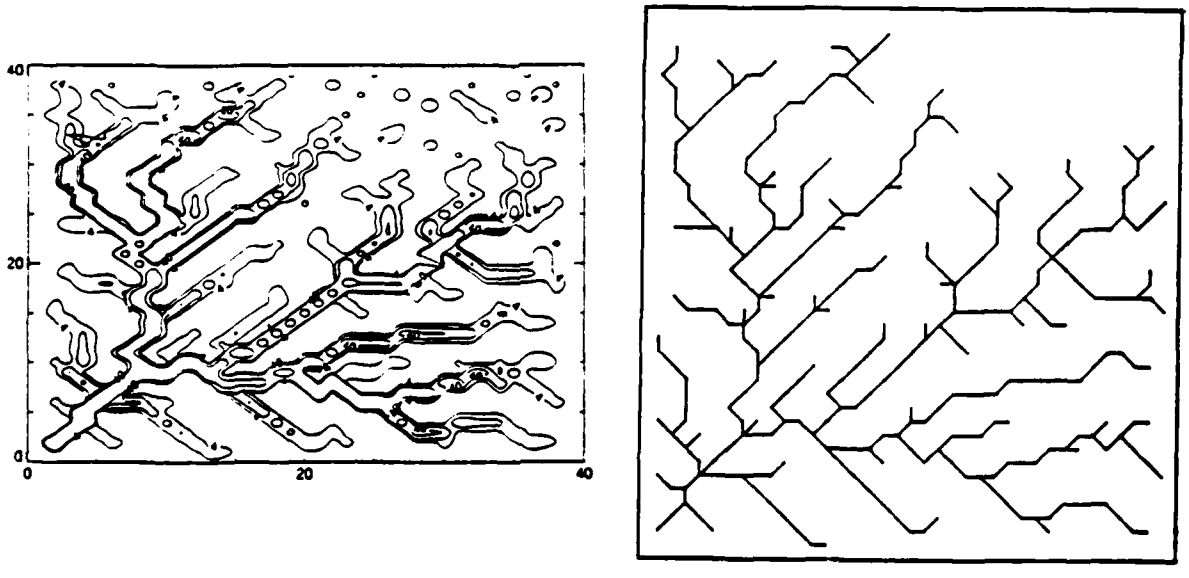

Figure 3-12: Contributing Area Spatial Distribution Timestep 5000

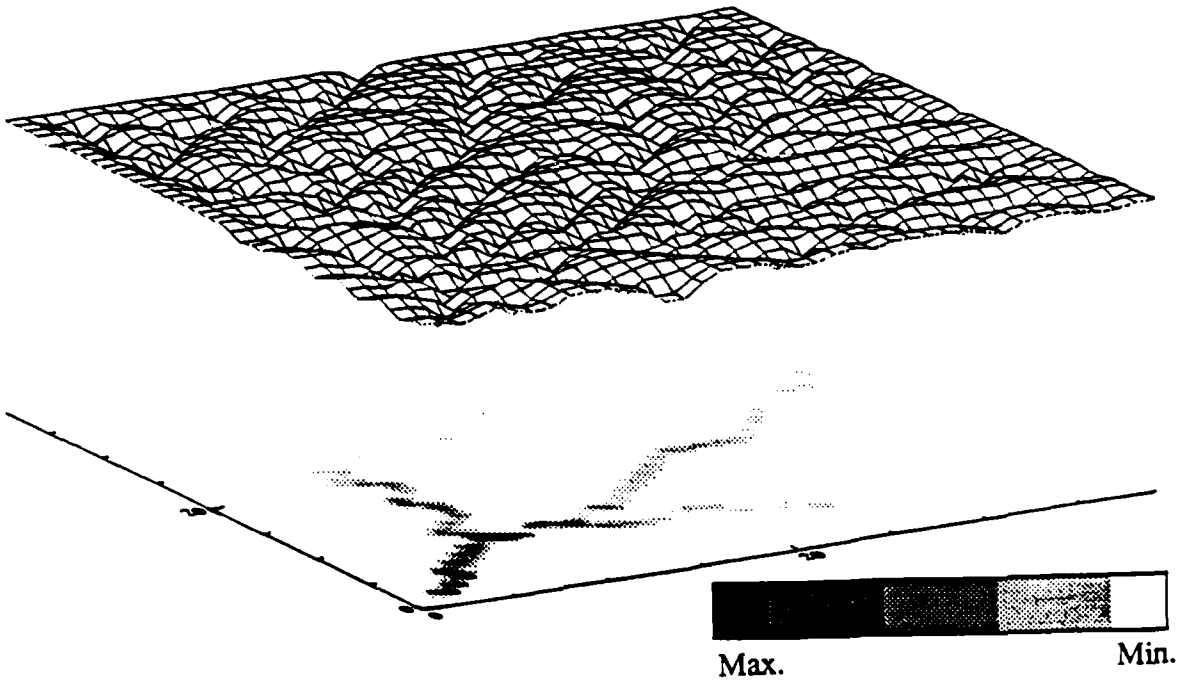

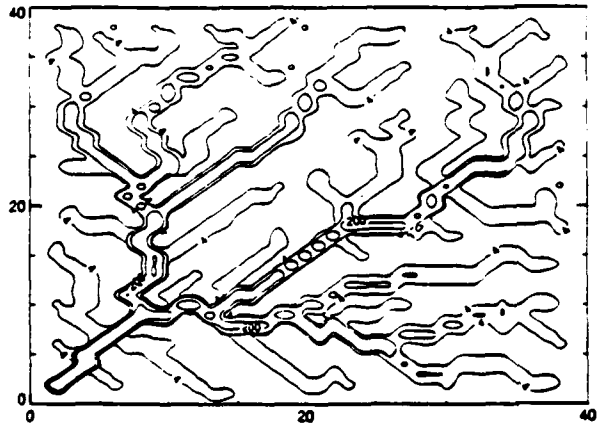

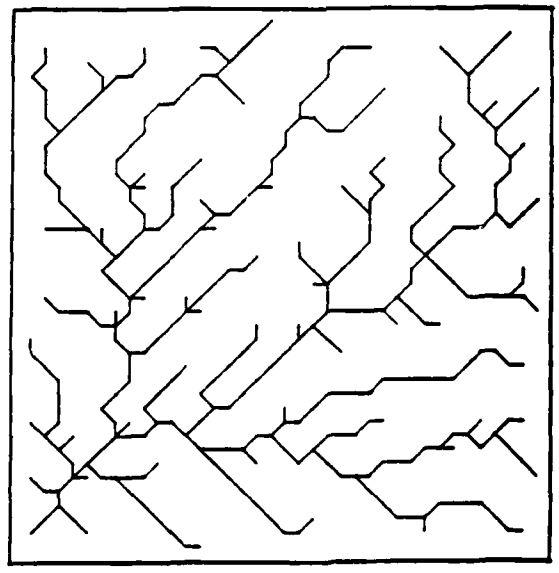

Figure 3-13: Contributing Area Spatial Distribution Timestep 7000

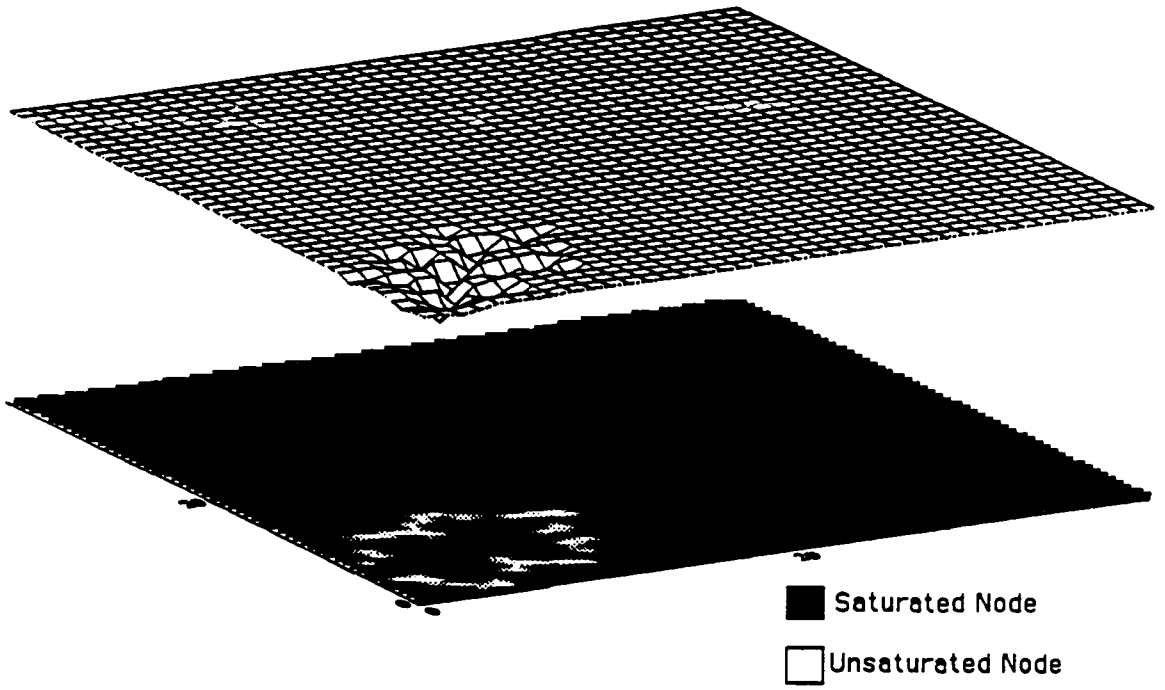

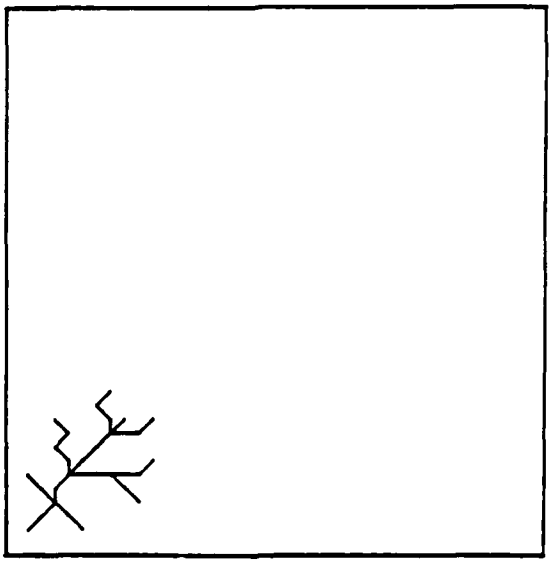

Figure 3-14: Saturated and Unsaturated Nodes Timestep 1000

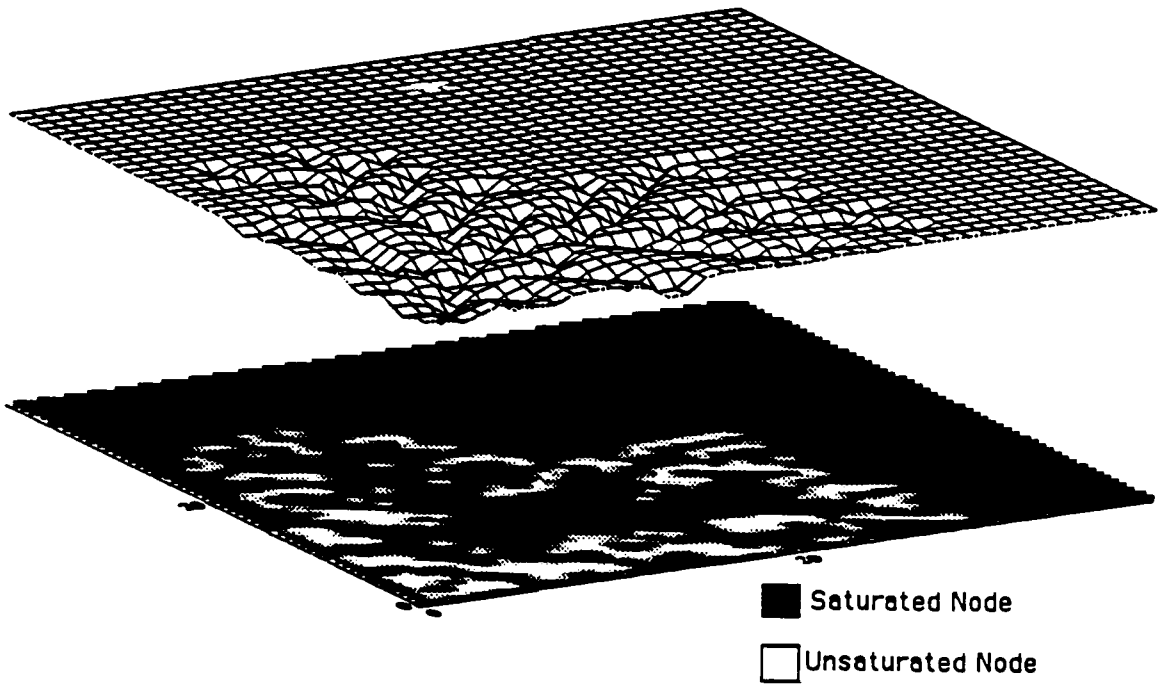

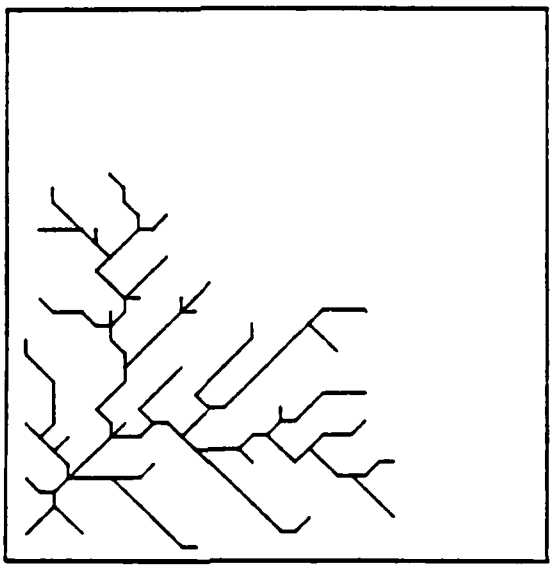

Figure 3-15: urated and Unsaturated Nodes Timestep 3000

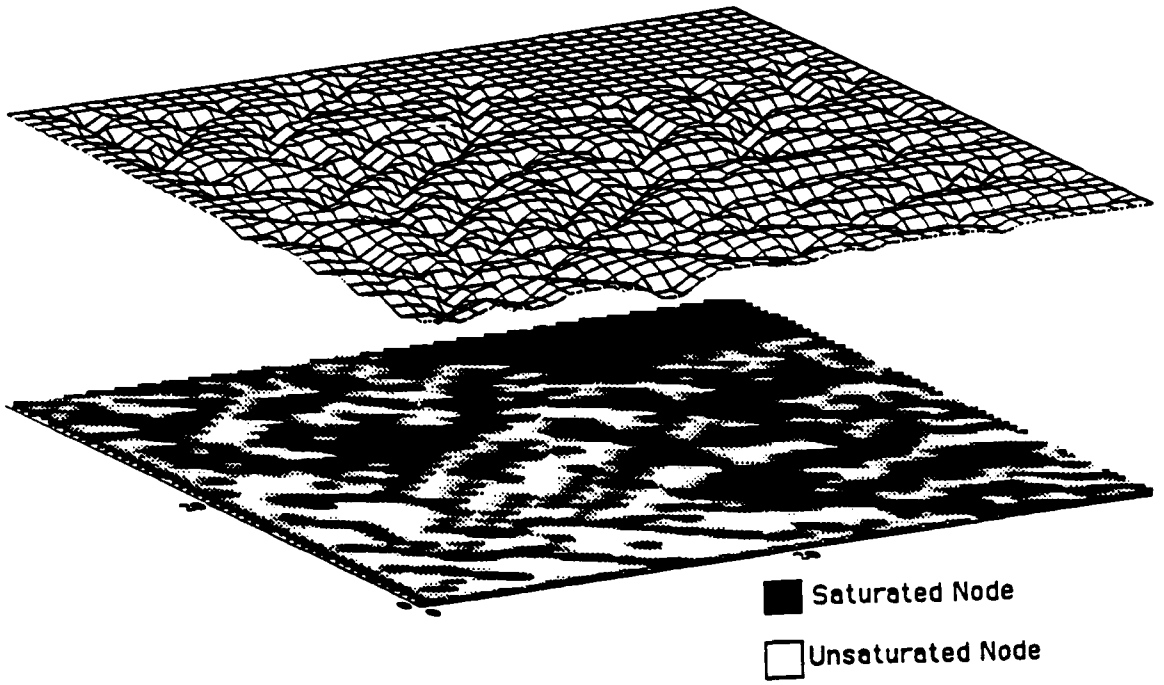

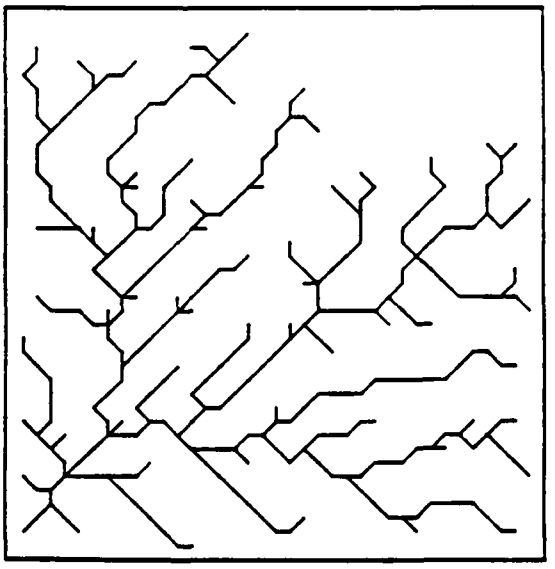

Figure 3-16: Saturated and Unsaturated Nodes Timestep 5000

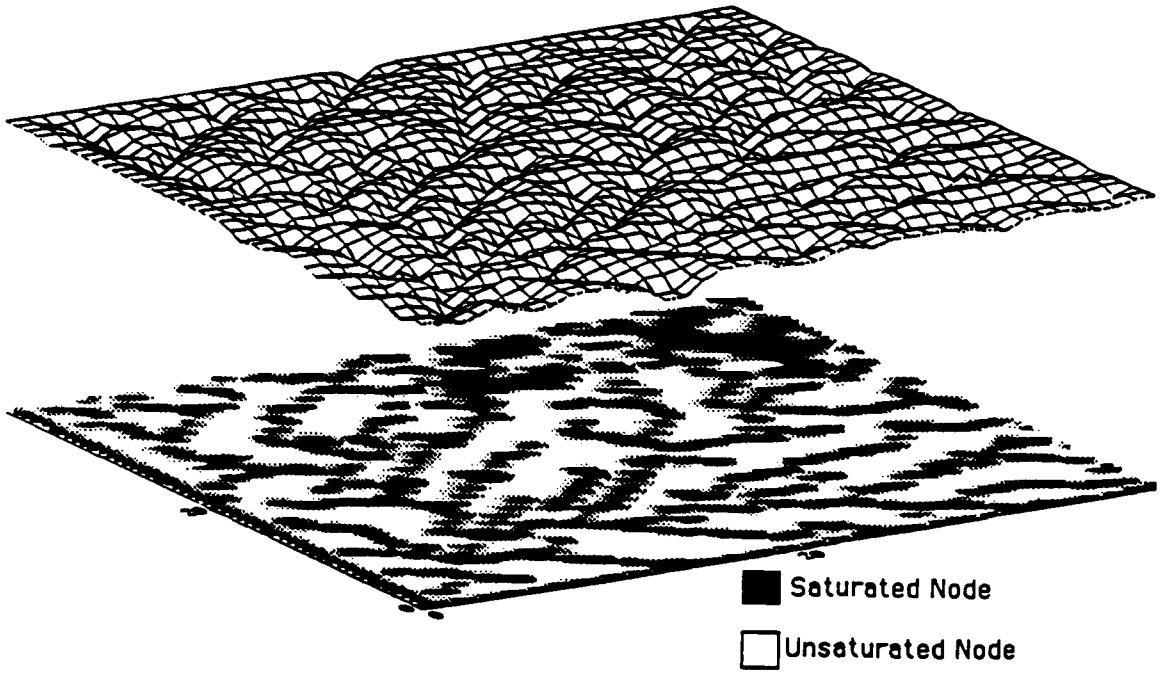

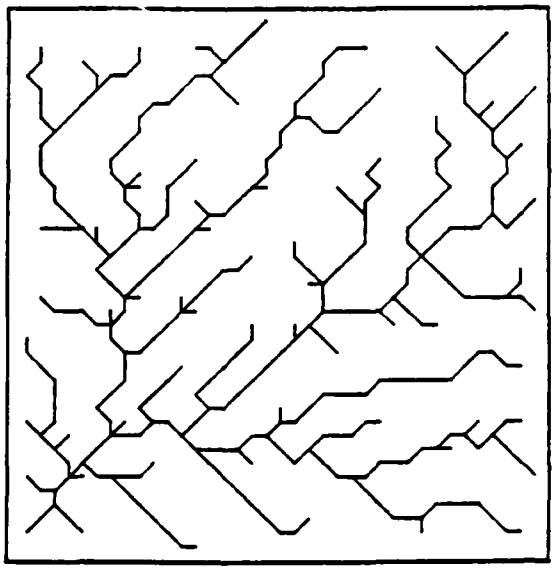

Figure 3-17: Saturated and Unsaturated Nodes Timestep 7000

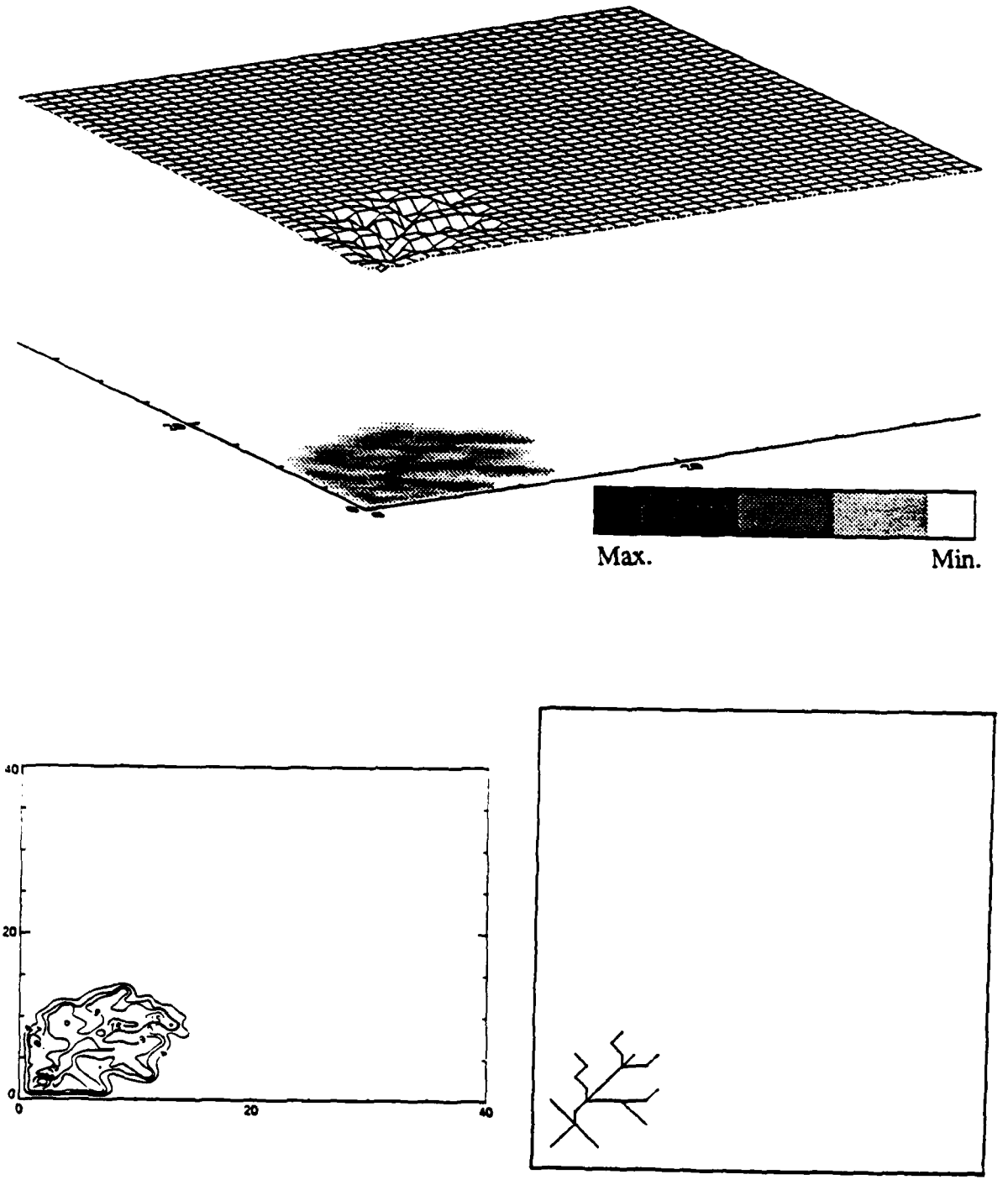

Figure 3-18: Channel Formation Function Spatial Distribution Timestep 1000

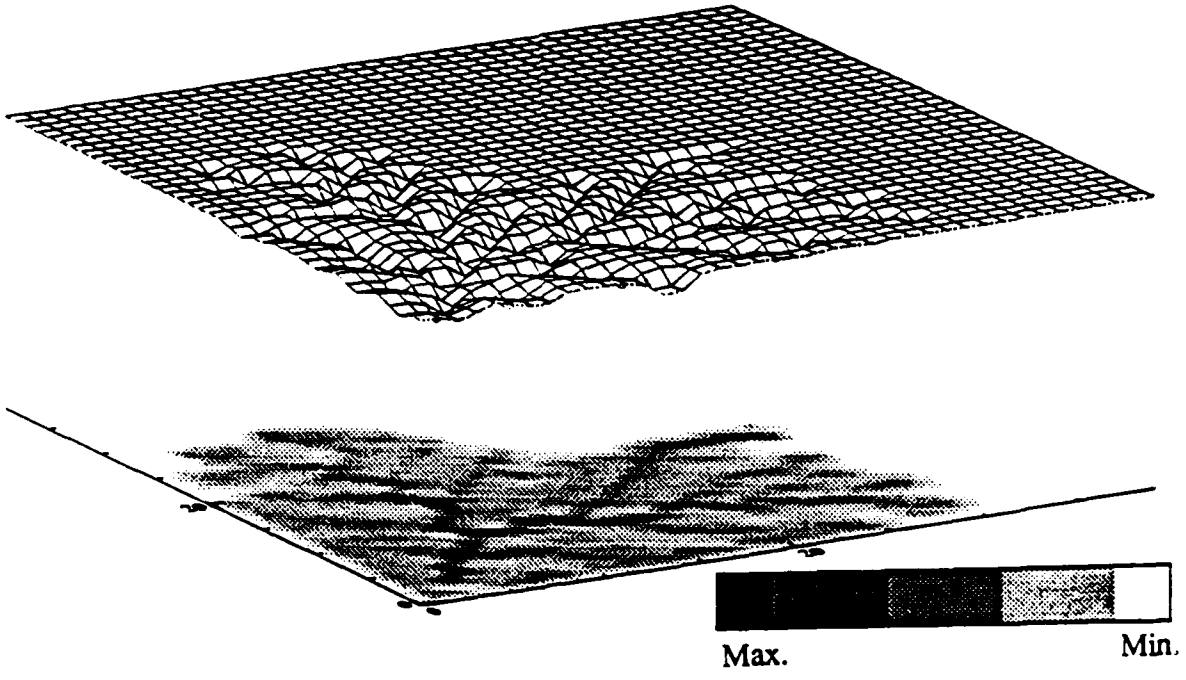

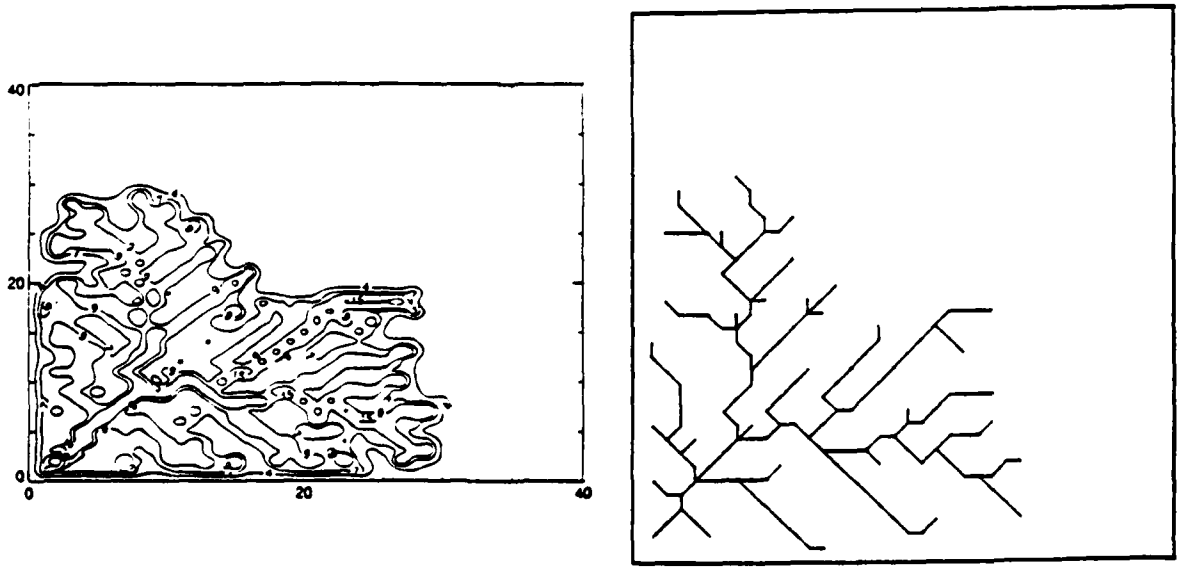

Figure 3-19: Channel Formation Function Spatial Distribution Timestep 3000

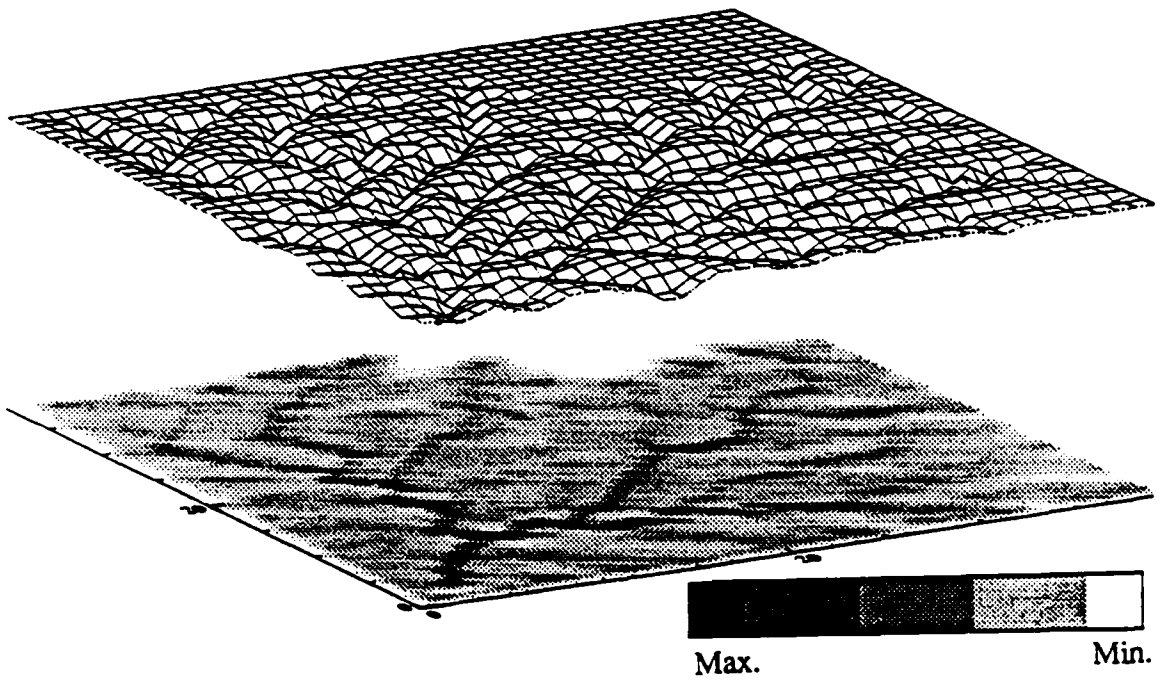

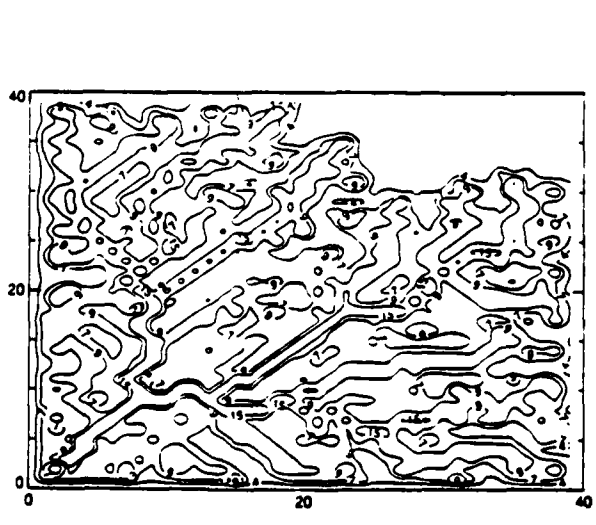

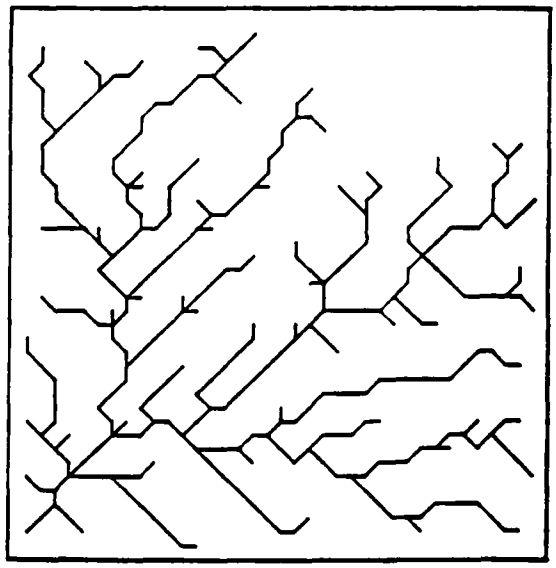

Figure 3-20: Channel Formation Function Spatial Distribution Timestep 5000

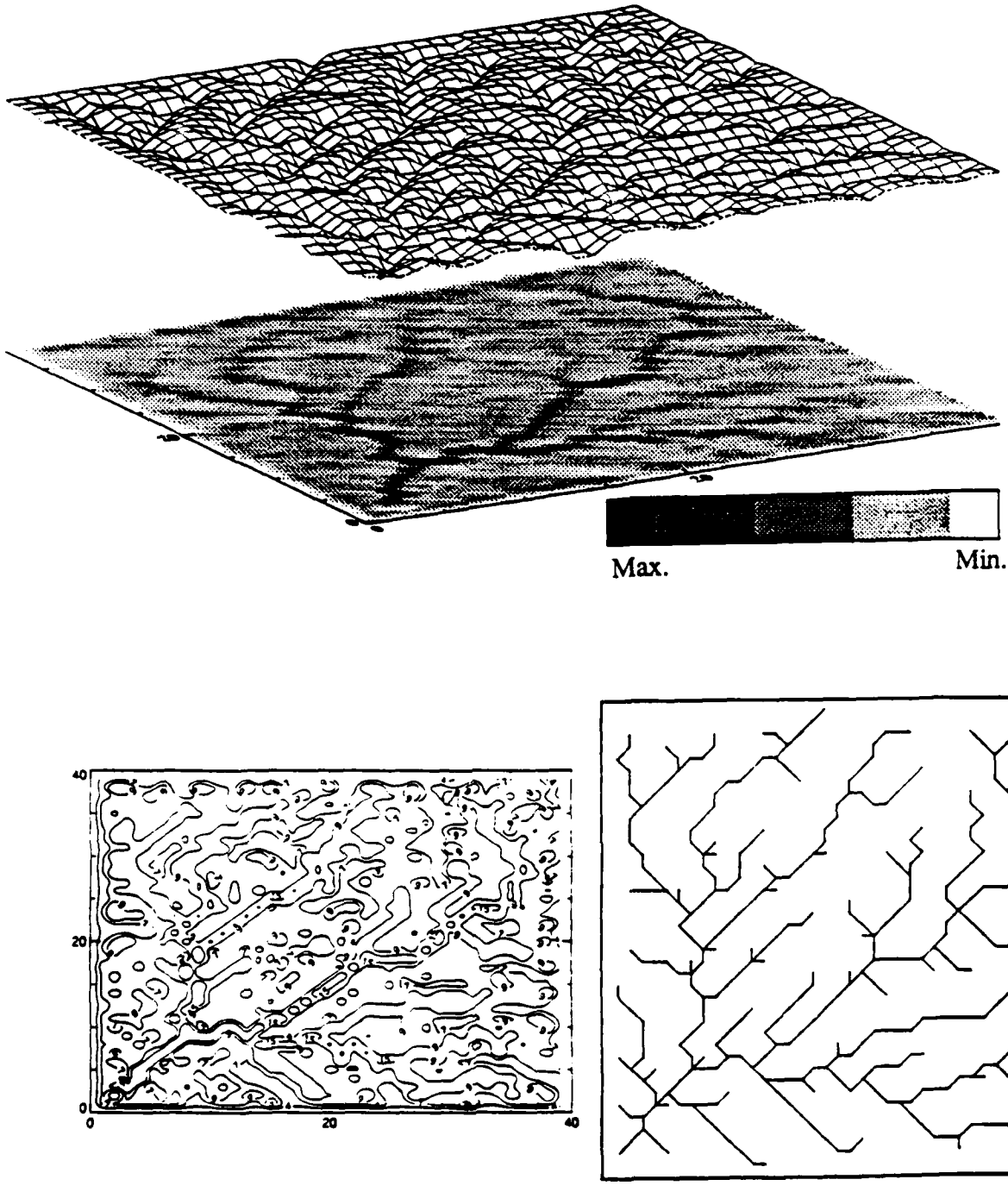

Figure 3-21: Channel Formation Function Spatial Distribution Timestep 7000

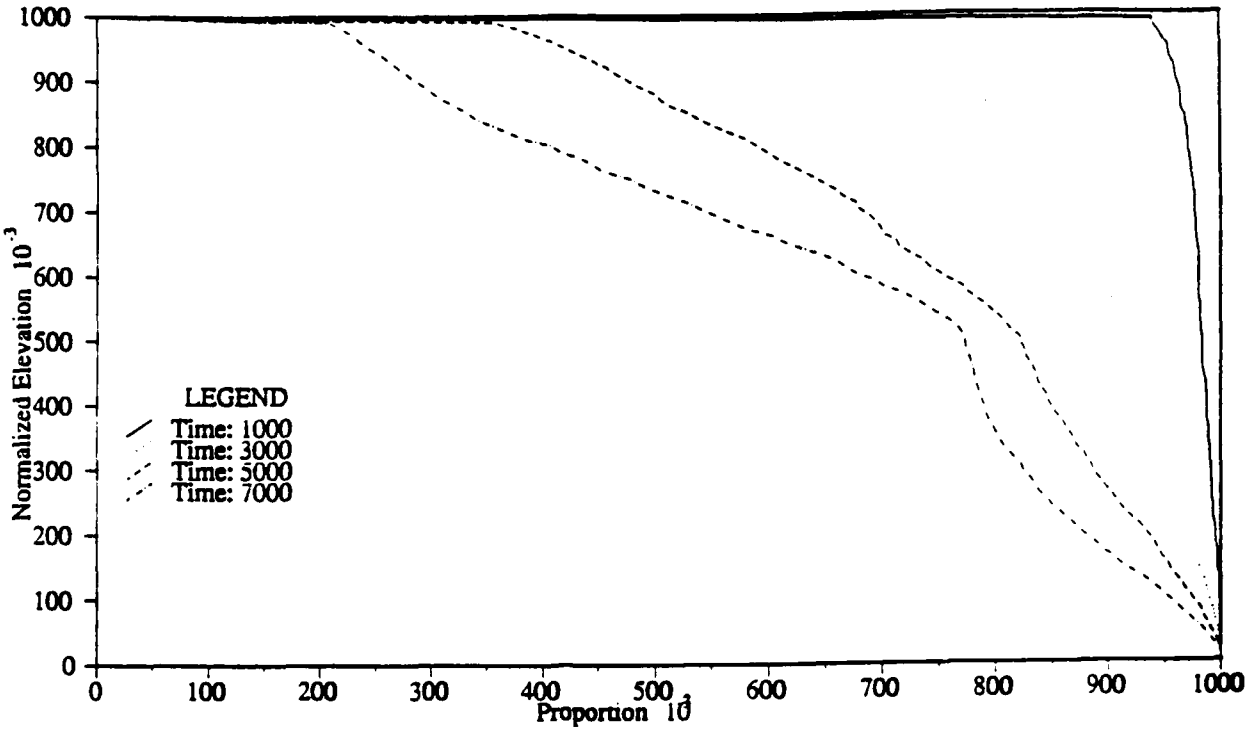

Figure 3-22: Hypsometric Curve Variation in Time

Statistic	Value
$R_b(1\text{-}2)$	5.08
$R_S(1\text{-}2)$	2.85
$R_L(1\text{-}2)$	2.60
$R_A(1\text{-}2)$	5.85
$R_b(2\text{-}3)$	4.00
$R_S(2\text{-}3)$	2.15
$R_L(2\text{-}3)$	1.82
$R_A(2\text{-}3)$	4.96
R_b	4.75
R_S	2.67
R_L	2.35
R_A	5.53
K	1.96
ε_1	2.67
D_d'	11.54
Magnitude	61
Mean Relief	9.90
Mean Stream Relief	3.12

Table 3-I: Final Network Statistic Values Simulation BR643SATU10

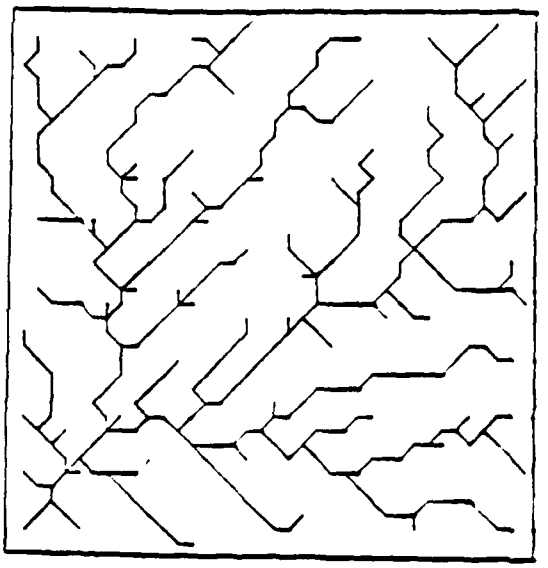

BR643SATU10

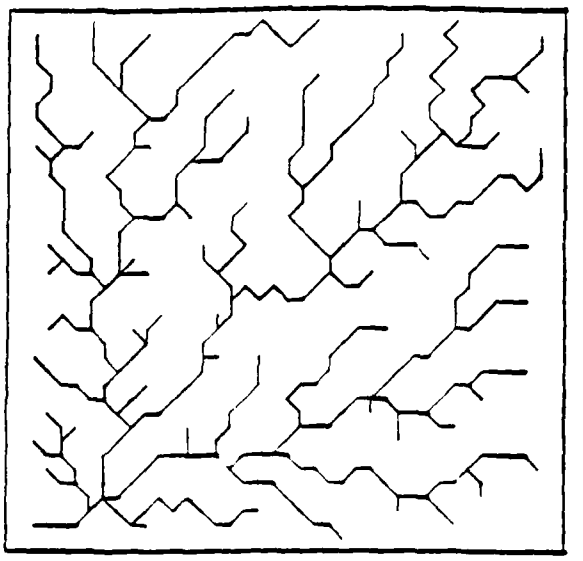

BR643SATU34

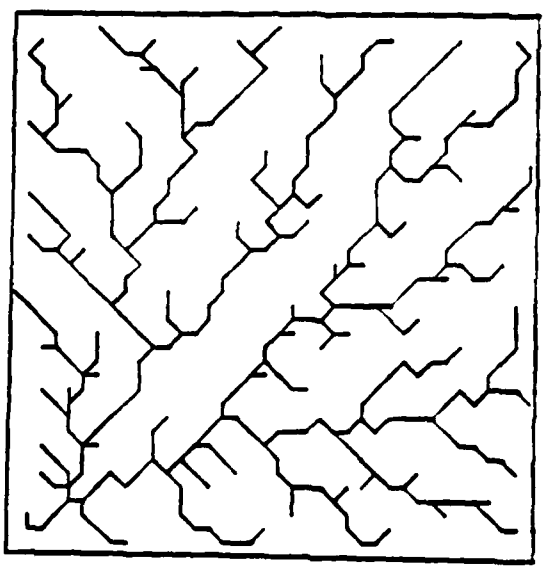

BR643SATU35

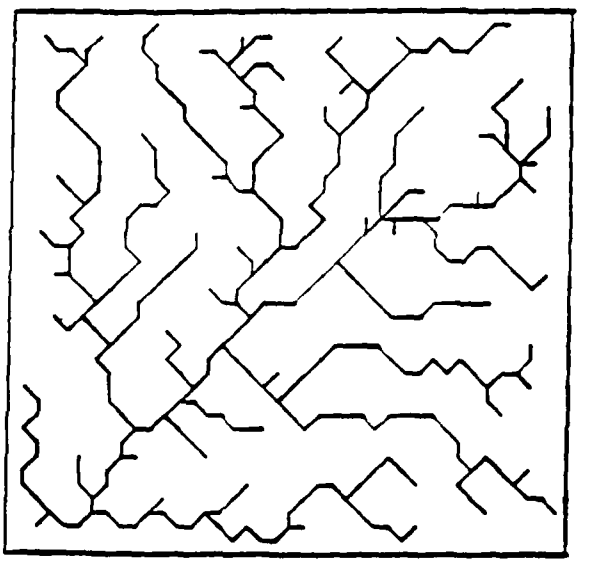

BR643SATU36

Figure 3-23: Final Catchments for Simulations with Different Initial Elevation Fields

each of these measures appears in Figures 3-24 to 3-31. These ratios were calculated between links of order 1 and 2 and between links of order 2 and 3 according to Strahler's ordering system. Notice that even though the values are within reasonable limits, a scatter of results is apparent.

Figures 3-32, 3-33 and 3-34 correspond to the time evolution of drainage density, magnitude and mean link lengths respectively. Notice how the variability in drainage density is much smaller than the variability of those measures based on topological variables.

Finally, Figure 3-35 shows the variation of the hypsometric curve with time. The variation of both the hypsometric curves and the drainage density for the different evolutions is relatively small. The advantage of these two measures is that they are physically rather than topologically based.

Chapter 4 will look in greater detail at this inherent variability of the catchment evolution model. This variability will be related to the concept of transient chaos and quantitative measures will illustrate this effect.

3.6 Hypsometric Curves for Cases with Continuous and Instantaneous Uplift

In this section the time evolution of the hypsometric curves for simulations BR643SATU10 and BR643SATU33 are studied. Both simulations have the same parameter values. The difference between them is in the way tectonic uplift is applied. In simulation BR643SATU10 the uplift is given as a single event at the beginning of the evolution while in simulation BR643SATU33 the tectonic input is a continuous, constant and uniformly distributed process in time. Figures 3-36 and 3-37 present the hypsometric curve evolutions for both cases. The jump at the upper part of the curves is an effect of the lower outlet elevation. With time, the elevation jump at the outlet corner is reduced because of the sediment transport, and a smoother field of elevations appears.

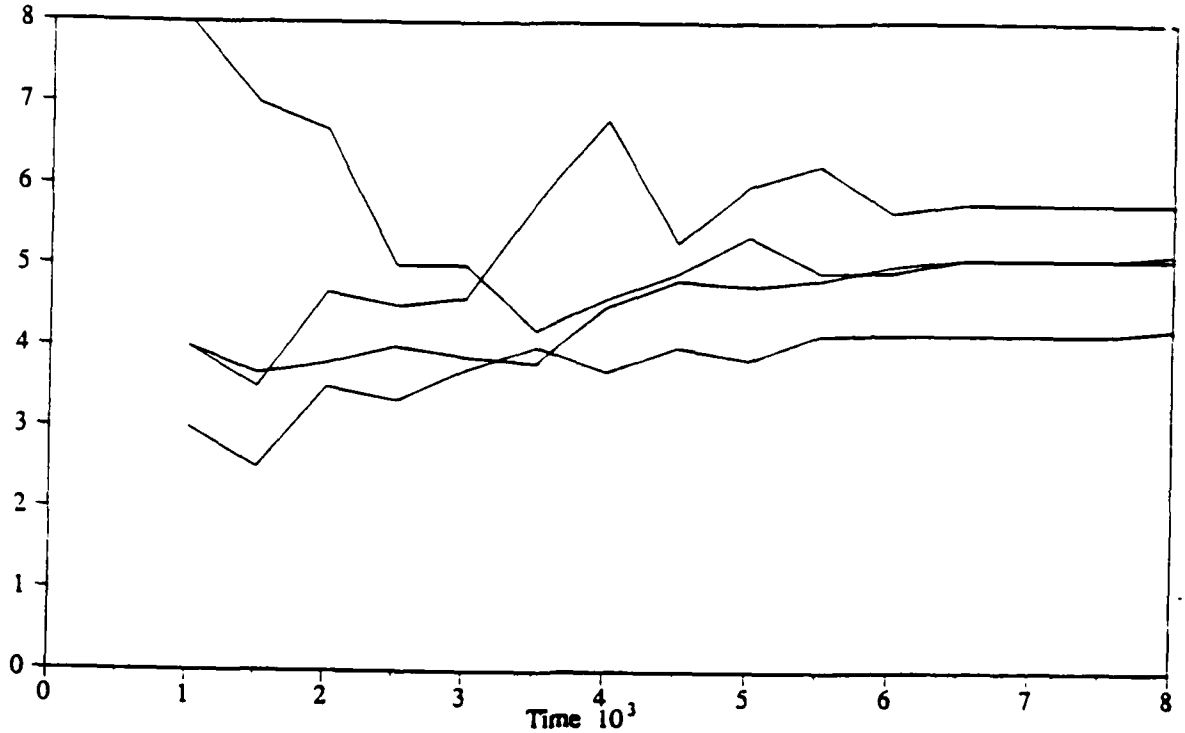

Figure 3-24: Strahler Bifurcation Ratio. Order 1-2

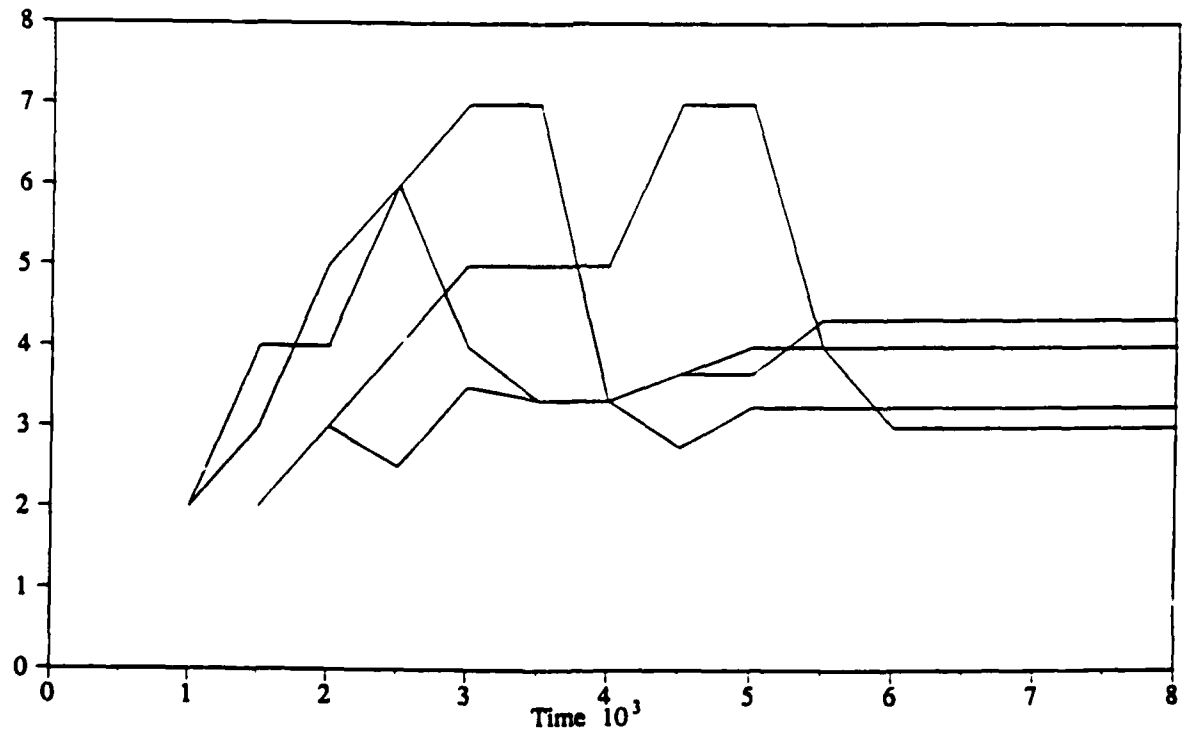

Figure 3-25: Strahler Bifurcation Ratio. Order 2-3

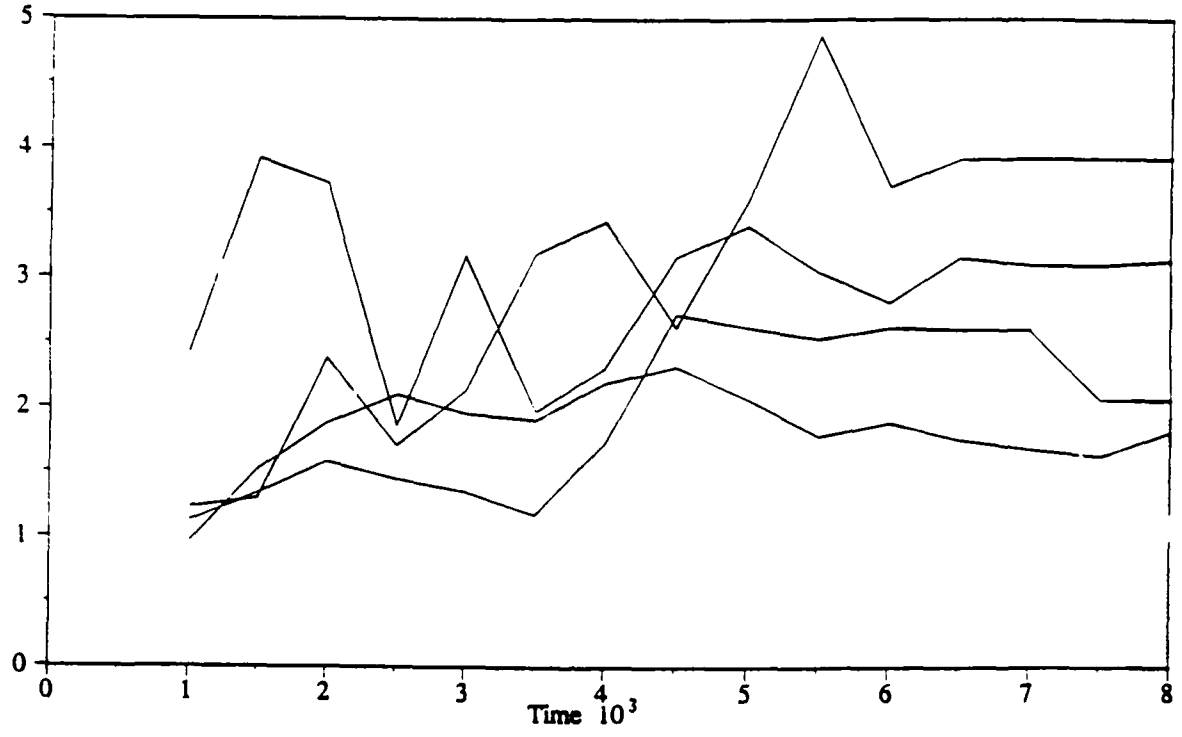

Figure 3-26: Strahler Length Ratio. Order 1-2

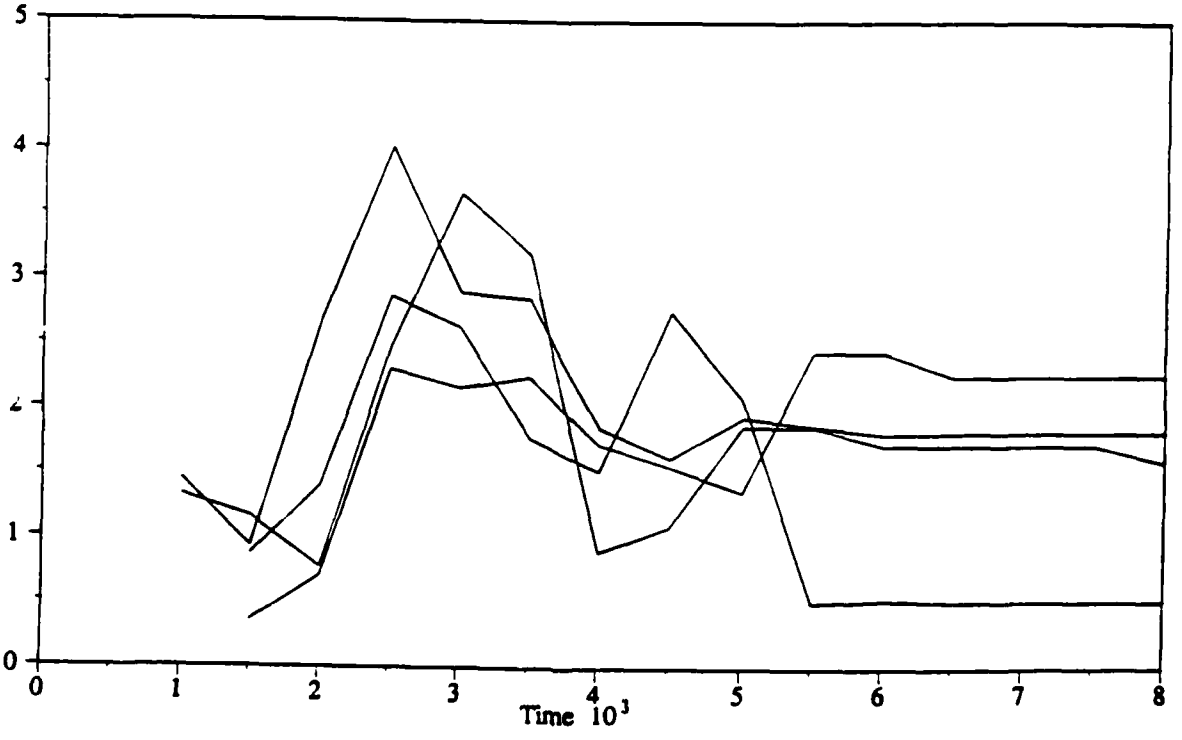

Figure 3-27: Strahler Length Ratio. Order 2-3

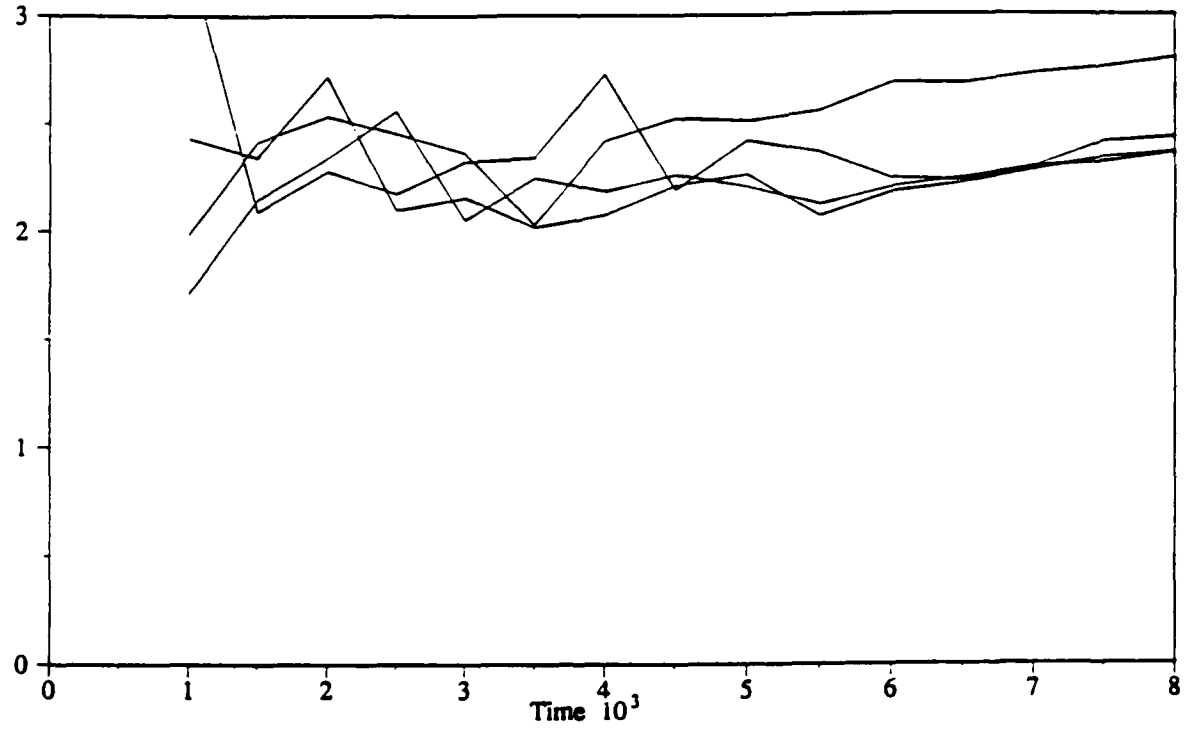

Figure 3-28: Strahler Slope Ratio. Order 1-2

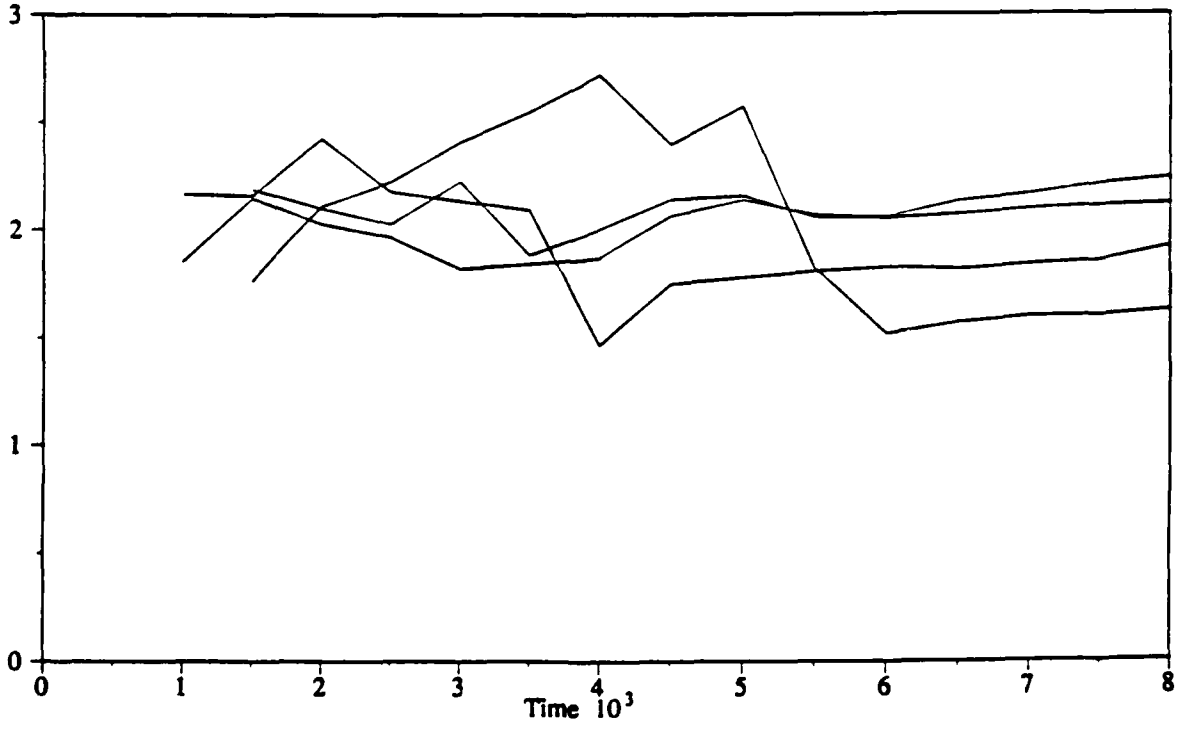

Figure 3-29: Strahler Slope Ratio. Order 2-3

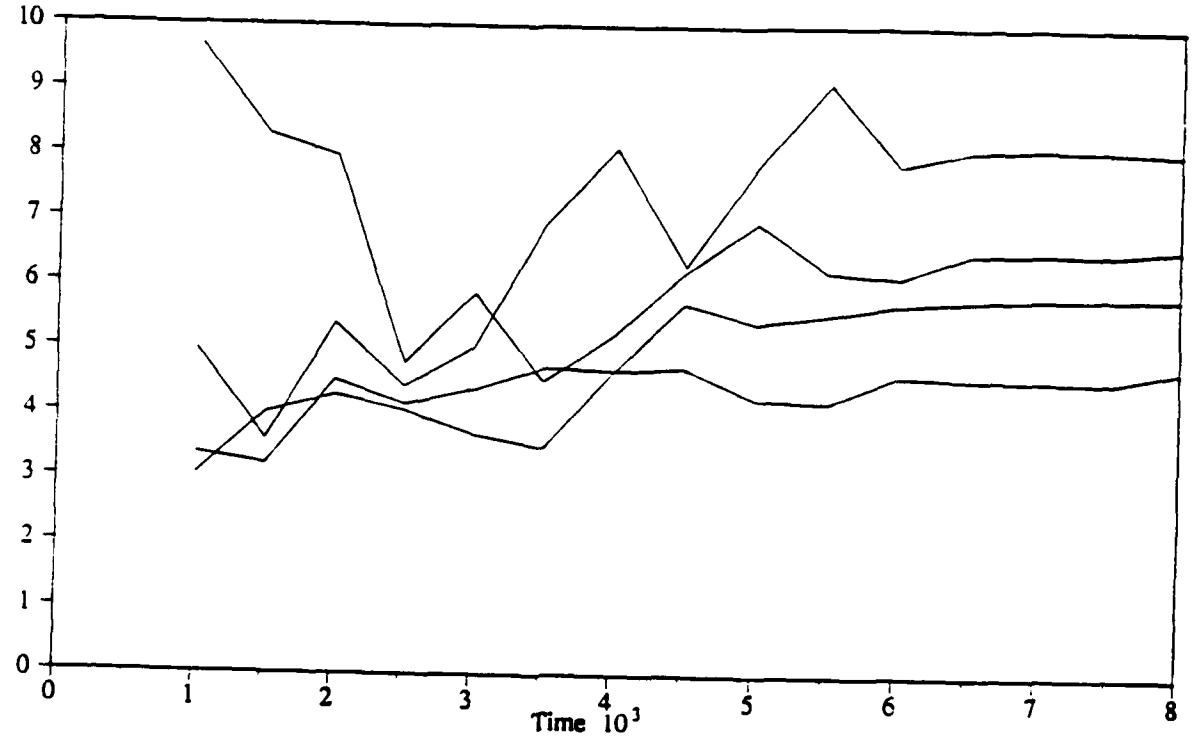

Figure 3-30: Strahler Area Ratio. Order 1-2

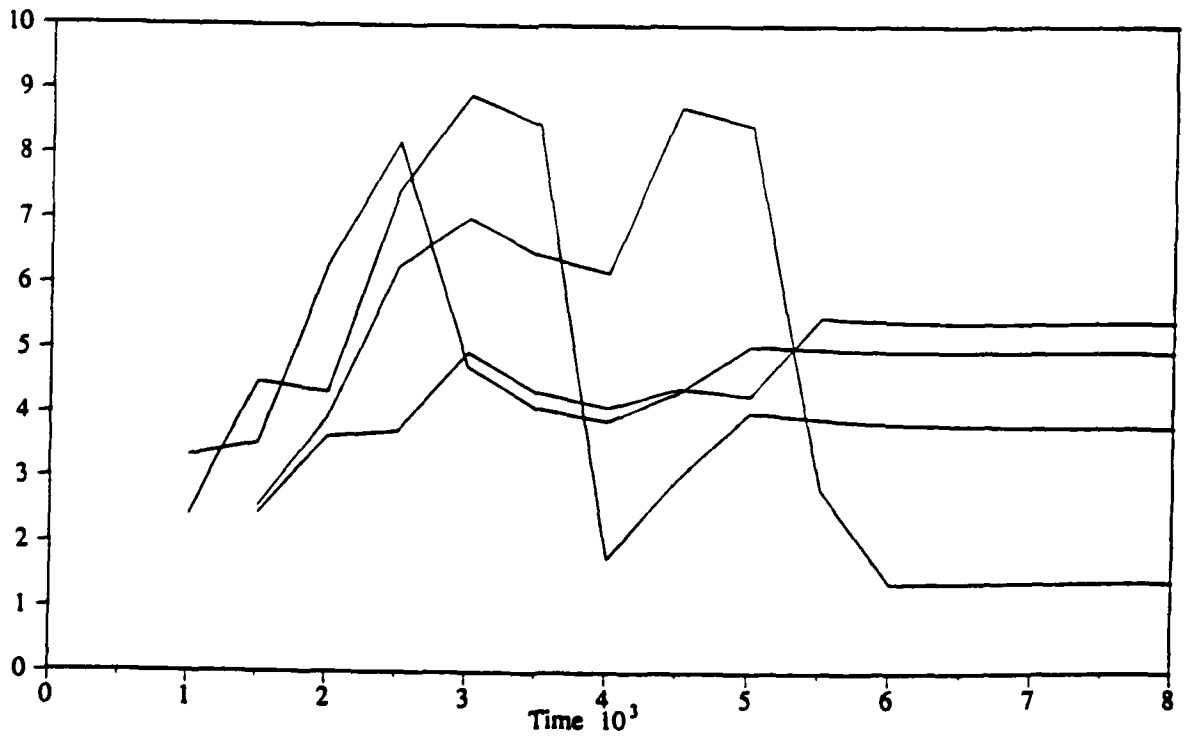

Figure 3-31: Strahler Area Ratio. Order 2-3

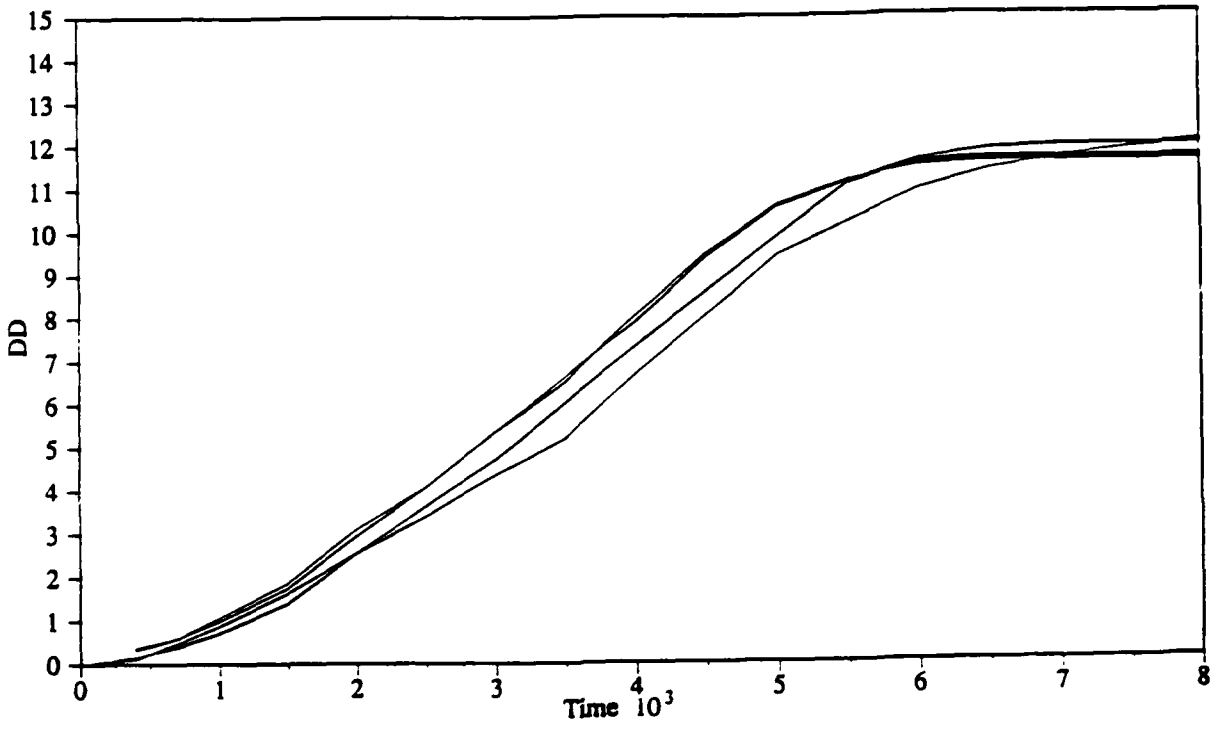

Figure 3-32: Time Evolution of Drainage Density

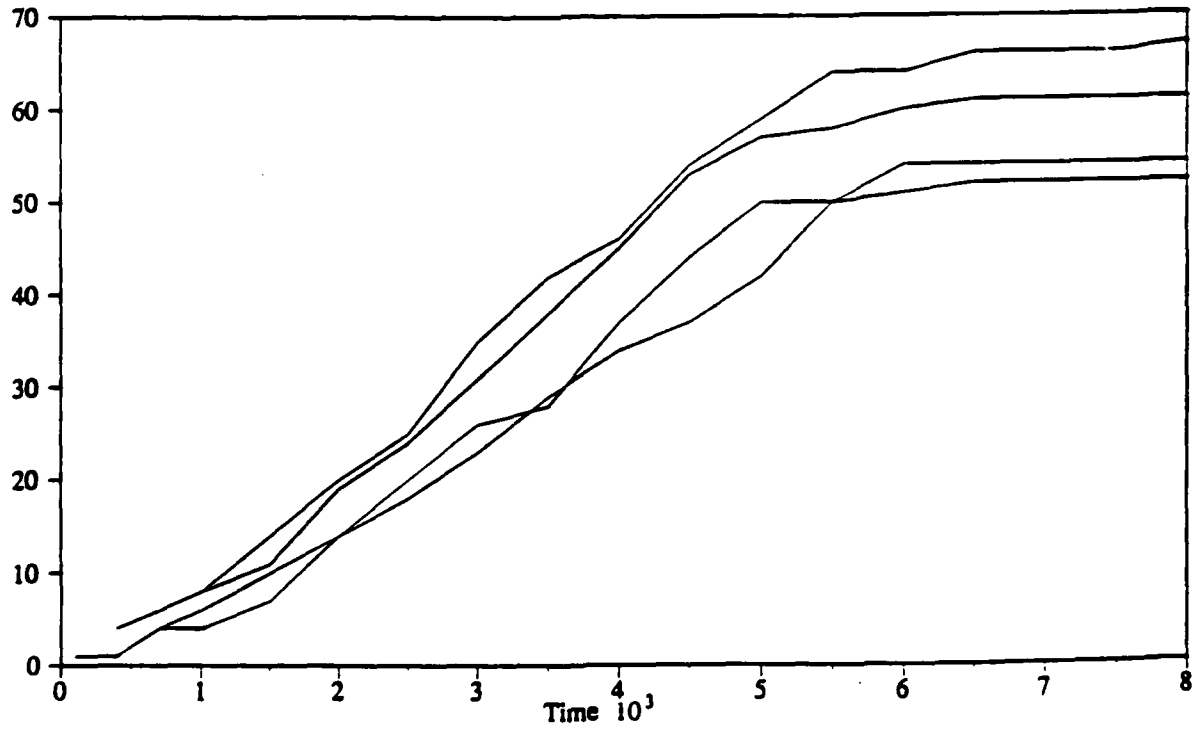

Figure 3-33: Time Evolution of Magnitude

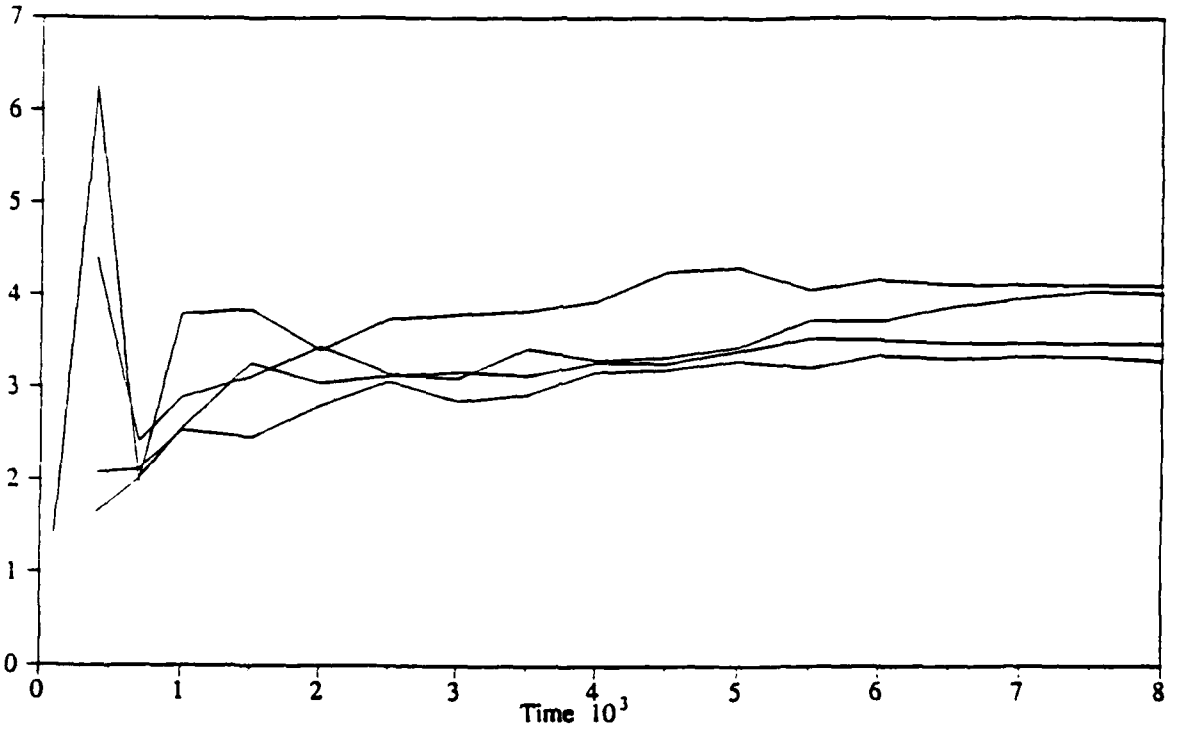

Figure 3-34: Time Evolution of Mean Link Length

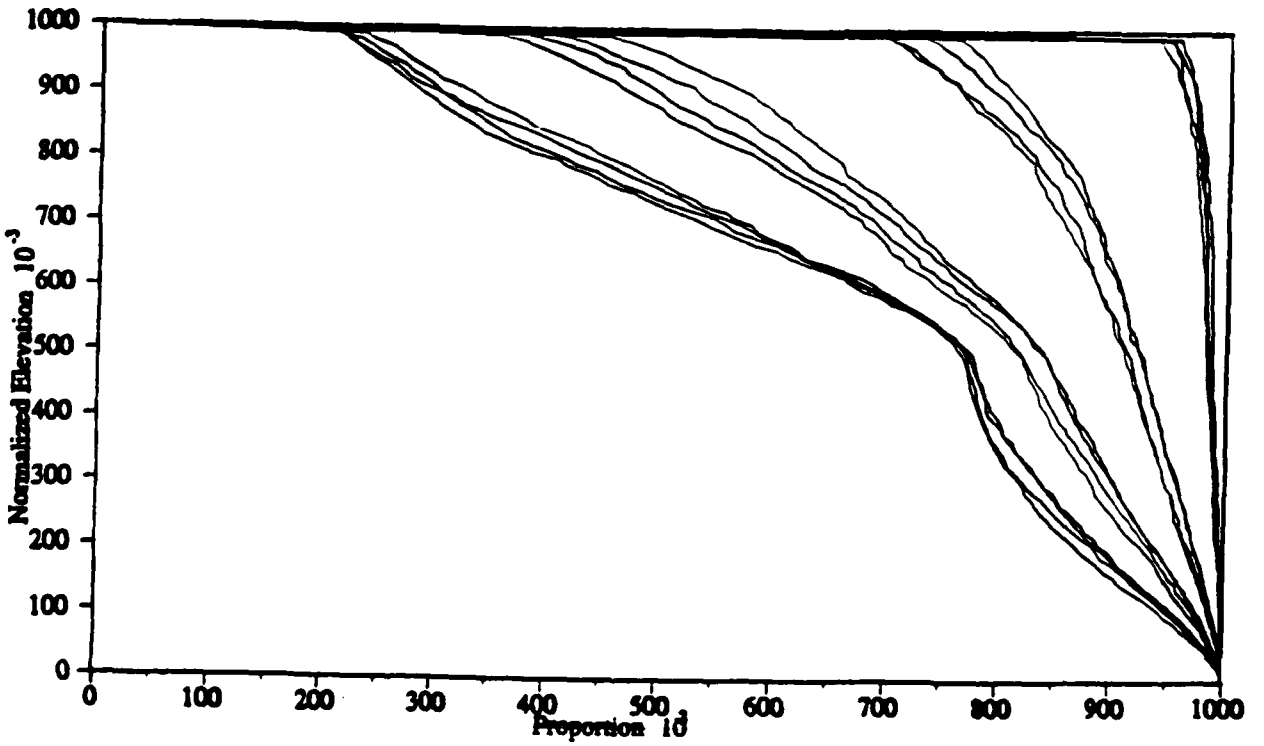

Figure 3-35: Time Evolution of Hypsometric Curve

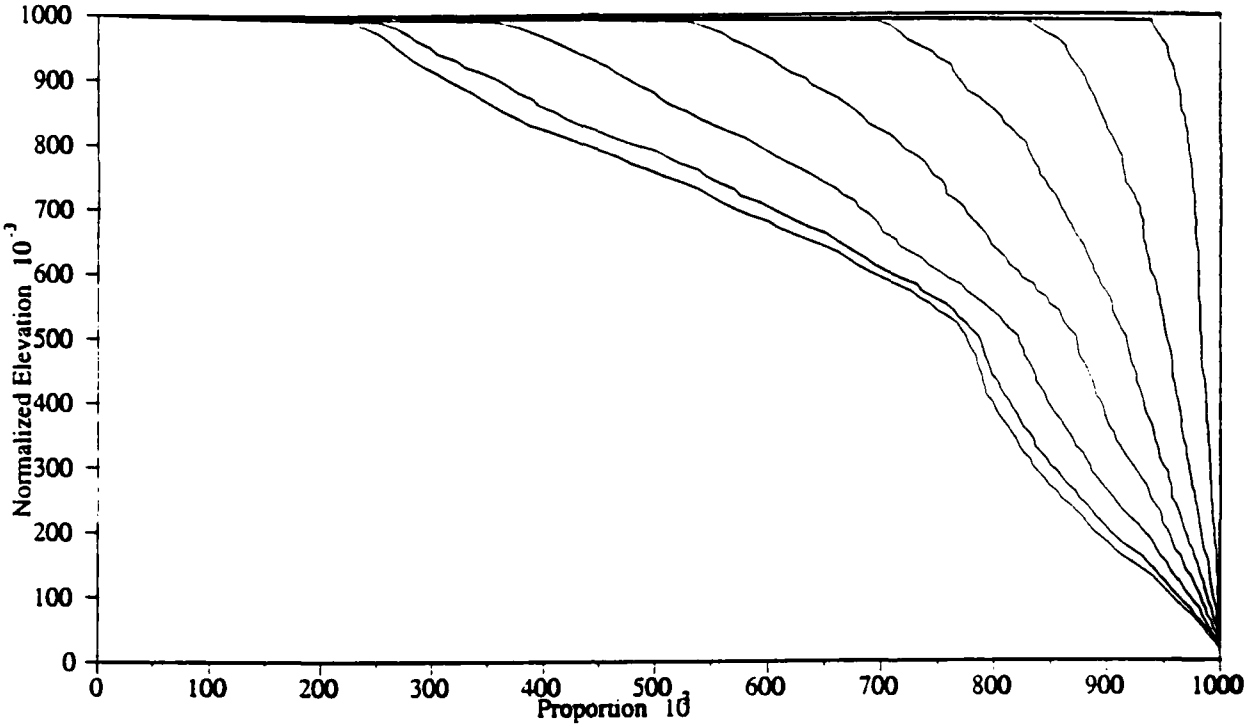

Figure 3-36: Hypsometric Curve Evolution.
Episodic Uplift Case 10

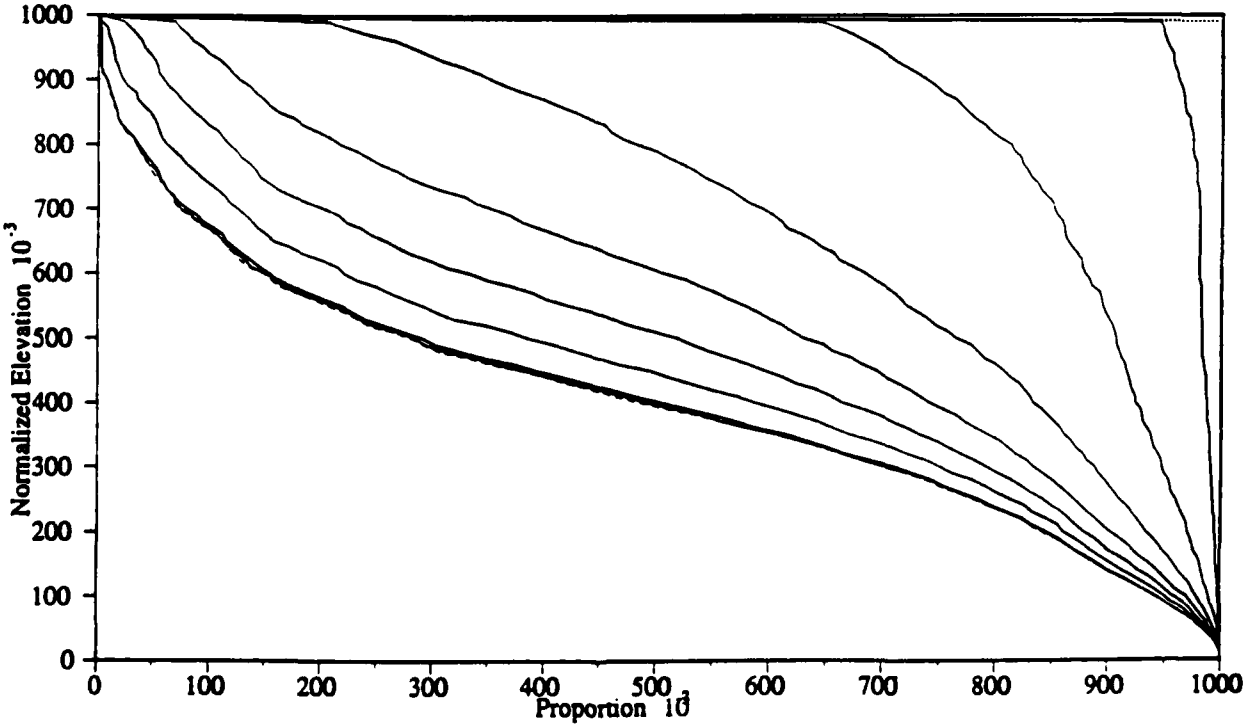

Figure 3-37: Hypsometric Curve Evolution.
Continuous Uplift Case 33

The case with continuous tectonic uplift tends to evolve into an S-shaped hypsometric curve. This form appears because the tectonic input is applied everywhere in the elevation field at the same rate. The erosion at hillslopes with high elevation is small because the subsurface saturation threshold reduces contributing overland flow. Therefore, those nodes with higher elevation in the catchment increase in their elevation while lower nodes decrease further in elevation to the point of dynamic equilibrium where the S-shape is attained. Notice, however, that the variable shown is normalized elevation.

The case with instantaneous tectonic uplift has a kink that is created because of the differences in sediment transport between saturated and unsaturated nodes. It will be seen in the next section how diffusive sediment transport processes have a major influence on the evolution of the hypsometric curves.

3.7 Influence of Diffusion in Simulations

The evolution equation (3.12) for elevation in the catchment evolution model has three components of which the two most important are the tectonic input and the fluvial sediment transport. The third component corresponds to diffusive processes like rainsplash and rockslide. Their effect is specially important on unsaturated hillslope nodes. While in the original WBR model overland flow occurred at every node, in its subsurface saturation modification there is no overland flow in unsaturated nodes. It is at those nodes where diffusive processes are the impotant mechanism for sediment transport.

Simulations BR643SATU10 and BR643SATU32 share the same parameter values except for the value of the diffusion coefficient D_z. In the first case $D_z=0$ while in the second case $D_z=3.5\text{x}10^{-5}$. Figure 3-38 shows the temporal evolution of the drainage density for both simulations.

Figure 3-39 corresponds to the hypsometric curves as time varies. Notice how in the

case with diffusion, hypsometric curves decrease faster because of the increased sediment transport that comes especially from unsaturated nodes. In contrast with the original WBR model where overland flow was present at every node and therefore the influence of diffusion was small, in the subsurface saturation modification the diffusive sediment transport processes have an interesting influence on the evolution of hypsometric curves. In those cases with D_z=0 nodes at high elevation do not erode as fast -or do not erode at all- as lower nodes that usually have larger contributing areas and smaller slopes which makes them susceptible to saturation. The presence of diffusion makes the difference in behavior between both sets of nodes smaller, smoothing out the kink that appears in the cases with no diffusion.

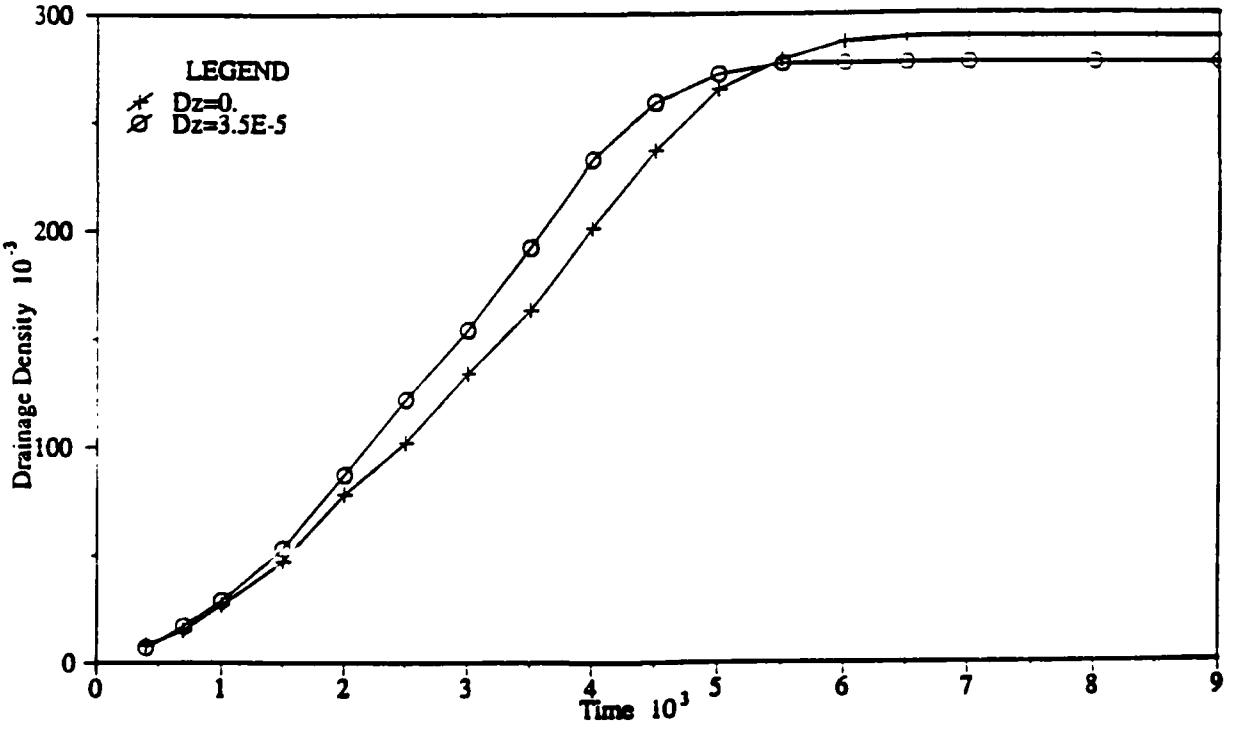

Figure 3-38: Drainage Density Evolution.
Cases 10 and 32

Despite the influence that diffusive processes have on the evolution of hypsometric curves, physically-based geomorphological measures do not differ very much in both cases, which reinforces the preference of these measures over the topologically based. Notice,

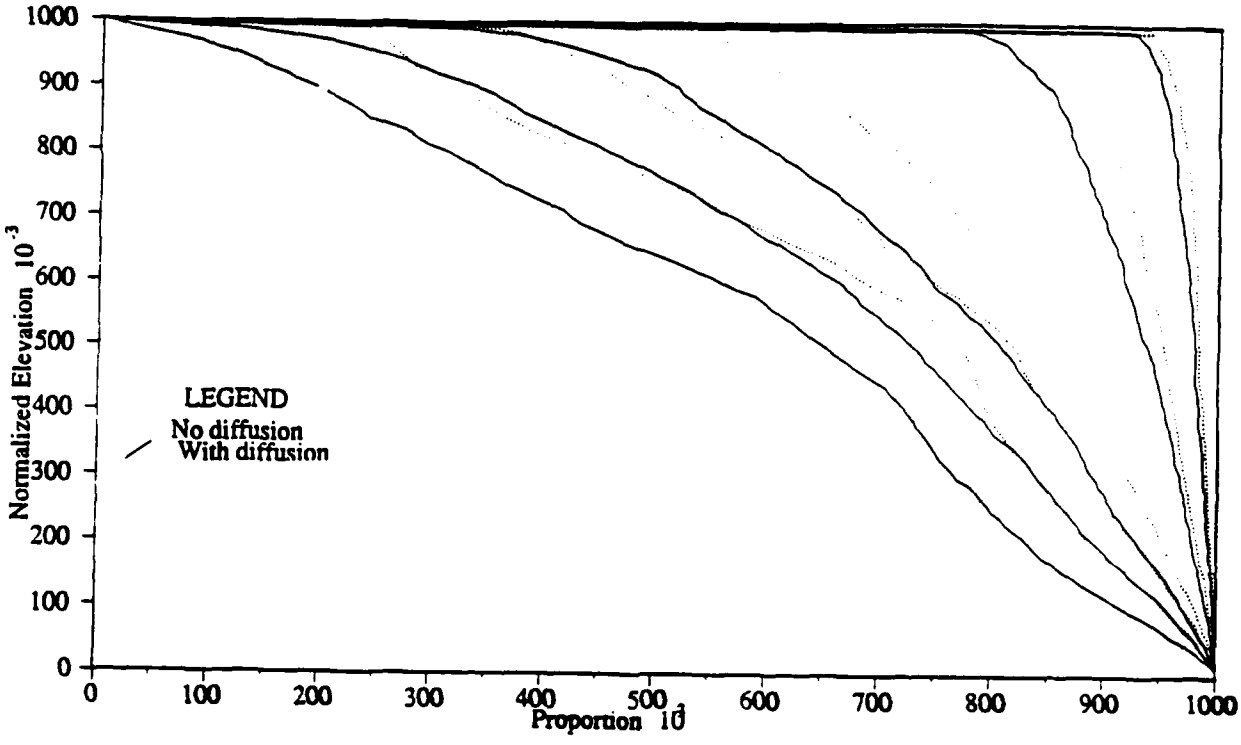

Figure 3-39: Hypsometric Curve Evolution.
Cases 10 and 32

however, that the form of the final networks is completely different; it also results in different values of topologically-based network measures. Figure 3-40 presents the form of the final networks. Chapter 4 will examine how small perturbations, in this case produced by a new sediment transport factor, can affect the entire catchment evolution.

3.8 Non-Dimensional Formulation of the Model

Given that the different parameters and variables of the model are strongly interconnected in the differential equations, in order to make thoughtful comparisons between basin evolutions in different points of the parameter space, a non-dimensional version of the model has to be defined. The basic idea is to combine parameters that work in the same phenomena and to generate lumped non-dimensional parameters. This section is mostly based on [47].

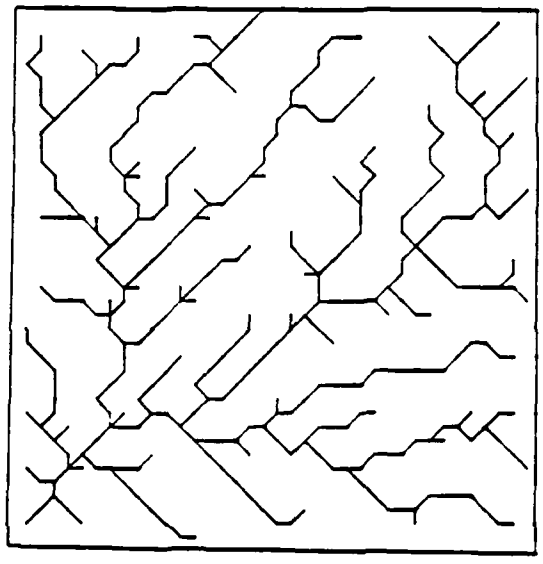

BR643SATU10

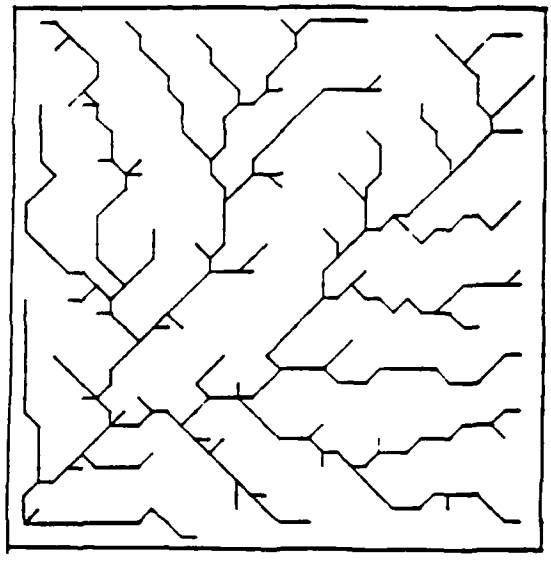

BR643SATU32

Figure 3-40: Final Networks.
Cases 10 and 32

The first step is to define the basic non-dimensional variables:

$$z' = \frac{z}{L_z} \tag{3.19}$$

$$x' = \frac{x}{L_x} \tag{3.20}$$

$$R' = \frac{T_R R}{L_R} \tag{3.21}$$

$$t' = \frac{t}{T} \tag{3.22}$$

where z', x', R' and t' are non-dimensional elevation, horizontal distance, runoff rate and time respectively. L_z, L_x, L_R, T_R and T are the corresponding scales in elevation, horizontal length, runoff depth, runoff time and catchment evolution time respectively. The expressions are self explanatory, except perhaps Equation (3.21) that comes from the assumption of uniform rainfall over the area, which in terms of the model implies $R=\beta_3$.

The second step is to define second-level variables of the model in this framework:

$$S' = \frac{L_x}{L_z} S \tag{3.23}$$

$$A' = \frac{1}{L_x^2} A$$

$$Q' = \frac{T_R}{L_x^2 L_R} Q \tag{3.24}$$

$$Q_s' = \frac{T_R^{m_1}}{L_z^{n_1} L_R^{m_1} \overline{\beta}_1 L_x^{2m_1 - n_1}} Q_s \tag{3.25}$$

$$a' = \frac{T_R^{m_5}}{L_z^{n_5} L_R^{m_5} \overline{\beta}_5 L_x^{2m_5 - n_5}} a \tag{3.26}$$

$$f'(Y) = \frac{f(Y)}{\overline{\beta}_1} \tag{3.27}$$

$$D' = \frac{T_R}{L_x^2 L_R} D \tag{3.28}$$

$$T_c' = \frac{T_R}{\bar{\alpha}_2 L_R} T_c \tag{3.29}$$

where $S', A', Q_s', a', f'(Y)$ and T_c' are the nondimensional expressions of the analogous variables in the model. The only factors in the above expressions that remain to be defined are:

$$\beta_1'(x,y) = \frac{\beta_1(x,y)}{\bar{\beta}_1} \tag{3.30}$$

$$\beta_5'(x,y) = \frac{\beta_5(x,y)}{\bar{\beta}_5} \tag{3.31}$$

$$\alpha_2'(x,y) = \frac{\alpha_2(x,y)}{\bar{\alpha}_2} \tag{3.32}$$

$$C_0'(x,y) = \frac{C_0(x,y)}{\bar{C}_0} \tag{3.33}$$

The Equations (3.30) to (3.33) express the fact that β_1, β_5, α_2 and C_0 may vary in space. Therefore, they are defined in terms of a mean scale for each variable. This scale cannot be related to the basic non-dimensional variables because they correspond to different processes: β_1 and β_5 to details of the sediment transport phenomena like particle size; c_0 to the tectonic uplift process; and α_2 to hydraulic conductivity decrease in the soil.

The last step in the process is to lump the original parameters in order to form the non-dimensional parameters. The way the original parameters are combined comes from the specific form of the equations. The non-dimensionalized governing equations are now:

$$\frac{\partial z_i'}{\partial t'} = \mathbf{TT}\, C_{0_i}' + \mathbf{TS} \sum_j Q_{s_j}' I_{ji} + \mathbf{TD}\, D_z L_g \frac{\partial^2 z_i'}{\partial x_j'^2} \tag{3.34}$$

$$\frac{\partial Y_i}{\partial t'} = \mathbf{TC}\left[0.0025\mathbf{TA}\, a_i' + \left(-0.1Y_i + \frac{Y_i^2}{1+9Y_i^2}\right)\right] \tag{3.35}$$

which together with the non-dimensional subsurface saturation criteria and the definitions of second-level variables (Q,a,Q_s and D) forms the model. The saturation criteria in non-dimensional form is:

$$\mathbf{TSC}\, T_c' < \frac{A'}{S'} \tag{3.36}$$

TT,**TS**, **TD**, **TC**, **TA** and **TSC** are the nondimensional tectonic uplift, sediment transport, diffusion, channelization rate, channel formation function and saturation criteria numbers respectively. Their definitions follow from the model equations and are now presented:

$$\mathbf{TT} = \frac{T\bar{C}_0}{L_z} \tag{3.37}$$

$$\mathbf{TS} = \frac{T L_x^{2m_1-n_1} L_z^{n_1-1} L_R^{m_1} \bar{\beta}_1}{L_g^2 T_R^{m_1} \rho_s (1-n)} \tag{3.38}$$

$$\mathbf{TD} = \frac{L_g T D_z}{L_x^2} \tag{3.39}$$

$$\mathbf{TC} = T d_t \tag{3.40}$$

$$\mathbf{TA} = \frac{L_z^{n_5} L_x^{2m_5-n_5} L_R^{m_5} c_1 \bar{\beta}_5}{T_R^{m_5}} \tag{3.41}$$

$$\mathbf{TSC} = \frac{\bar{\alpha}_2 L_x^3 T_R}{\nu_R L_z} \tag{3.42}$$

Based on these non-dimensional numbers, comparisons can be made between catchment evolutions. When two catchments have identical nondimensional parameters as well as identical distributions of nondimensional catchment properties like discharge Q', sediment transport $f'(Y)$, elevation z' and tectonics C'_0, they can be considered physically similar.

Willgoose et al. [47] present two definitions of non-dimensional numbers. The definitions presented before correspond to transient conditions. There are analogous expressions for catchments in dynamic equilibrium.

3.9 Influence of TSC in the Catchment Evolution

The value of the threshold that determines whether a node is saturated or not has important implications on the overall behavior of the system. The value of TC (and in a broader sense the value of **TSC**) affects the amount of overland flow that is distributed to the nodes. In this section three different simulations with varying values of TSC will be shown. The cases to be presented are BR643SATU10, 38 and 39 which have values of **TSC** equal to 0.92×10^3, 4.6×10^3 and 0.28×10^3 respectively. All the other parameter values are the same. Figures 3-41 to 3-43 show an isometric view of the catchment once the network stops growing, a contour of elevations and the final network.

With decreasing values of **TSC**, a larger number of grid nodes enter into the saturated group where overland flow and fluvial sediment transport is produced. An increase of overland flow production produces a higher value of channel formation function, triggering the growth of new channels as can be seen by comparing Figures 3-42 and 3-41. Channel valleys are wider in case 39 compared with case 10 because of the increased fluvial transport in hillslope nodes surrounding channels.

If the value of TSC is small enough, then all the nodes would be saturated and the behavior of the modified model would be identical to the original WBR model. Finally, it should be noticed that it is the difference in overland flow distribution, produced by the saturation deficits, that makes analytical calculations more difficult in the subsurface saturation case compared to the original model.

3.10 Analysis of Geomorphological Relationships in Simulated Catchments

In this section a series of hypotheses and relationships that have been studied and tested in real basins will be examined in the final catchments generated by the subsurface modification to the WBR model.

The relationships studied are: the hypothesis of area-slope renormalization in channels and the possibility of using analysis of this kind to distinguish channels from hillslopes in digital elevation maps; statistical properties of link lengths and contributing areas; and the behavior of some fundamental scales of the catchment.

3.10.1 Area-Slope Renormalization

Flint [9] found empirically that slopes and channels scale. He found a relationship between area A and slope S of the form:

$$S = CA^{-\theta} \tag{3.43}$$

with θ ranging from 0.37 to 0.83 with a mean of 0.6. Recently, Tarboton [44] also found that this scaling relationship holds between areas and slopes in catchments using digital elevation maps. The scaling relation was tested for simulations with the WBR model in [47] and an excellent fit was found in catchments at dynamic equilibrium.

In this subsection simulations using the subsurface saturation modification are examined. Figure 3-44 shows the data points of area and slope for channelized nodes. The simulation case under consideration was BR643SATU33 at dynamic equilibrium.

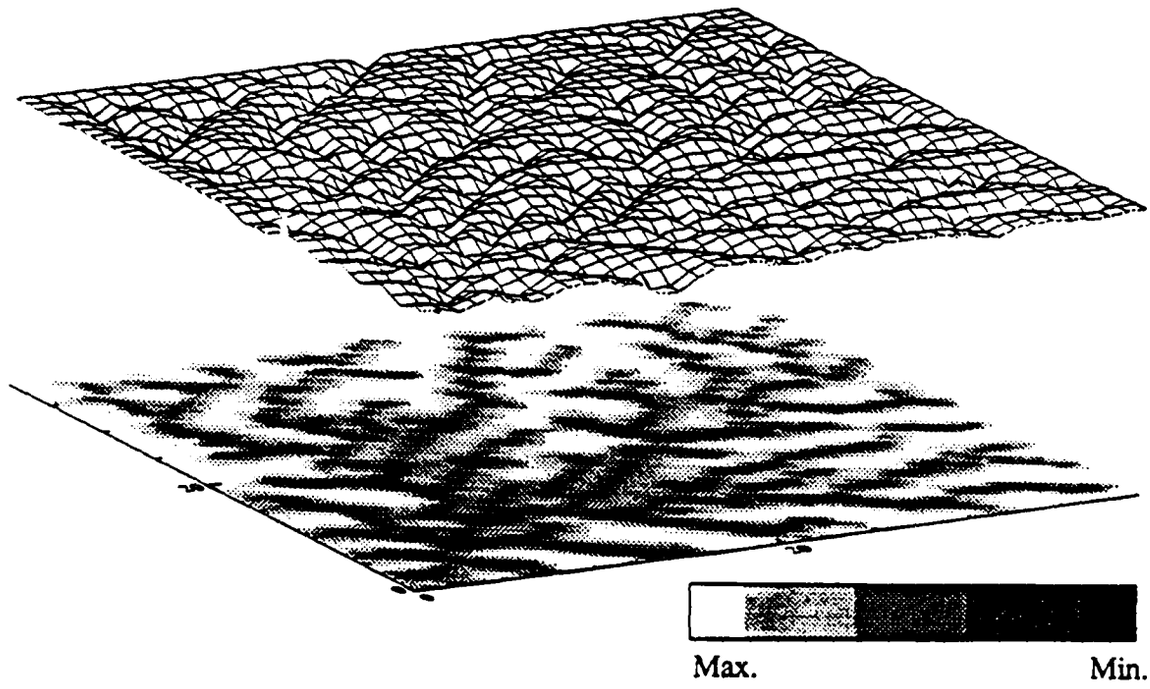

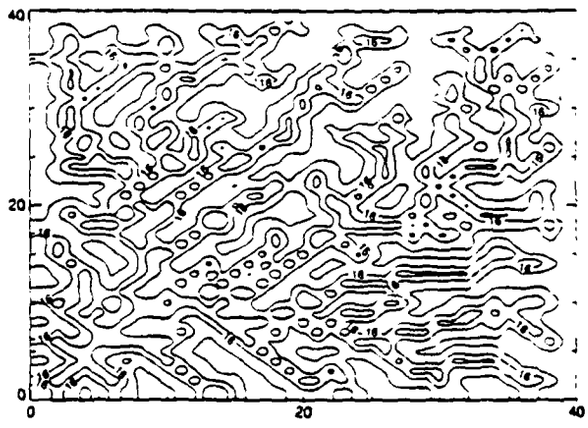

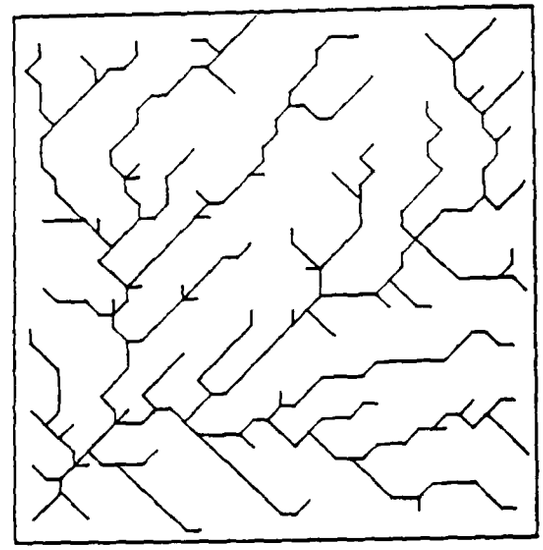

Figure 3-41: Elevation Spatial Distribution. Case 10

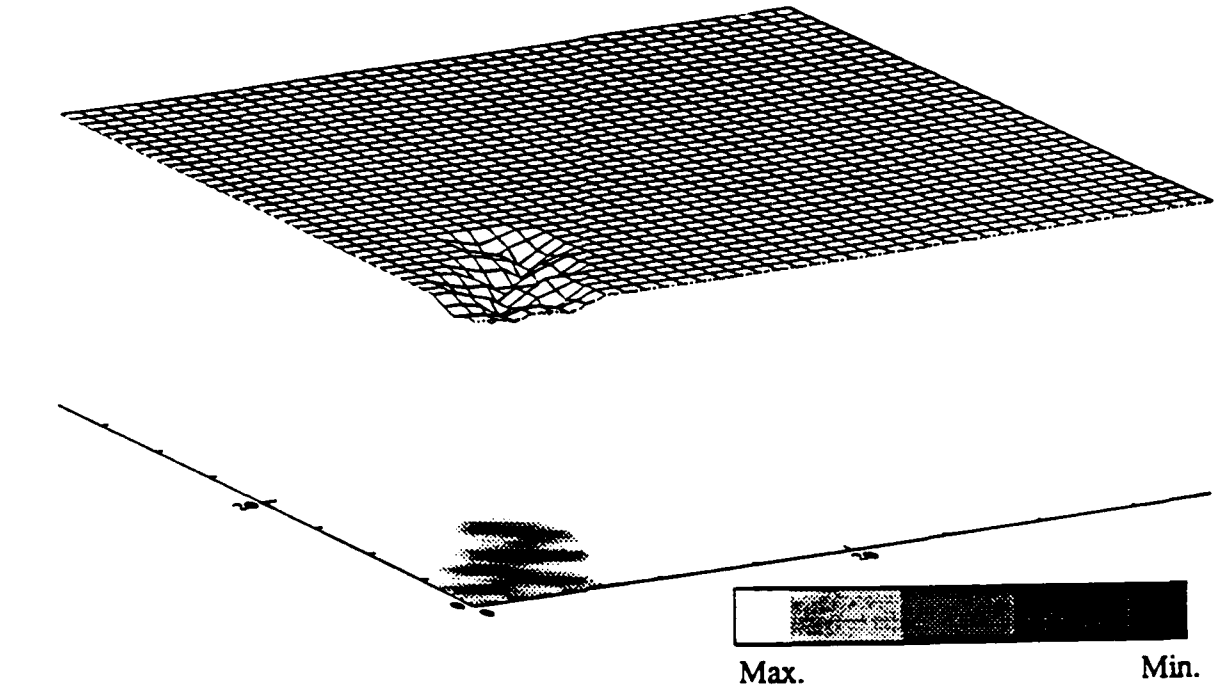

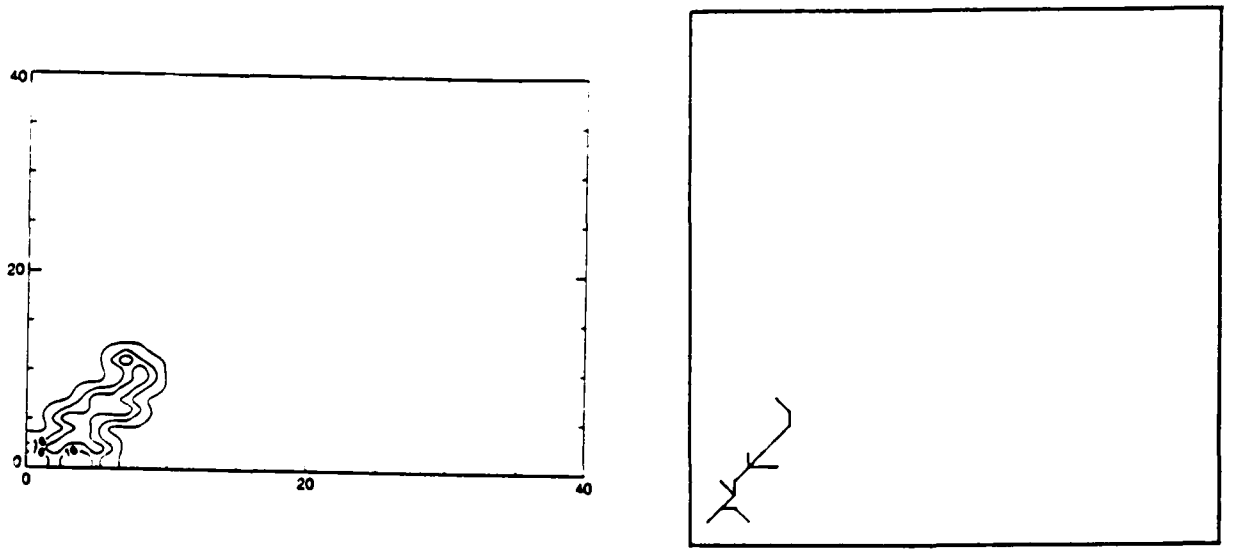

Figure 3-42: Elevation Spatial Distribution. Case 38

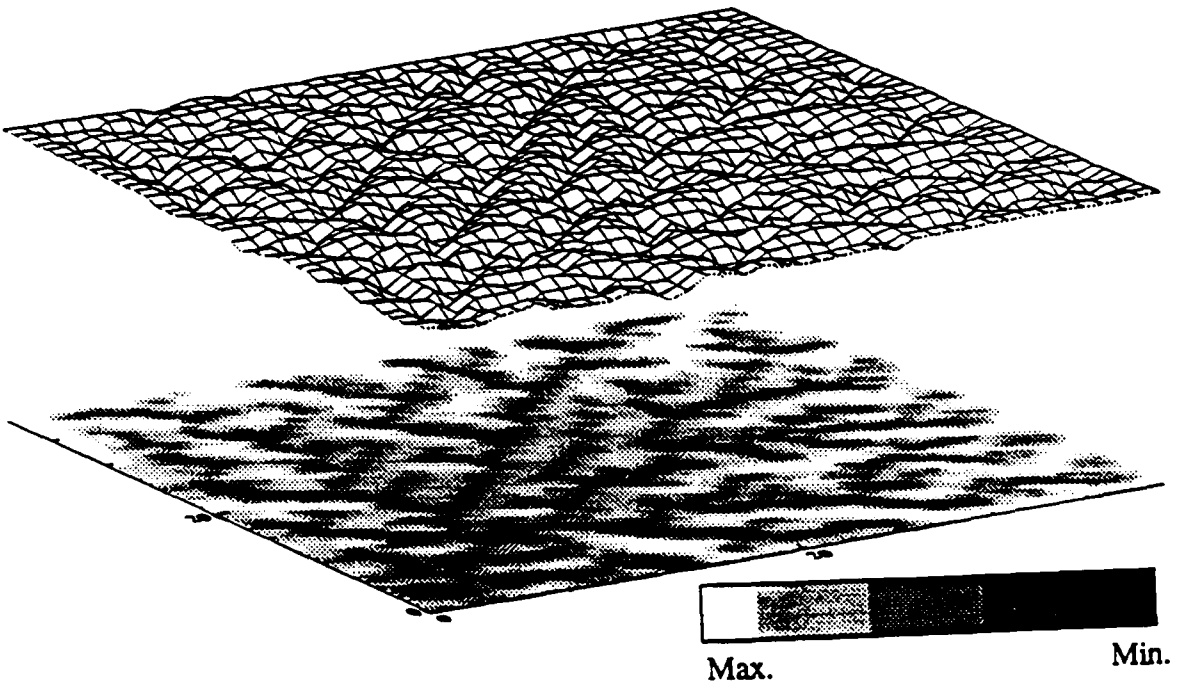

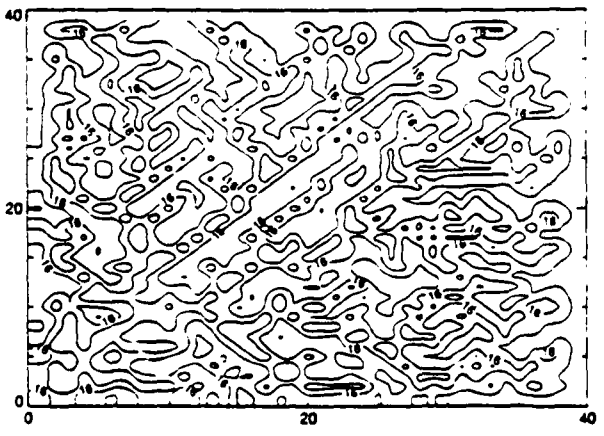

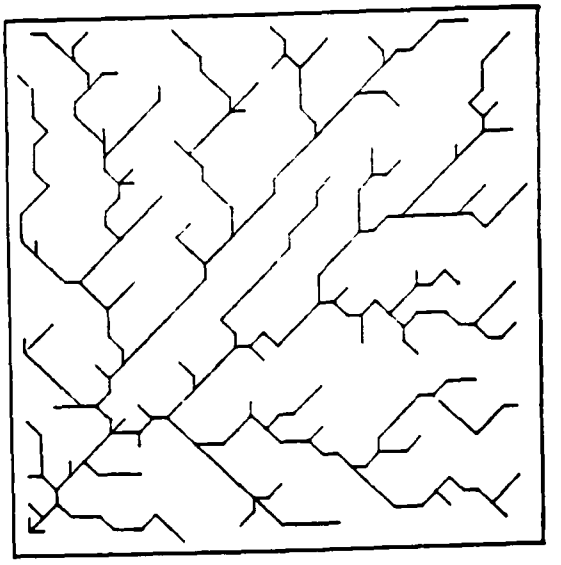

Figure 3-43: Elevation Spatial Distribution. Case 39

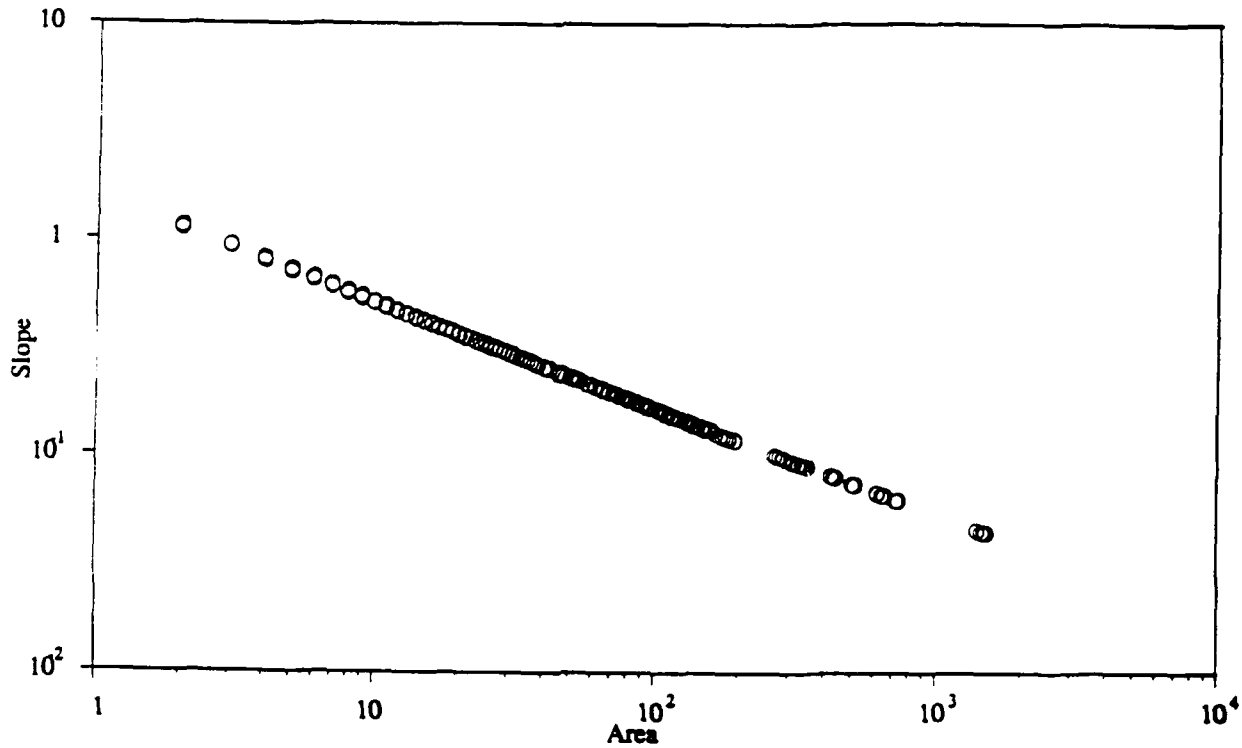

Figure 3-44: Area-Slope Renormalization.
Case 33 at Dynamic Equilibrium

The fit of Equation (3.43) is also excellent in this modified model. The observed value of θ is 0.38. The analysis of Willgoose et al. [47] to calculate the value of θ from the parameters of the model cannot be applied to the subsurface saturation modification. The reason is that in the modified model there is no a simple and direct relationship between Q and A as in the original model ($Q=\beta_3 A$) because of the presence of saturation deficits.

Tarboton [44] hypothesizes that channels and hillslopes can be distinguished in a digital elevation map based on a slope break that appears in the renormalization analysis when every pixel in the map is studied. The indicator function which defines exactly whether a node is channelized or not in the WBR model permits this hypothesis to be tested. Willgoose et al. [47] found that the criteria for hillslope distinction was not a break in slope; instead he found a separate hillslope renormalization line. This behavior of the model has to do with the fact that the only difference in sediment transport mechanisms

between channels and hillslopes is the multiplicative factor O_i. Figures 3-45 and 3-46 show the area-slope renormalization analysis for the case with continuous tectonic uplift before the system reaches dynamic equilibrium. All the grid nodes are included in these graphs. It can be seen at Figure 3-45 that at time 4000 transient points are present in the bottom left-hand corner. These points correspond to those nodes where the action of the network has not arrived. As time passes, the dispersion of the points in the graph reduces until it reaches the straight line renormalization at dynamic equilibrium.

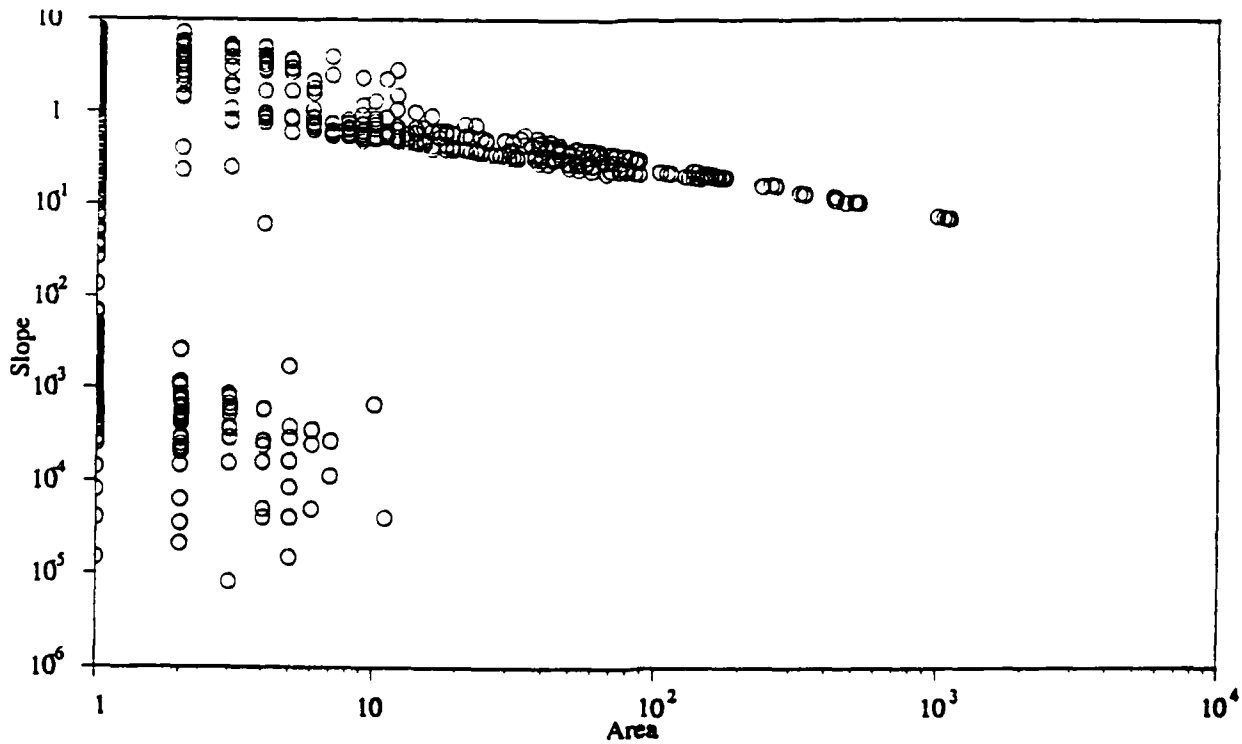

Figure 3-45: Area-Slope Renormalization. All Nodes Included.
Case 33 Before Dynamic Equilibrium.Time 4000

Figures 3-47, 3-48 and 3-49 show the area-slope graphs at three different times in the evolution of a system that includes diffusive sediment transport processes but instantaneous tectonic uplift. Again, there are transient points with small area and very small slope. These points in the graph dissapear later in the evolution from the effect of sediment wash. However, even though the fit of expression (3.43) is good as can be seen in Figure 3-49, it is not as precise as it was in the continuous uplift case. In the diffusion case, a reduction of

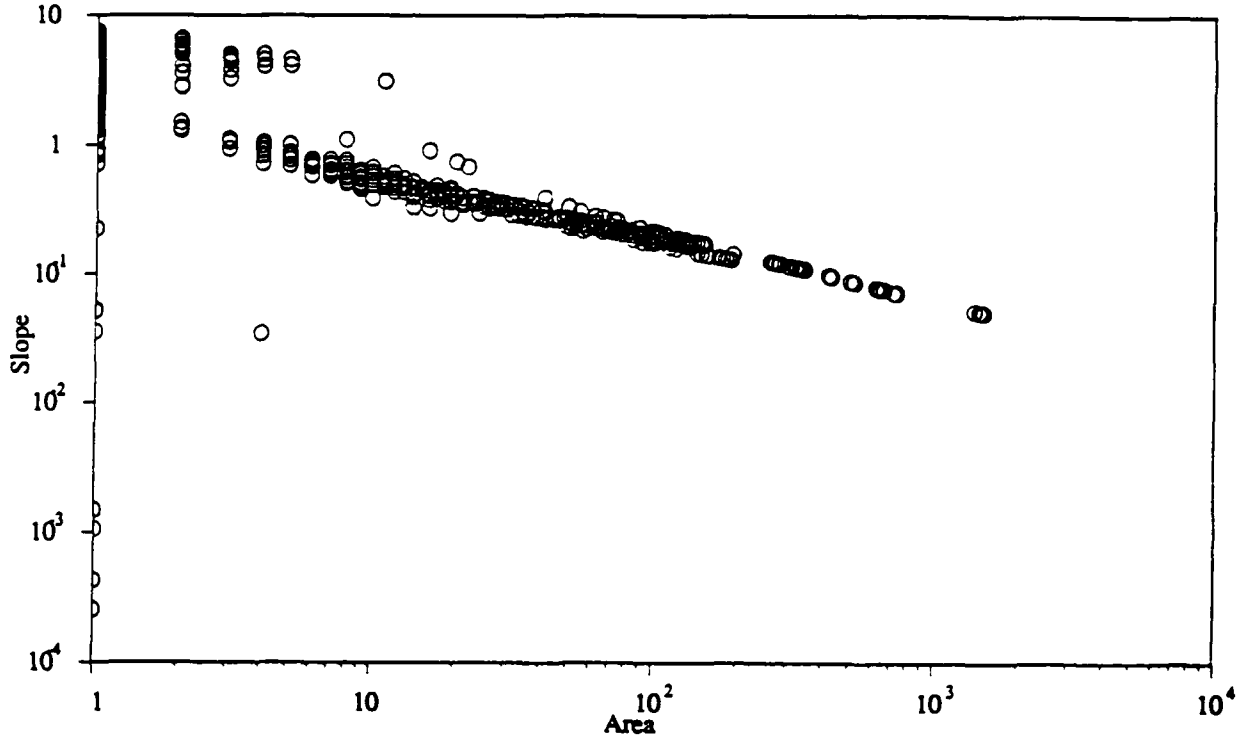

Figure 3-46: Area-Slope Renormalization. All Nodes Included.
Case 33 Before Dynamic Equilibrium.Time 6000

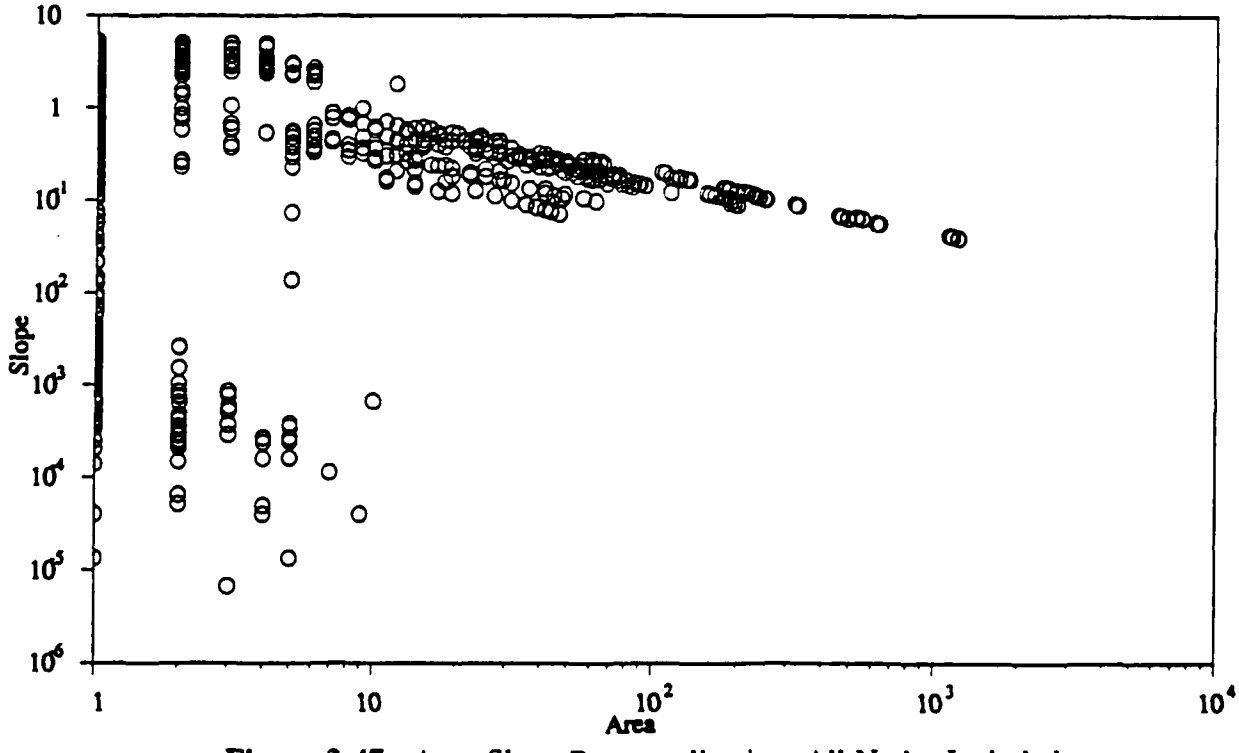

Figure 3-47: Area-Slope Renormalization. All Nodes Included.
Case 32. Time 4000

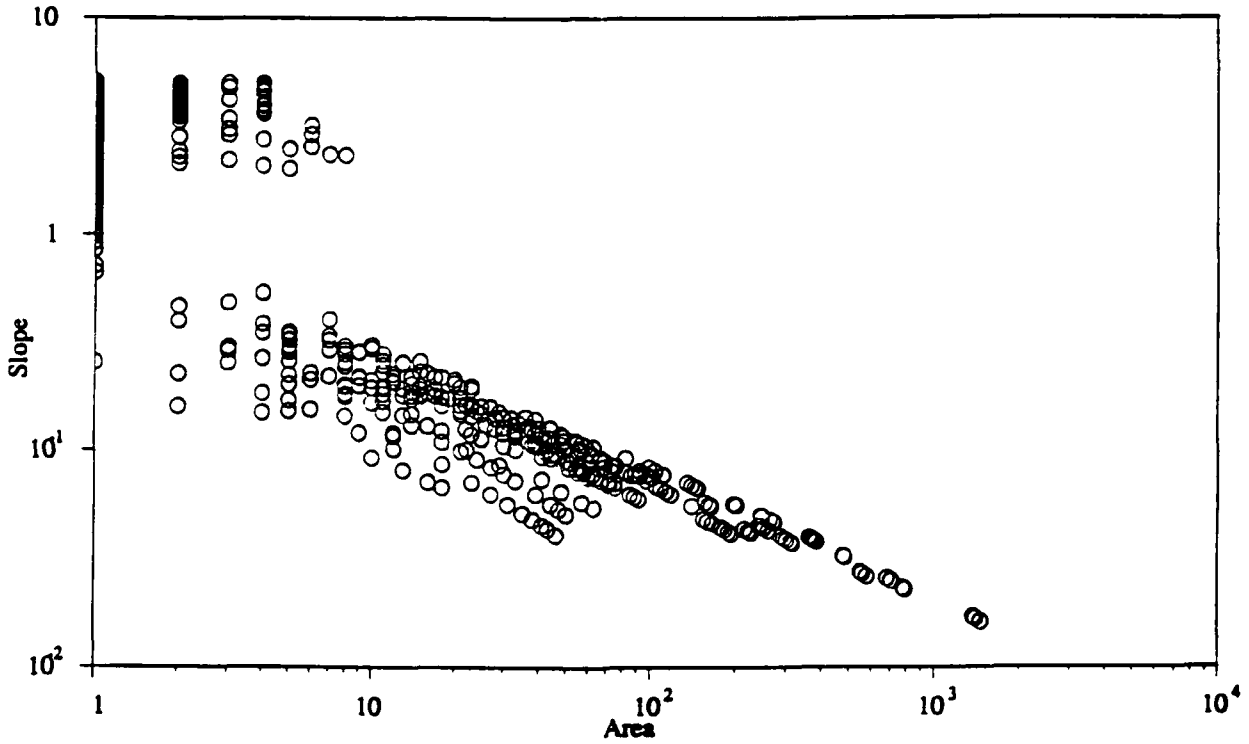

Figure 3-48: Area-Slope Renormalization. All Nodes Included.
Case 32. Time 6000

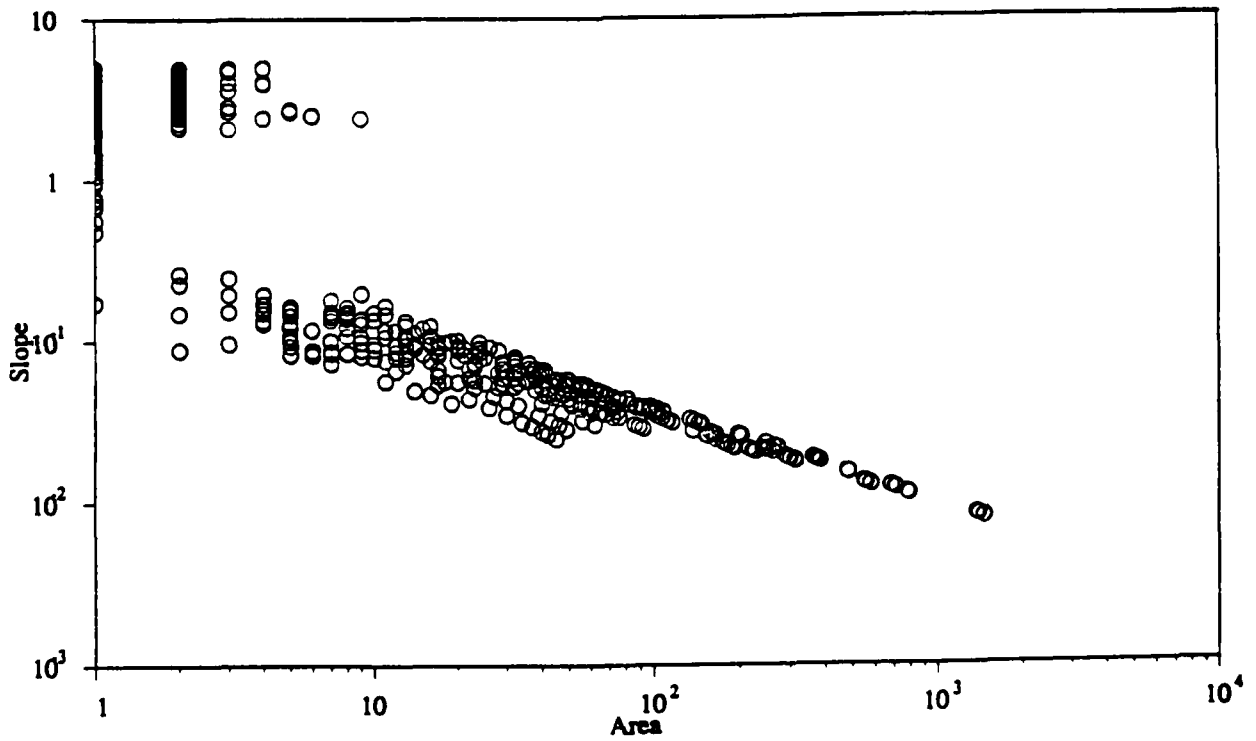

Figure 3-49: Area-Slope Renormalization. All Nodes Included.
Case 32. Time 10000

slope is present as areas decrease. Later on, some hillslope nodes are left behind in the sediment wash process because they belong to the unsaturated group.

3.10.2 Link Lengths of Simulated Catchments

This section will study the planar properties of the simulated catchments using the subsurface saturation modification. The results will be compared to the simulations performed with the original model. Also some relationships that have been studied by field workers will be examined. The relationships to be considered are: that the probability distribution of exterior and interior link lengths are different [37]; that the link length distribution is exponential [37] or Gamma [46]; and that link lengths are correlated with link magnitude or the downstream link magnitude [39] and [1].

In order to test the different hypotheses, Table 3-II presents the mean link length for exterior, interior and the whole set of links (denoted by $\overline{L}_e$, $\overline{L}_i$ and $\overline{L}_t$ respectively). Following [47] a t-test was performed in order to find out whether a statistically significant difference existed between interior and exterior mean lengths. The null hypothesis is:

$$\mathbf{H}_o : \frac{\overline{L}_e/\overline{L}_i - 1}{\sigma_{\overline{L}_e/\overline{L}_i}} = 0 \qquad (3.44)$$

The mean value of the test variable is 0.29. Therefore the hypothesis cannot be rejected at the 5% confidence limit, i.e. no statistical difference was found between the mean values of exterior and interior link lengths.

Based on this result, it is possible to study the distribution of all the links at once, both interior and exterior. Both the mean and the standard deviation of L_t for different simulations are presented in Table 3-III. Also in this table the shape factor for a moment-fitted gamma distribution was calculated. The mean value of the shape factor was 1.43 ± 0.28 which is consistent with the hypothesis that link lengths are gamma distributed with a shape parameter factor of about 1.5 to 2.0 [46].

SIMULATION	L_e	L_i	$\frac{L_e/L_i-1}{\sigma_{L_e/L_i}}$
BR643SATU10	3.81	3.14	+0.85
BR643SATU21	2.71	2.62	+0.14
BR643SATU29	3.91	3.83	+0.08
BR643SATU30	2.63	3.36	-0.86
BR643SATU31	3.03	2.49	+0.86
BR643SATU32	3.42	3.19	+0.29
BR643SATU33	2.74	3.10	-0.46
BR643SATU34	4.59	3.44	+1.33
BR643SATU35	4.20	4.02	+0.18
BR643SATU36	3.22	3.37	-0.18
BR643SATU37	4.36	3.90	+0.47
BR643SATU39	3.28	3.22	+0.07
BR643SATU40	5.09	7.50	-1.28
BR643SATU42	5.17	2.81	+3.34
BR643SATU43	2.58	2.55	+0.05
BR643SATU44	6.55	5.52	+0.74
BR643SATU45	2.21	2.69	-0.70

Table 3-II: T-test for Mean Exterior and Interior Link Lengths

Finally, link lengths were plotted against magnitude of the same link and the following link downstream. Figures 3-50 and 3-51 correspond to these plots. The case under consideration corresponds to runs BR643SATU10,34,35 and 36 which have the same different parameters but different initial random elevation fields. Correlations for case 10 were found to be low (-0.15 for link length vs. magnitude and -0.18 for link length vs. downstream magnitude) in agreement with results by [47] and [1].

SIMULATION	$\bar{L}_t$	σ_{L_t}	$\bar{L}_t^2/\sigma_{L_t}^2$
BR643SATU10	3.48	3.04	1.31
BR643SATU21	2.66	2.17	1.50
BR643SATU29	3.87	3.21	1.45
BR643SATU30	2.99	2.33	1.65
BR643SATU31	2.77	2.20	1.59
BR643SATU32	3.31	3.21	1.06
BR643SATU33	2.91	2.11	1.90
BR643SATU34	4.02	3.39	1.41
BR643SATU35	4.11	3.88	1.12
BR643SATU36	3.29	2.34	1.41
BR643SATU37	4.13	3.44	1.44
BR643SATU39	3.25	2.68	1.21
BR643SATU40	6.26	5.89	1.13
BR643SATU42	4.00	4.27	0.88
BR643SATU43	2.57	1.98	1.68
BR643SATU44	6.05	4.36	1.93
BR643SATU45	2.45	1.89	1.67

Table 3-III: Shape Parameter of a Gamma Distribution fitted to Link Lengths

3.10.3 Link Contributing Areas in Simulated Catchments

In Subsection 3.10.2 it was shown that the mean values of exterior and interior link lengths were not statistically different. Smart in his paper [38] also suggested different distributions for areas draining to an exterior and interior link. A t-test similar to the test

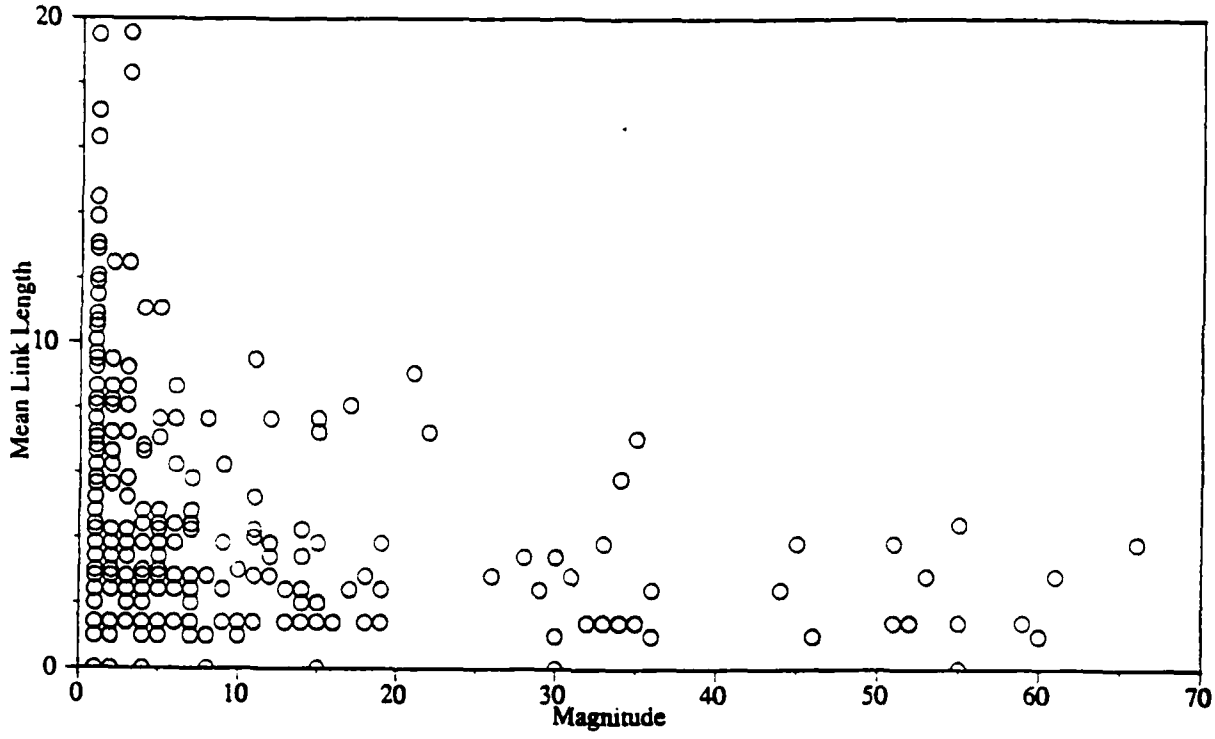

Figure 3-50: Link Length vs. Magnitude.
Cases 10,34,35,36

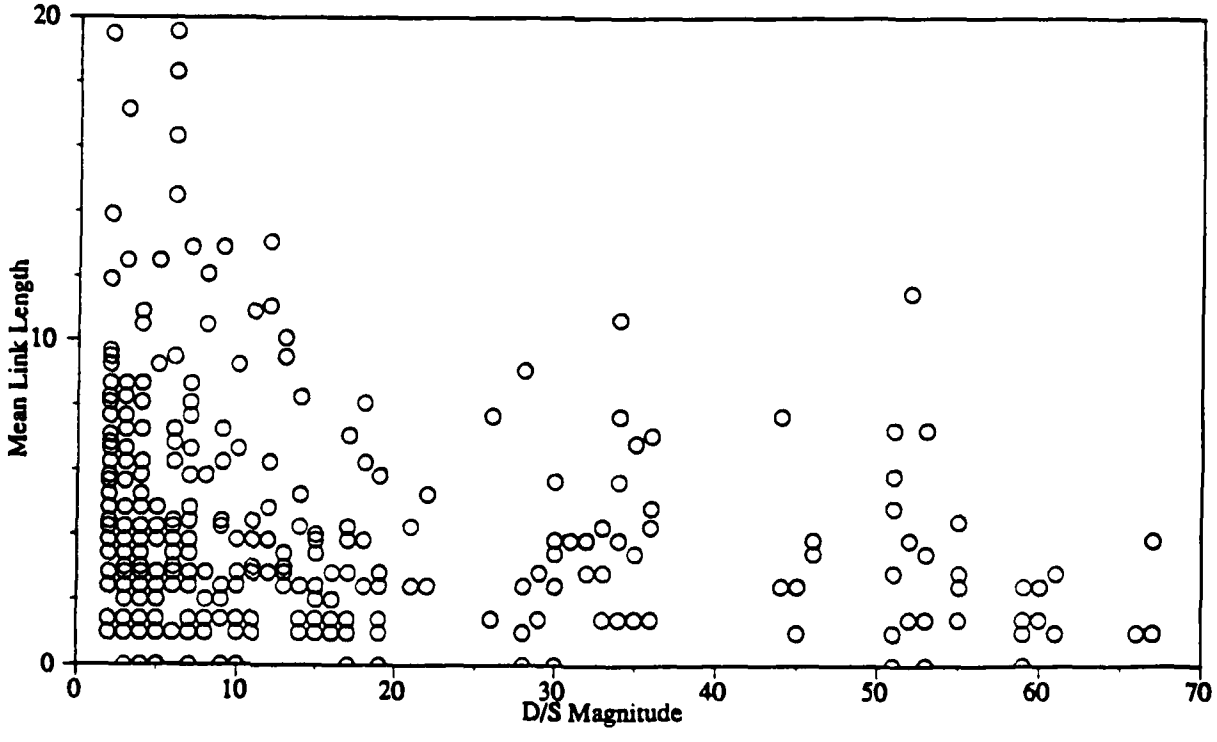

Figure 3-51: Link Length vs. Downstream Magnitude.
Cases 10,34,35,36

performed in Section 3.10.2 was done using mean contributing areas ($\overline{A}_e$ and $\overline{A}_i$ for exterior and interior areas respectively) instead of link lengths. The values of $\overline{A}_e$, $\overline{A}_i$ are shown in Table 3-IV. The t-test at the 5% level of significance shows $\overline{A}_e/\overline{A}_i$ to be larger than 1. This result is in agreement with [47]. The difference in the mean of the area distributions comes from the source area that contributes only to exterior links. Given that no statistical difference was found between mean exterior and interior link lengths and that lateral area and link length are strongly correlated, then the difference between $\overline{A}_e$ and $\overline{A}_i$ comes basically from source areas. The mean proportion of source areas to total area is 27% which is a little low when compared to the value of the proportion calculated from digital elevation maps where its value is around 35-40% (Moglen and Bras, unpublished data).

3.10.4 Fundamental Length Scales in Simulated Catchments

In this subsection commonly studied catchment length scales will be measured in the resulting simulated networks generated with the subsurface saturation modification to the WBR model. These measures address the problem of determining a meaningful definition of mean hillslope length. The lengths to be studied are: the mean link lengths of exterior, interior and the whole set of links ($\overline{L}_e$, $\overline{L}_i$ and $\overline{L}_t$ respectively); the drainage density-based hillslope length ($L_h=1/2D_d$) proposed by Horton [14]; the square root of the mean first order Strahler area $\sqrt{\overline{A}_1}$; the mean value $\sqrt{\overline{A}_s}$ of the area contributing to channel heads (called source area by Montgomery and Dietrich [28]); and the lateral hillslope length (defined in [47] as the mean hillslope length of the lateral contributing areas).

In order to make a comparison between the results of the original WBR model and its subsurface saturation modification, a simple linear least-square regression was fitted pairwise to the different length scales described before. Results appear in Tables 3-V and 3-VI

SIMULATION	$\overline{A}_e$	$\overline{A}_i$	$\frac{\overline{A}_e/\overline{A}_i - 1}{\sigma_{\overline{A}_e/\overline{A}_i}}$
BR643SATU10	15.38	7.07	2.34
BR643SATU21	8.02	4.09	1.91
BR643SATU29	20.11	9.40	2.26
BR643SATU30	10.27	7.42	0.75
BR643SATU31	9.63	4.00	2.80
BR643SATU32	14.27	7.20	1.79
BR643SATU33	10.82	6.63	1.25
BR643SATU34	18.00	7.11	3.04
BR643SATU35	16.69	9.78	1.41
BR643SATU36	12.85	7.37	1.47
BR643SATU37	18.16	9.10	1.99
BR643SATU39	13.31	6.83	1.89
BR643SATU40	51.00	36.44	0.79
BR643SATU42	20.98	5.86	5.12
BR643SATU43	8.97	4.45	2.02
BR643SATU44	53.11	25.06	2.22
BR643SATU45	6.76	4.50	0.99

Table 3-IV: t-Test for Mean Exterior and Interior Link Areas

The correlation between the different length scales is generally good. The only exceptions are the correlation values between the mean exterior link length and the other scales, even though the correlation between $\overline{L}_e$ and $\sqrt{\overline{A}_1}$ is high. In the WBR model the variable with less correlation against the others was the mean interior link length. Notice

also that the mean first Strahler order area is approximately 75% larger than the mean source area and this influences the relation between mean and exterior areas that were studied in the Subsection 3.10.3.

X\Y	$\overline{L}_e$	$\overline{L}_i$	$\overline{L}_t$	L_h	$\sqrt{\overline{A}_1}$	A_s	L_{lh}
$\overline{L}_e$	1.00	0.62	0.96	1.32	0.79	0.92	1.99
$\overline{L}_i$	0.62	1.00	1.05	1.82	0.85	1.23	2.64
$\overline{L}_t$	0.96	1.05	1.00	1.56	0.82	1.07	2.31
L_h	1.32	1.82	1.56	1.00	0.43	0.61	1.36
$\sqrt{\overline{A}_1}$	0.79	0.85	0.82	0.43	1.00	1.32	2.84
$\sqrt{\overline{A}_s}$	0.92	1.23	1.07	0.61	1.32	1.00	2.13
L_{lh}	1.99	2.64	2.31	1.36	2.84	2.13	1.00

Table 3-V: Linear Regression Between Fundamental Length scales

X\Y	$\overline{L}_e$	$\overline{L}_i$	$\overline{L}_t$	L_h	$\sqrt{\overline{A}_1}$	A_s	L_{lh}
$\overline{L}_e$	1.00	0.67	0.91	0.71	0.90	0.77	0.76
$\overline{L}_i$	0.67	1.00	0.92	0.91	0.90	0.96	0.93
$\overline{L}_t$	0.91	0.92	1.00	0.89	0.99	0.95	0.93
L_h	0.71	0.91	0.89	1.00	0.92	0.95	0.96
$\sqrt{\overline{A}_1}$	0.90	0.90	0.99	0.92	1.00	0.97	0.95
A_s	0.77	0.96	0.95	0.95	0.97	1.00	0.97
L_{lh}	0.76	0.93	0.93	0.96	0.95	0.97	1.00

Table 3-VI: Correlation Coefficients Between Fundamental Length scales

3.11 The Influence of the Probabilistic Distribution of Rainfall

In Section 3.2 the excess water at every node was calculated as the difference between the rainfall β_3 at the mean flood event and the deficit D_i calculated using Equation (3.10). The sum along the elevation gradient of the excess water at each point gives the contributing overland flow as in Equation (3.14). In all the simulations examined up to this point, the calculations of the amount of overland flow at every node were based on the fixed mean value β_3. This implies that in the calculations some nodes were not saturated and therefore no erosion due to overland flow is possible. However, given that the timescales considered in the simulations are very long, typically on the order of millions of years, it would be expected that some rainfall events corresponding to floods above the mean value β_3 would produce erosion on those nodes considered as unsaturated before. Following Willgoose (personal communication) and [19], a way to modify the overland flow calculation procedure is to assume a probabilistic distribution over the rainfall amounts and calculate the excess water based on this distribution.

If an exponential distribution of rainfall amounts R with mean β_3 is assumed, then the excess water at a node i is:

$$E_i = \int_0^\infty \frac{<R-D_i>}{\beta_3} e^{-R/\beta_3}\, dR = \frac{1}{\beta_3}\int_{D_i}^\infty (R-D_i)\, e^{-R/\beta_3}\, dR = \beta_3\, e^{-D_i/\beta_3} \qquad (3.45)$$

where again <x> stands for max(x,0).

A node is saturated if D_i is equal to 0 and in this case $E_i=\beta_3$ as in the original formulation. The difference in the overland flow distribution in the new formulation comes from the originally unsaturated nodes which now have some excess water production. Equation (3.45) can be seen as a probabilistic proportion of overland flow assigned to the nodes. Notice however, that in this approach, even though the probabilistic distribution of R is taken into account, no stochastic term is included in the model's formulation.

Furthermore, because of the special form of the exponential distribution, the calculation of E_i still depends on the parameters of the original model.

The overland flow at a node i is now:

$$Q_i = E_i + \sum_j Q_j I_{ji} \tag{3.46}$$

and the other equations of the model remain the same.

Using the same parameters and the initial elevation field of the simulation example presented in Section 3.4, a new simulation including the approach of this section was performed. Comparisons between both runs will now be presented. Figure 3-52 shows the final networks for the original simulation BR643SATU10 and the modified version BR661SATU10. The differences are small but noticeable. Figure 3-53 to 3-56 show the evolution of the elevation distribution with time. Figures 3-57 and 3-58 correspond to the evolution in time of the drainage density and magnitude of the network.

Finally, Figure 3-59 shows the evolution of the hypsometric curves for both cases. This figure shows clearly the effect of the new overland flow distribution on the catchment evolution. It can be seen that those nodes at higher elevation, which usually fall into the group of unsaturated nodes because of their smaller areas and larger slopes, are eroded faster in the new formulation. The sharpness of the knee is reduced because of the erosion in the unsaturated nodes and the hypsometric curves in both cases are almost identical in the zones of channel and saturated nodes. The overland flow in the unsaturated nodes, even though small, is enough to produce changes in the network. Similar behavior was observed in different simulations that used the same parameter values as the experiments described in previous sections. Figure 3-60 shows the hypsometric curve evolution for case 33 that was analyzed in Section 3.6.

At the beginning of the basin evolution almost all the nodes are saturated and no difference exists between both simulations. As time passes, some nodes become

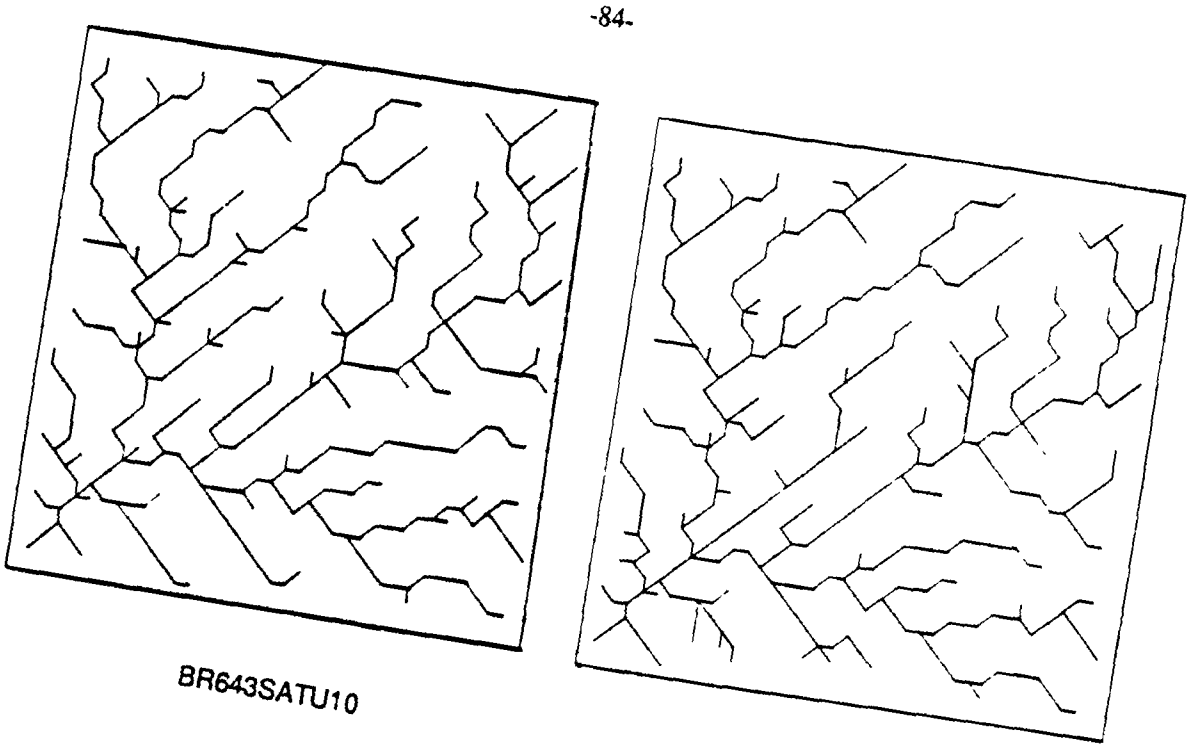

Figure 3-52: Final Networks. Cases BR643SATU10 and BR661SATU10

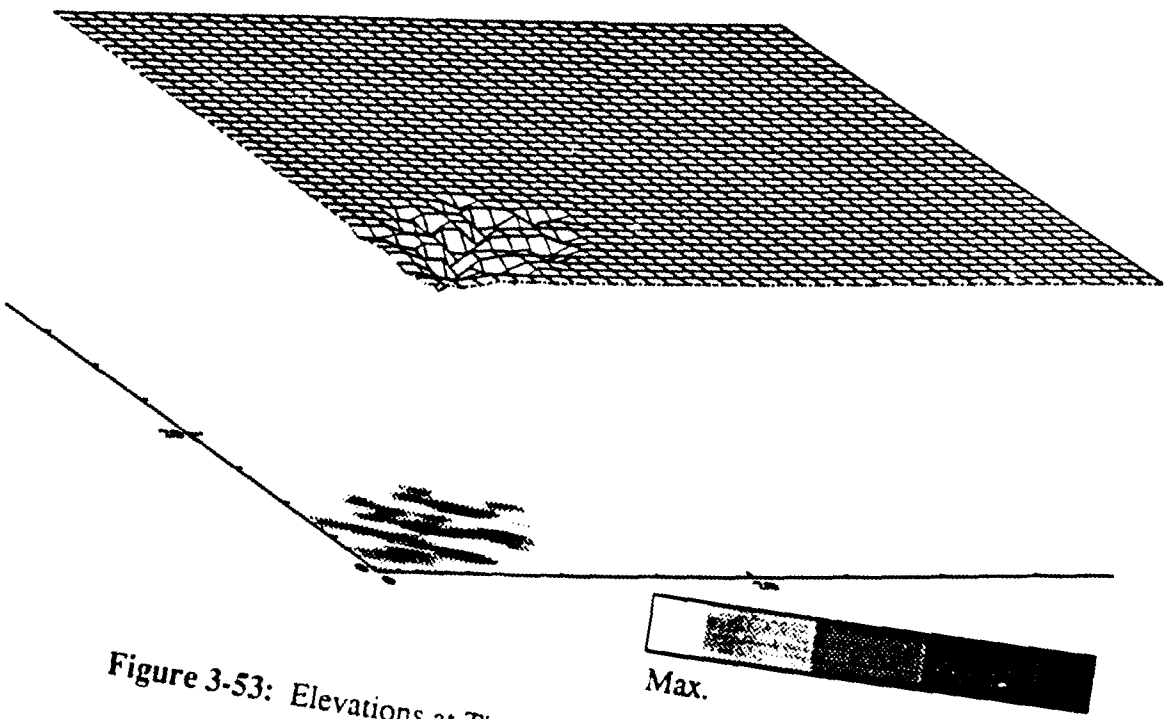

Figure 3-53: Elevations at Time 1000. Case BR661SATU10

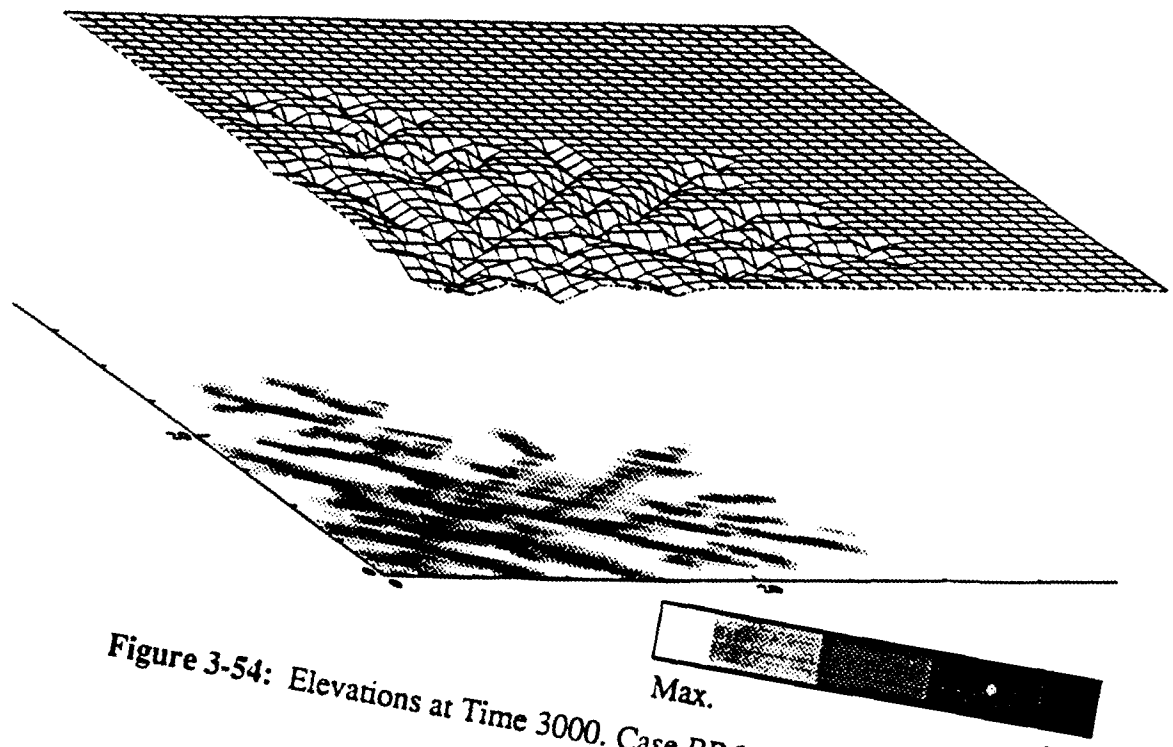

Figure 3-54: Elevations at Time 3000. Case BR661SATU10

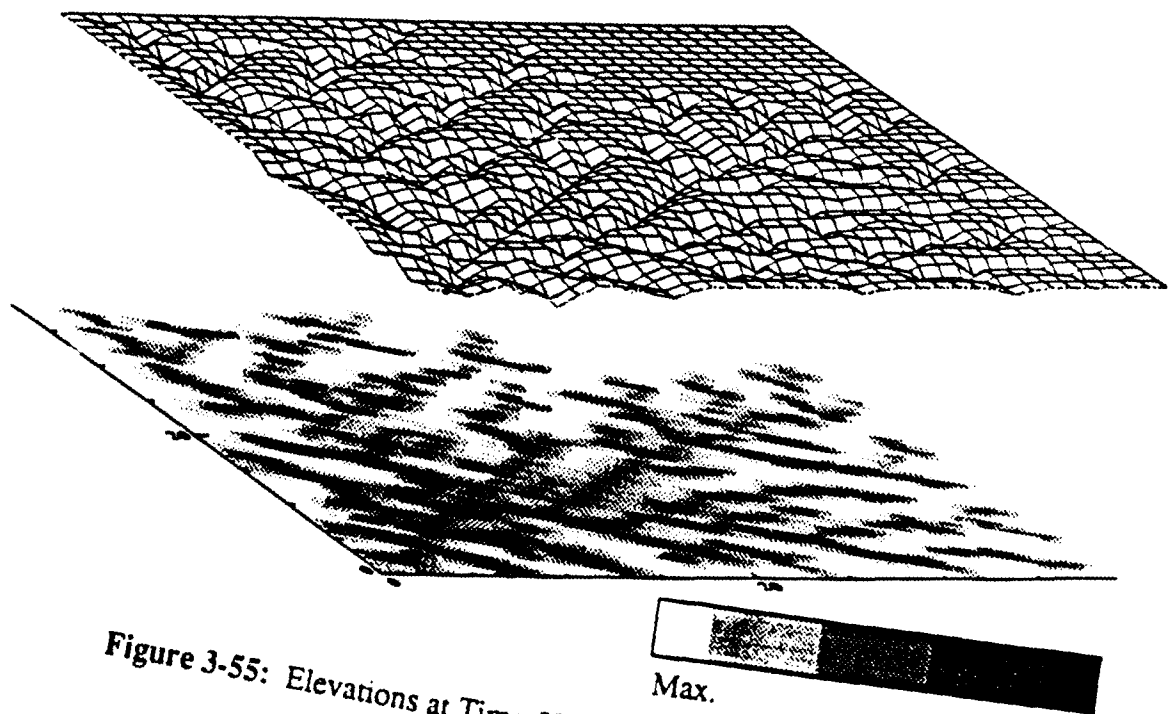

Figure 3-55: Elevations at Time 5000. Case BR661SATU10

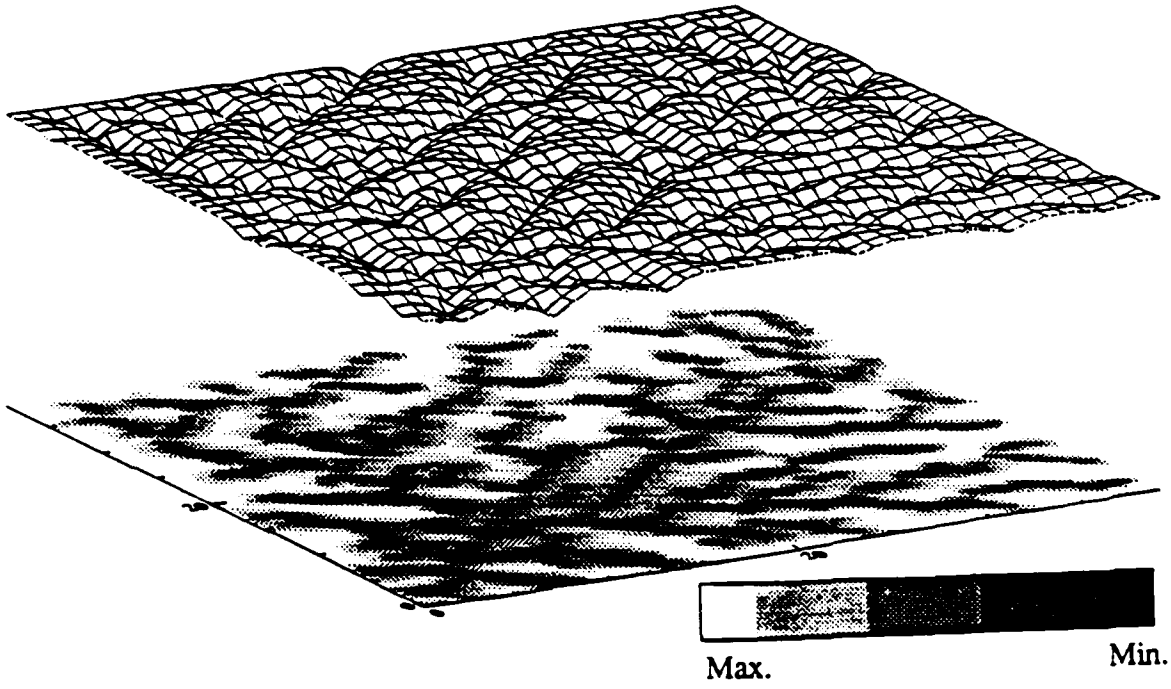

Figure 3-56: Elevations at Time 7000. Case BR661SATU10

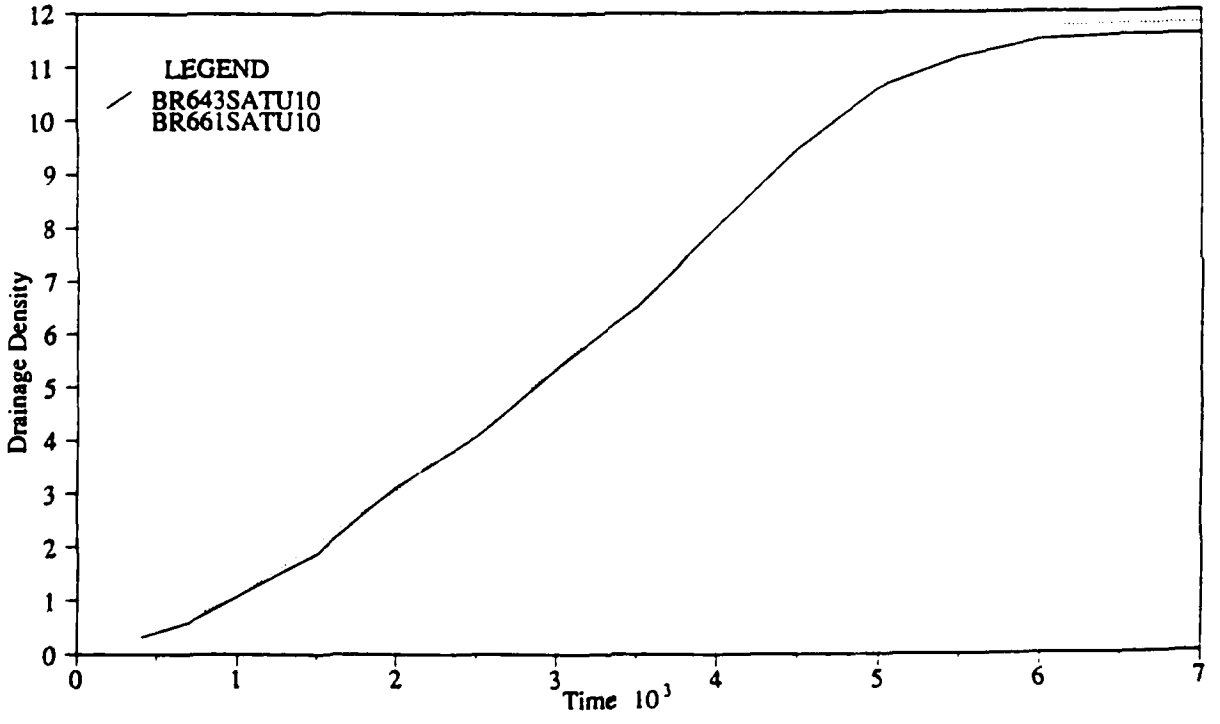

Figure 3-57: Drainage Density Evolution. Cases BR643SATU10 and BR661SATU10

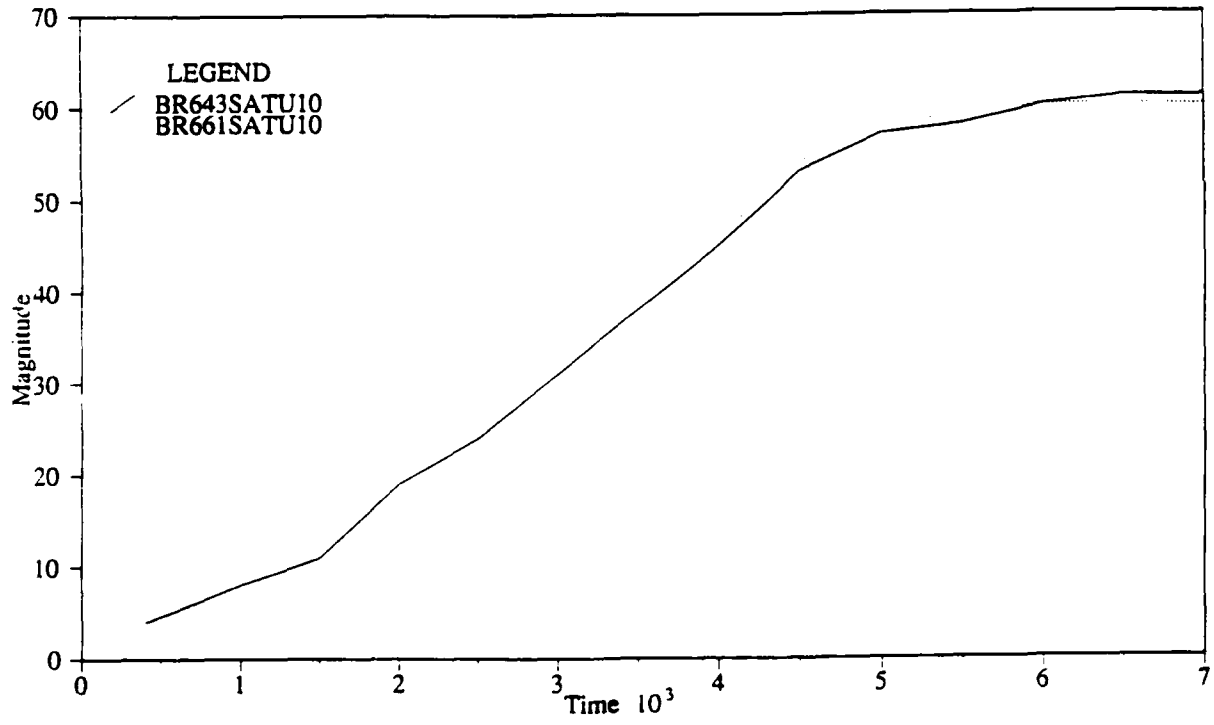

Figure 3-58: Magnitude Evolution. Cases BR643SATU10 and BR661SATU10

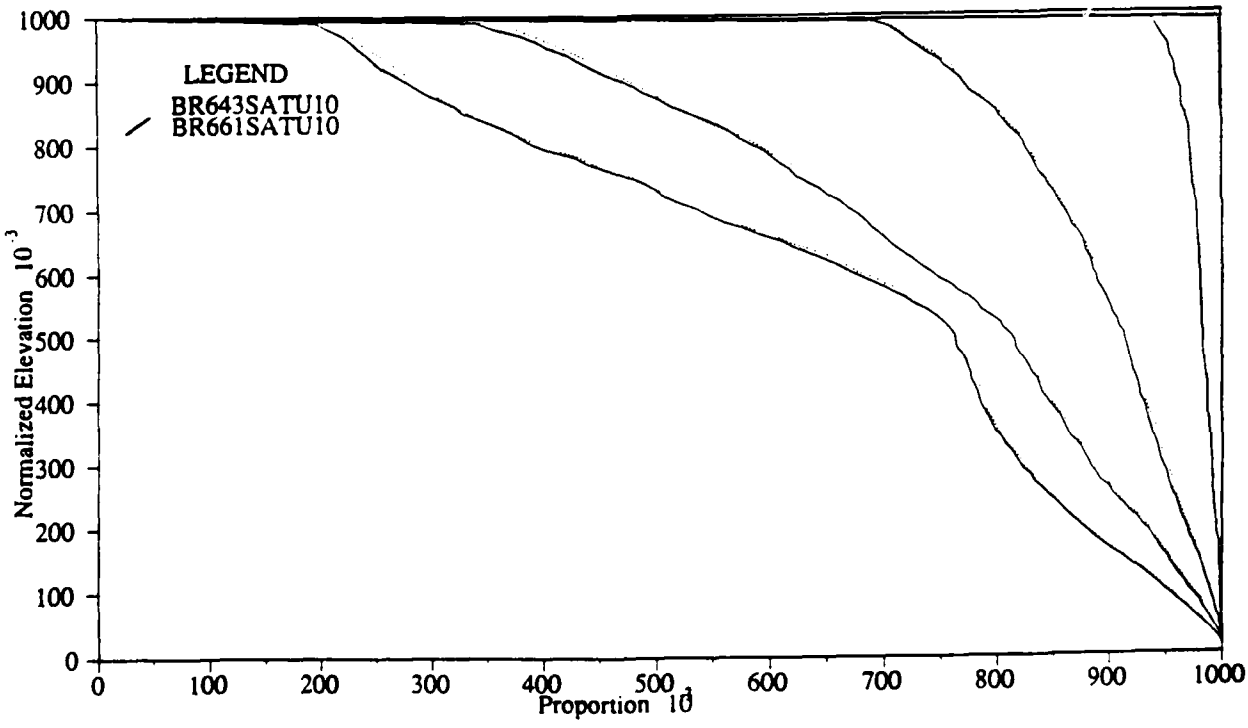

Figure 3-59: Hypsometric Curve Evolution. Cases BR643SATU10 and BR661SATU10

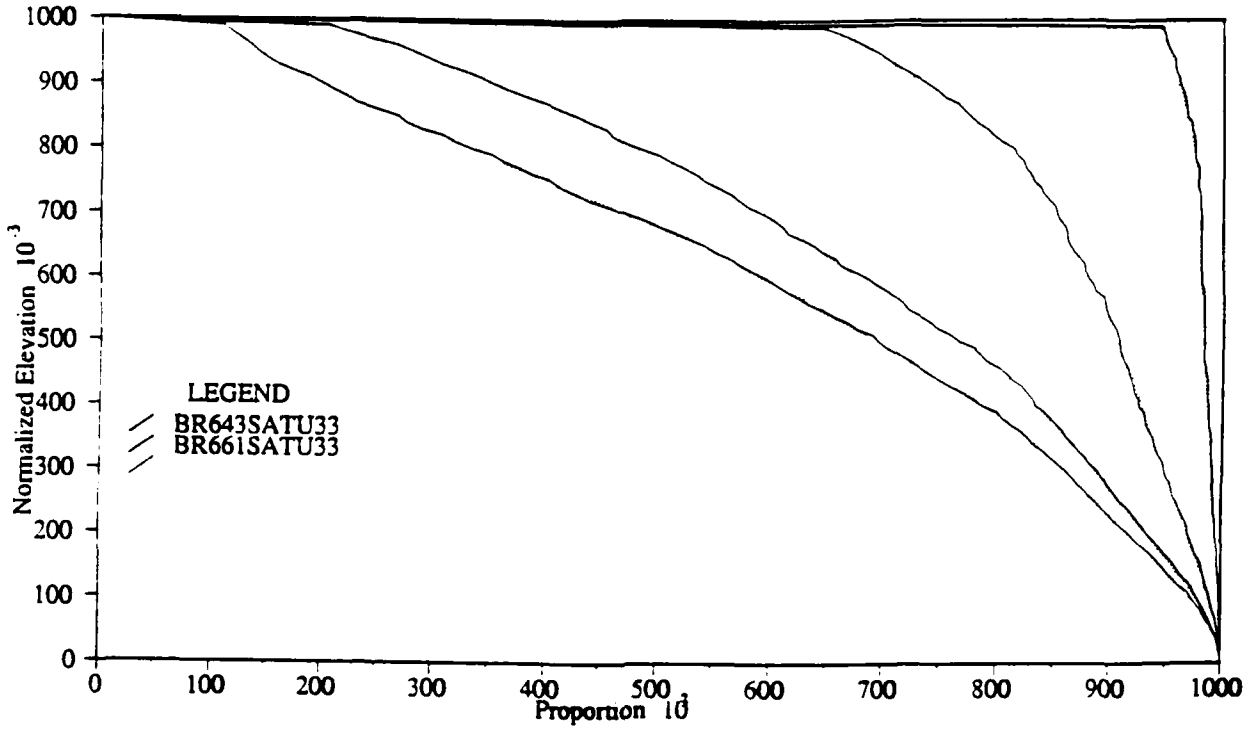

Figure 3-60: Hypsometric Curve Evolution. Cases BR643SATU33 and BR661SATU33

unsaturated and do not contribute to overland flow in the original formulation. However, even though excess water is produced in those nodes in the second fomulation, the exponential form of the distribution makes this quantity small. For example, in simulation BR661SATU10 the probabilistic proportion of overland flow in unsaturated nodes was one to three orders of magnitude smaller than in saturated nodes. The effect of E_i is small in the overall evolution because in both cases the evolution of the catchments is led by the channelized nodes.

Table 3-VII compares the statistics of the network for the cases BR643SATU10 and BR661SATU10.

The role of T_c also changes, being more important in the new approach described in this section. In the original formulation T_c, through its effect on D_i, determined which nodes were saturated and which were not. T_c was also involved in the overland flow calculation in

Statistic	BR643SATU10	BR661SATU10
$R_b(1\text{-}2)$	5.08	4.62
$R_S(1\text{-}2)$	2.85	2.69
$R_L(1\text{-}2)$	2.60	2.91
$R_A(1\text{-}2)$	5.85	6.14
$R_b(2\text{-}3)$	4.00	4.33
$R_S(2\text{-}3)$	2.15	2.02
$R_L(2\text{-}3)$	1.82	1.64
$R_A(2\text{-}3)$	4.96	4.63
R_b	4.75	4.47
R_S	2.67	2.53
R_L	2.35	2.57
R_A	5.53	5.73
K	1.96	1.68
ε_1	2.67	2.26
D_d'	11.54	11.73
Magnitude	61	60
Mean Relief	9.90	9.90

Table 3-VII: Final Network Statistic Values.
Simulations BR643SATU10 and BR661SATU10

those nodes that were near complete saturation (i.e. those nodes with $D_i>0$ but $\beta_3-D_i>0$). In the approach described in this section, T_c is important in calculating the overland flow at every unsaturated node through Equation (3.45). T_c affects the probabilistic proportion of overland flow assigned to the unsaturated nodes. Figures 3-61 to 3-65 show simulations with increasing values of **TSC**. The elevation fields and the resulting networks are presented. The effect of T_c can be clearly seen in the variation of the hypsometric curves. Figures 3-66 to 3-68 correspond to simulations with **TSC** equal to $0.276\text{x}10^3$, $0.920\text{x}10^3$ and $4.600\text{x}10^3$. Notice how the knee in the hypsometric curves tends to reduce as **TSC** decreases. The increasing number of saturated nodes and the increasing overland flow production in unsaturated nodes are the reasons for this behavior. In the limit, as **TSC** decreases, the subsurface saturation modification tends to the original WBR model.

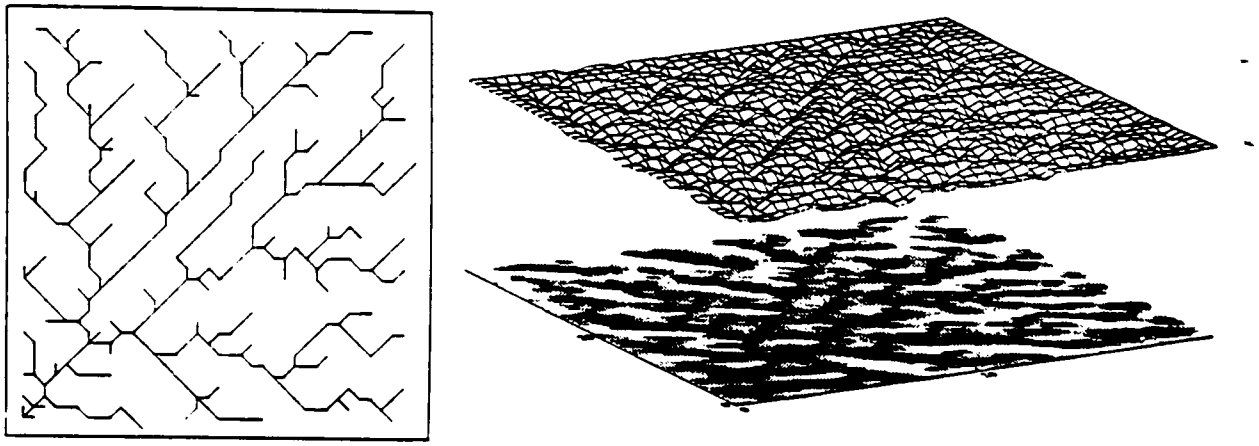

Figure 3-61: TSC=0.276x10^3

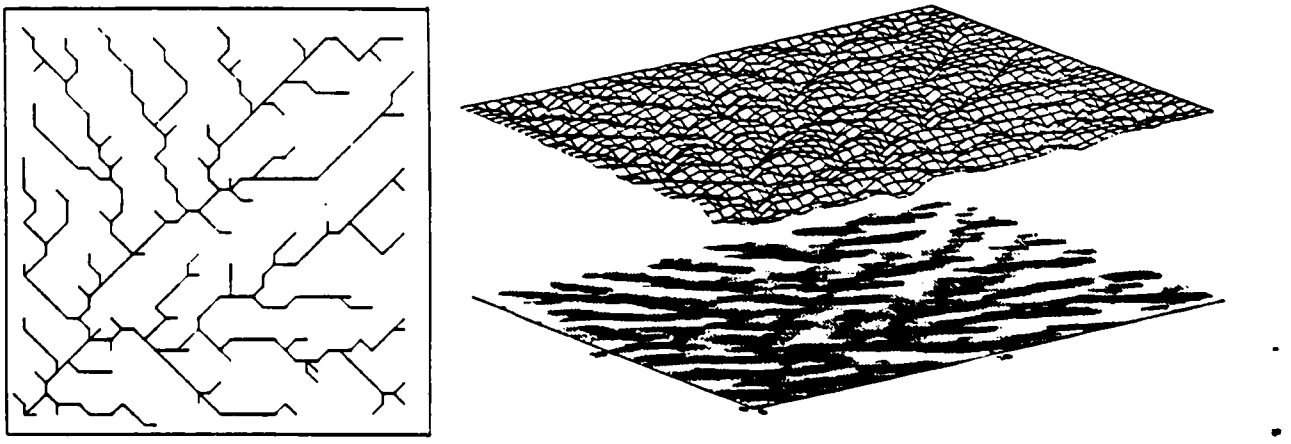

Figure 3-62: TSC=0.552x10^3

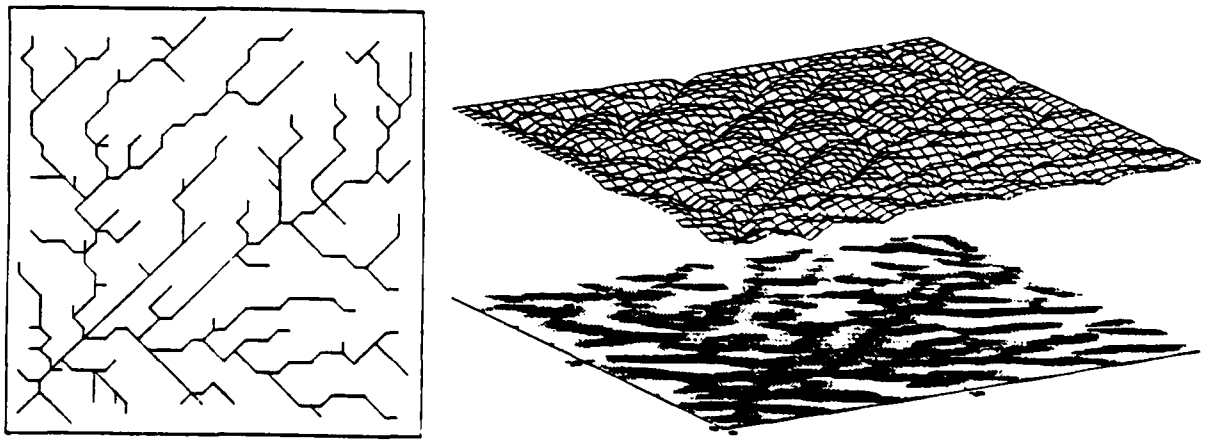

Figure 3-63: TSC=0.920x10^3

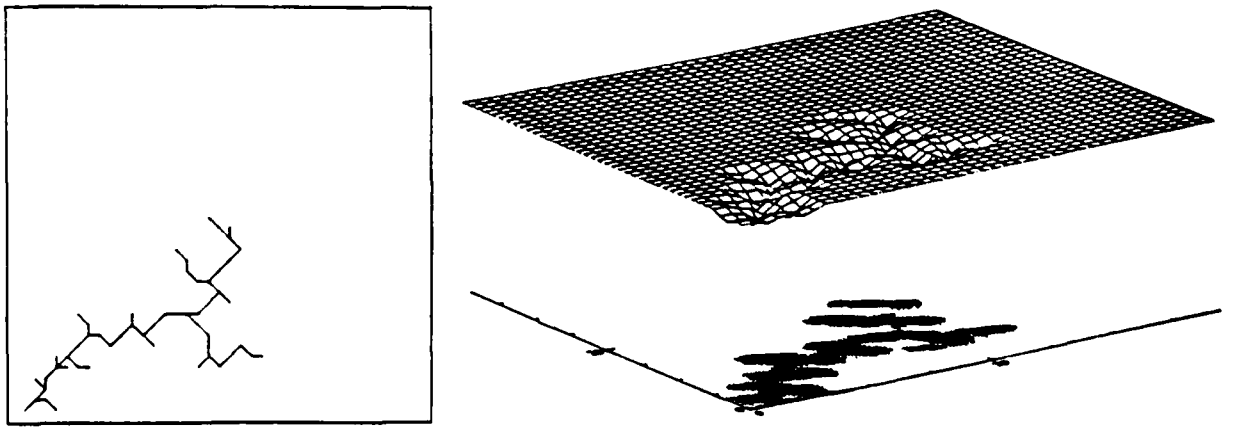

Figure 3-64: TSC=1.840x10^3

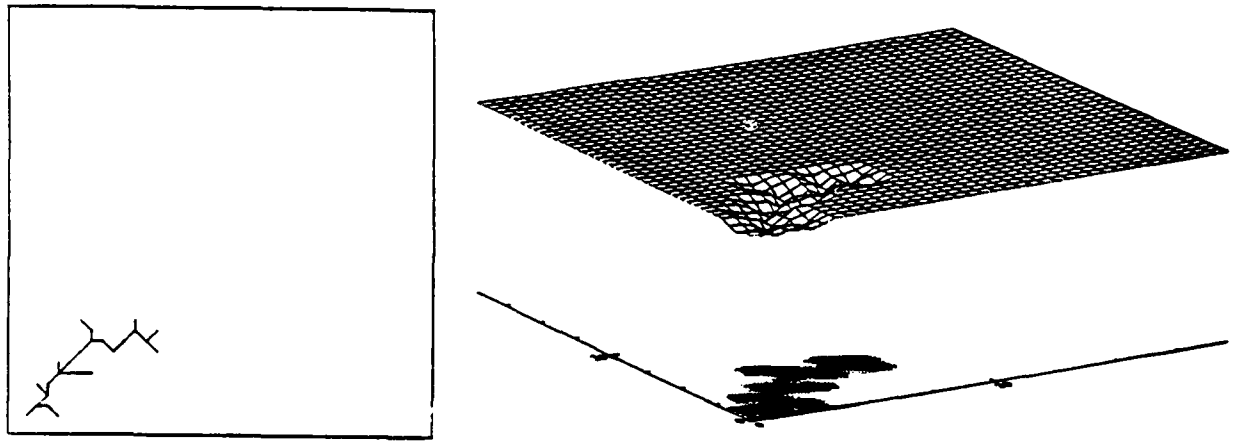

Figure 3-65: TSC=4.600x10^3

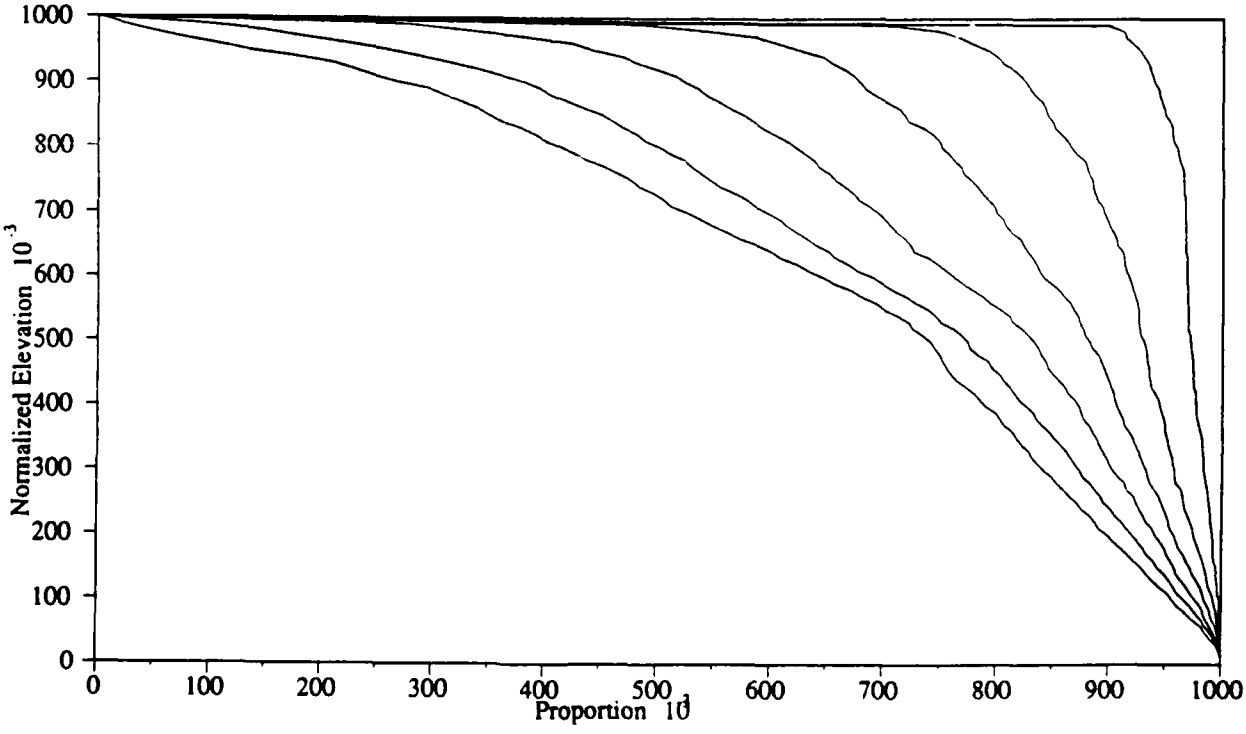

Figure 3-66: Hypsometric Curve Evolution TSC=0.276x10^3

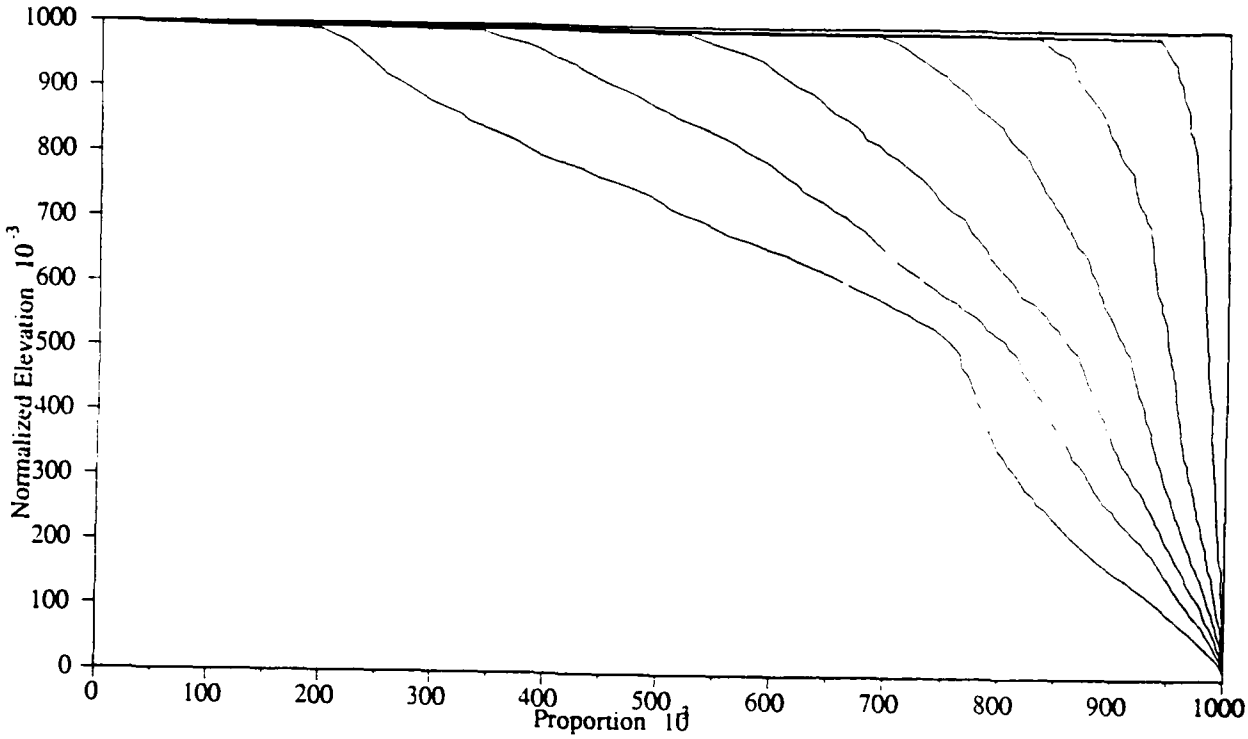

Figure 3-67: Hypsometric Curve Evolution **TSC**=0.920x10^3

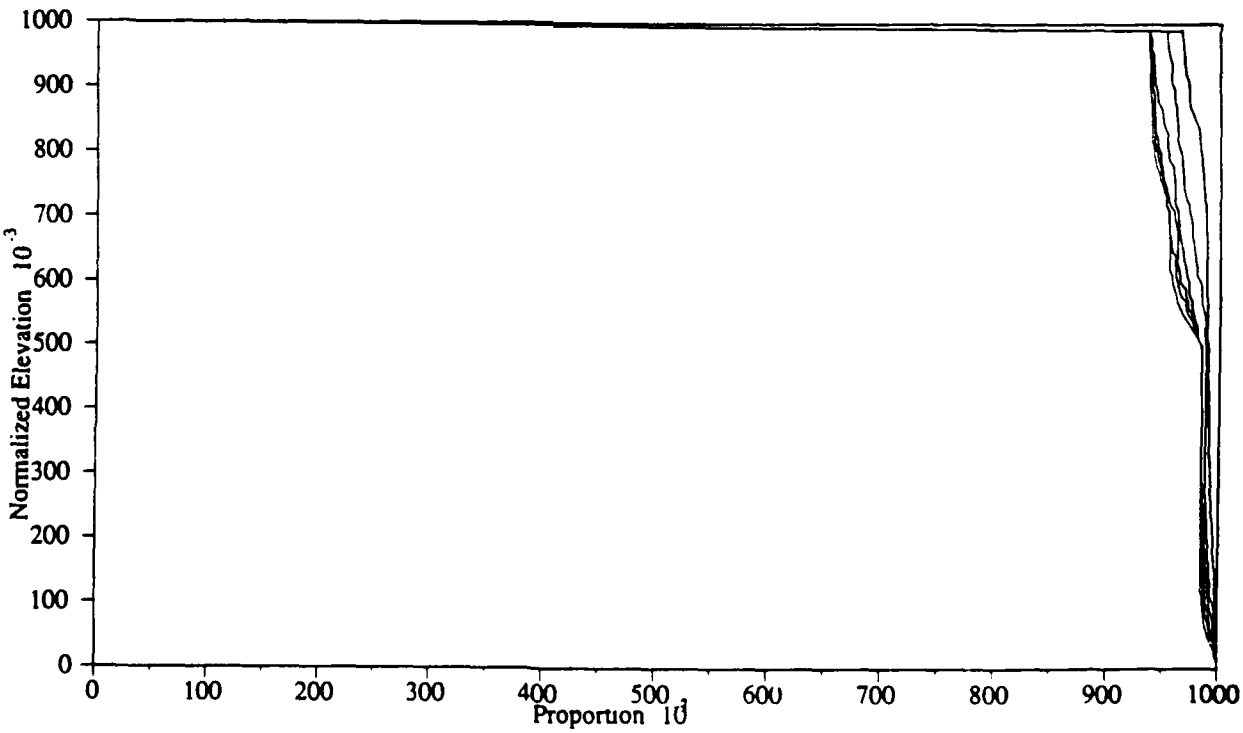

Figure 3-68: Hypsometric Curve Evolution **TSC**=4.60x10^3

Chapter 4

Sensitivity to Initial Conditions in the WBR model

4.1 Introduction

The networks produced by both the WBR model and its subsurface saturation modification have a random appearance. Keeping all the parameter values constant and varying the initial elevation field by a small amount produce completely different networks. Analytical results on the Meinhardt equations (described in Section 2.3.) show that small perturbations in the system can grow and produce completely different results, making the system chaotic; it is this transient chaos that causes the random appearance. The special form of the Meinhardt system allows an analytical derivation of these facts, but this procedure is not directly applicable to the WBR catchment evolution model. The integration of contributing flow to each node along the elevation gradient is one of the major difficulties. Nevertheless, numerical experiments can be performed in order to establish whether the chaotic behavior found in the Meinhardt system is similar to the WBR model and to what extent.

The organization of the chapter is as follows: a short review of definitions and common procedures in the study of chaotic dynamical systems is presented. Then, after defining an appropiate measure between elevation fields called the relief difference, various experiments are presented. All these experiments try to examine the validity of the hypothesis that evolutions that begin at very similar initial conditions evolve in a completely different manner. Finally, the influence of the different parameters of the WBR model over the dynamical evolution of the system is examined.

4.2 Sensitivity to Initial Conditions and Lyapunov Exponents

There is still no agreement for an exact definition of a chaotic dynamical system. Further research and stronger mathematical theory are required before a consensus about such definition is reached. However, there is one property that all chaotic systems share and which makes them interesting. This property is the sensitivity to initial conditions (henceforth called SIC). The SIC property means that nearby trajectories in the phase space will move away exponentially fast from each other on the average. It implies then that no matter how precisely variable measurements are taken in a chaotic system, errors will grow and dominate the solution making all long-term predictability impossible.

Complexity is by no means a requirement in order for a system to exhibit SIC. A system as simple as the logistic equation $x_{n+1}=ax_n(1-x_n)$ (with **a** a parameter in [0,4] and x_n in [0,1]) can exhibit this property. Figure 4-1 shows the evolution of two initial conditions $x_0=0.2$ and $x_0=0.2001$ in different regimes: one periodic and one chaotic. In the periodic regime (**a**=3.5) both solutions evolve side by side and the distance between them remains bounded for all time. On the other hand, in the chaotic regime (**a**=4.0) even though the difference between the two initial conditions is very small, after some time the solutions evolve in a completely different fashion. Any small error can produce loss of predictability in the long term.

The rates at which nearby solutions diverge are called Lyapunov exponents. Their sign indicates whether nearby trajectories diverge exponentially (i.e. if SIC is present or not); positive signs imply chaotic behavior. Lyapunov exponents also indicate the time scale on which predictions within a certain accuracy level can be performed.

In mathematical terms [27], if d_0 is a measure of the separation between two trajectories of a dynamical system at a certain time, the distance between them at a later time can be described as:

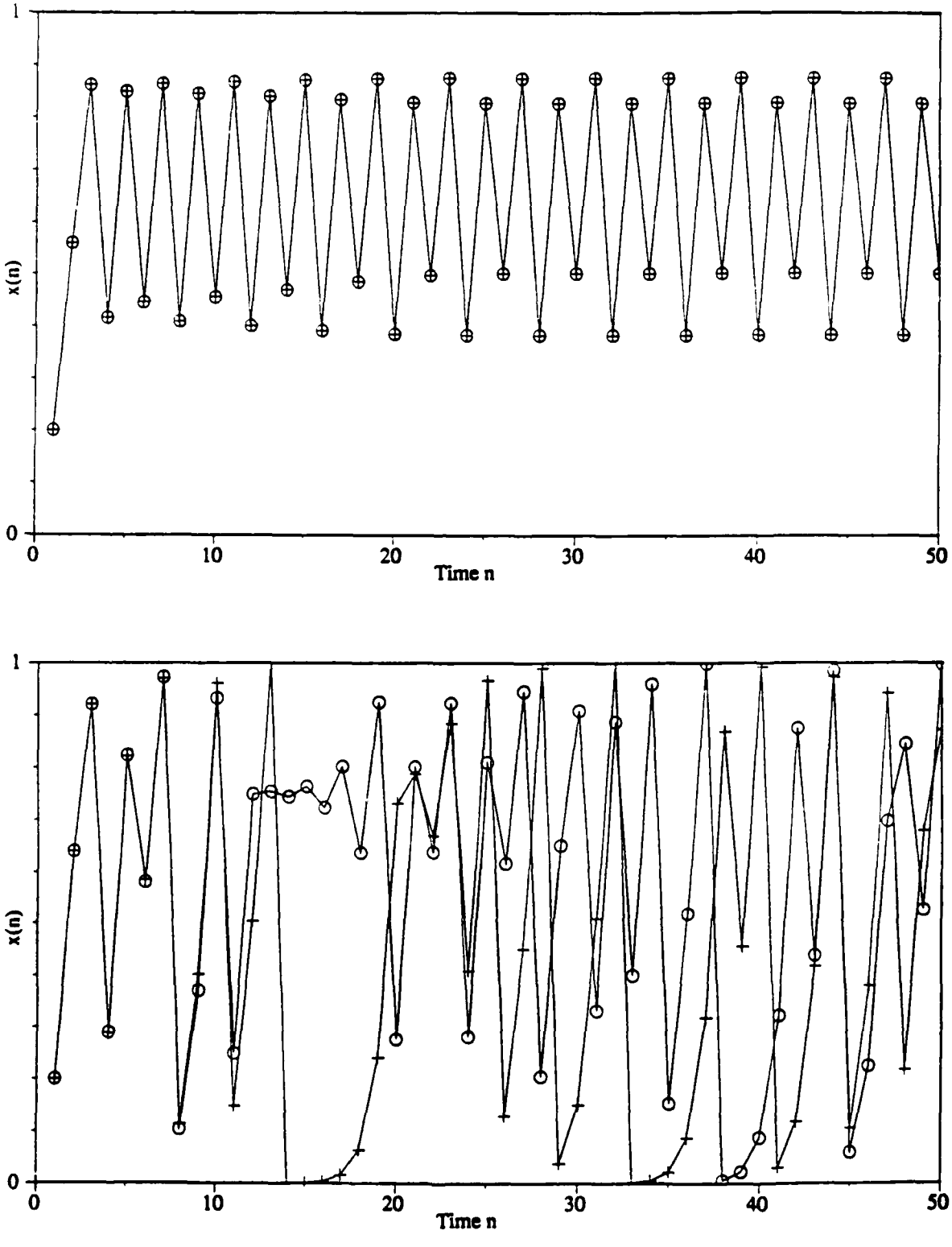

Figure 4-1: Logistic Equation. a=3.5 and 4.0 respectively

$$d(t) = d_0 e^{\lambda t} \tag{4.1}$$

where λ is the Lyapunov exponent. Figure 4-2 shows this property graphically. If λ is positive, the system displays SIC and behaves chaotically, otherwise the system behaves regularly. However, it is required that the dynamical system has dimensionality three or larger in order to exist the possibility of chaotic behavior.

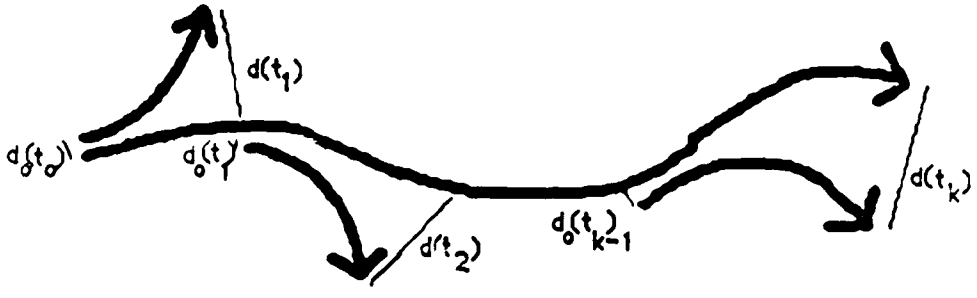

Figure 4-2: Exponential Separation of Trajectories in a Chaotic System

Of course, Equation (4.1) is not valid for all time because the system is bounded and the distance between trajectories cannot go to infinity. This is the reason why some average is required. Following Wolf et al. [48], a way to calculate the largest Lyapunov exponent is to take two nearby initial conditions, follow their trajectories in time and when the distance between them becomes too large, to replace one of the points with another one near the base trajectory. Section 4.6 will examine this idea in detail.

The Lyapunov exponent is calculated then as:

$$\lambda = \frac{1}{t_n - t_0} \sum_{k=1}^{n} log \frac{d(t_k)}{d_0(t_{k-1})} \tag{4.2}$$

where t_i is the time at which a new measurement is taken, $d(t_k)$ the distance between trajectories at time t_k and $d_0(t_k)$ the initial distance between the base trajectory and the new trajectory chosen at time t_k.

If the Lyapunov exponent λ is going to describe long-term behavior and have dependence on the initial condition used for its calculation, the average should continue for a long enough time. Notice also, if the system is 1-D and the time $t_k - t_{k-1}$ is small, the relation $d(t_k)/d_0'(t_{k-1})$ tends to the derivative $f'(x_{k-1})$ of the solution of the system.

For systems of dimensionality larger than one, a whole set of Lyapunov exponents can be defined, each of which describes the divergence of trajectories in a particular direction. In a n-dimensional system a small n-ball of initial conditions evolves into an n-ellipsoid with time. The exponential rate at which the different n principal axis of this ellipsoid grows or decays is the generalization of the concept of the 1-D Lyapunov exponent. Figure 4-3 from [27] explains this effect. The sum of all the Lyapunov exponents is the time-averaged divergence of its phase space. Wolf et al. [48] use this idea to calculate Lyapunov exponents: the growth of length elements (distance between two trajectories) gives the largest Lyapunov exponent; the growth of area elements (using three trajectories) gives the sum of the largest two exponents and so on.

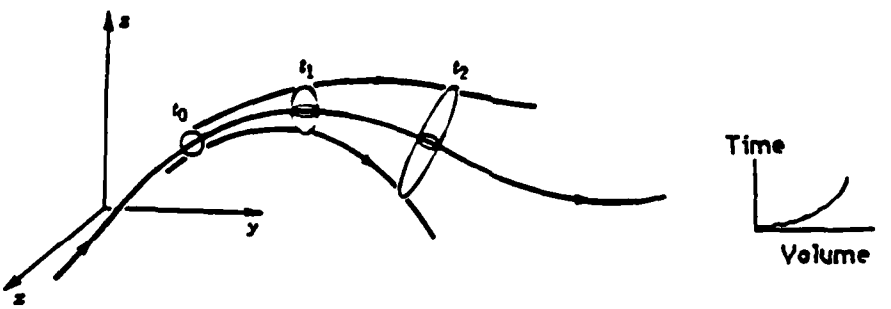

Figure 4-3: The Divergence of Volumes in Chaotic Systems

A word of caution is necessary at this point: there is a stricter definition of Lyapunov exponents and expansion rates of a dynamical system. This definition examines the eigenvalues of the transformation matrix corresponding to the linearization of the original dynamical system. Given that the linearization as well as the direction of its eigenvectors vary with time, an average over time of the eigenvalues is used to define Lyapunov

exponents (see Berge et al. [3] for details). In this case the exponents also measure average linearized expansions and contractions. It is expected that both definitions (the experimental and the theoretical) are strongly related but further research is still necessary.

4.3 SIC in the Catchment Evolution Model

The WBR model has not only non-linear time evolution but it is also a spatially extended system. Apart from some works by Kaneko and co-workers [16], [17] and [23] in coupled logistic maps, studies of chaotic behavior in spatially extended systems do not exist. They are to be expected in future years once the mathematical theory advances enough to look at problems of turbulence where both time and space are inherently unpredictable. This section will try to apply and generalize the concepts described in Section 4.2 to the WBR model.

The first problem is to define a measure of distance between trajectories in order to study the evolution of d(t) as in Equation (4.1). A plausible definition of the distance between two elevation fields $\mathbf{Z}_1$ and $\mathbf{Z}_2$ is:

$$d_{12}(t) = \|\mathbf{Z}_1(t) - \mathbf{Z}_2(t)\| = \sum_{allnodes} |z_1^{(t)}(i,j) - z_2^{(t)}(i,j)| \qquad (4.3)$$

where $z^{(t)}(i,j)$ is the elevation of node (i,j) at time t. Measure (4.3) will be called the relief difference between elevation fields $\mathbf{Z}_1$ and $\mathbf{Z}_2$. In stricter mathematical terms, if the elevation at each node is considered as an independent component of an n*m-dimensional vector (where m and n are the vertical and horizontal dimensions of the numerical grid respectively), then (4.3) is the L_0-norm in the n*m-D space. Of course, any other valid norm in this space, for example the square root of the sum of the squares of the elevation differences at grid nodes can also be used.

The SIC property can be tested then, under different conditions in the WBR model. Two initial elevation fields are taken such that the distance (i.e. the relief difference)

between them is small and the evolution of both catchments is followed measuring $d_{12}(t)$. If the system were regular $d_{12}(t)$ would remain bounded for all times. In the experiments performed, a base elevation field $\mathbf{Z}_b$ was chosen randomly: elevations were drawn from an uniform distribution with a very small coefficient of variation. Its evolution was compared against trajectories of points in phase space (initial elevation fields in real space) near the base elevation field. The details of how these points are chosen is described in the following two sections.

4.4 Behavior of One-Node Perturbations

Once the base initial elevation field $\mathbf{Z}_1(0)$ is fixed, a way to choose another elevation field $\mathbf{Z}_2$ "near" $\mathbf{Z}_1$ is to perturb the elevation at one of the nodes by a small amount. The measure of how separate $\mathbf{Z}_2$ is from $\mathbf{Z}_1$ is given by the relief difference between them. Given that only the elevation at one node is varied, $d_{12}(0)$ is equal to th variation in z at that node. Figure 4-4 shows the location of points at which the elevation was perturbed in each case. The final network is presented only for illustrative purposes; at the beginning of the simulation no channel network exists. The elevation was changed by the same amount in every experiment (approximately 3% of the notch). Figure 4-5 shows the evolution in time of the value of the relief difference (i.e. the distance in phase space) between $\mathbf{Z}_1$ and $\mathbf{Z}_2$. Notice how, for some of the cases, $d_{12}(t)$ grows exponentially with time and continue this expansion until the network captures the entire catchment. Once the catchment is captured, at approximately dimensionless time 1500 in the experiment shown, the growth of $d_{12}(t)$ stops. Then, the relief difference between the random fields begins to decrease slowly because in the case with episodic uplift both catchments tend ultimately to a flat plane. The exponential separation between trajectories is an indication of the transient chaos present in the WBR model. The logarithmic scale in the relief difference axis makes it possible to infer visually that the sign of the Lyapunov exponent (which corresponds to the slope of the graphs) is positive.

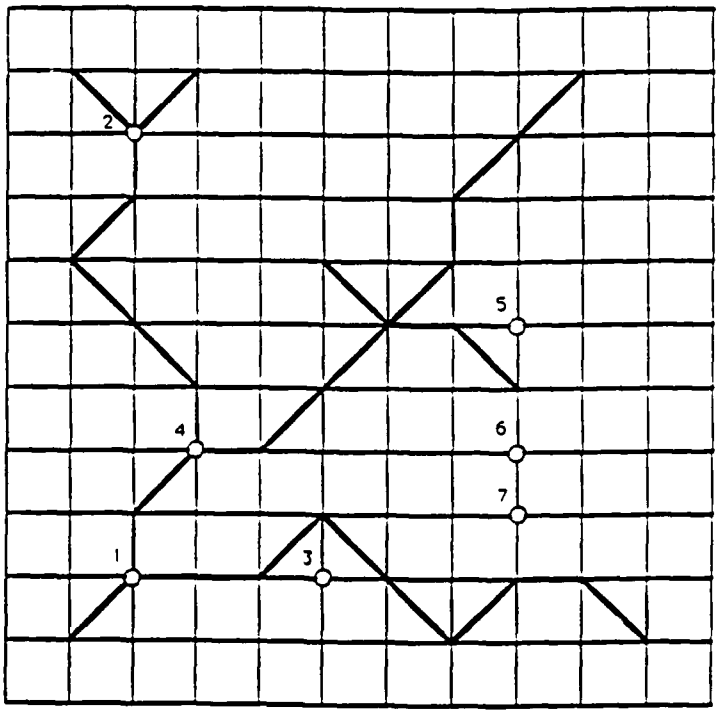

Figure 4-4: Location of Nodes with Perturbed Elevations

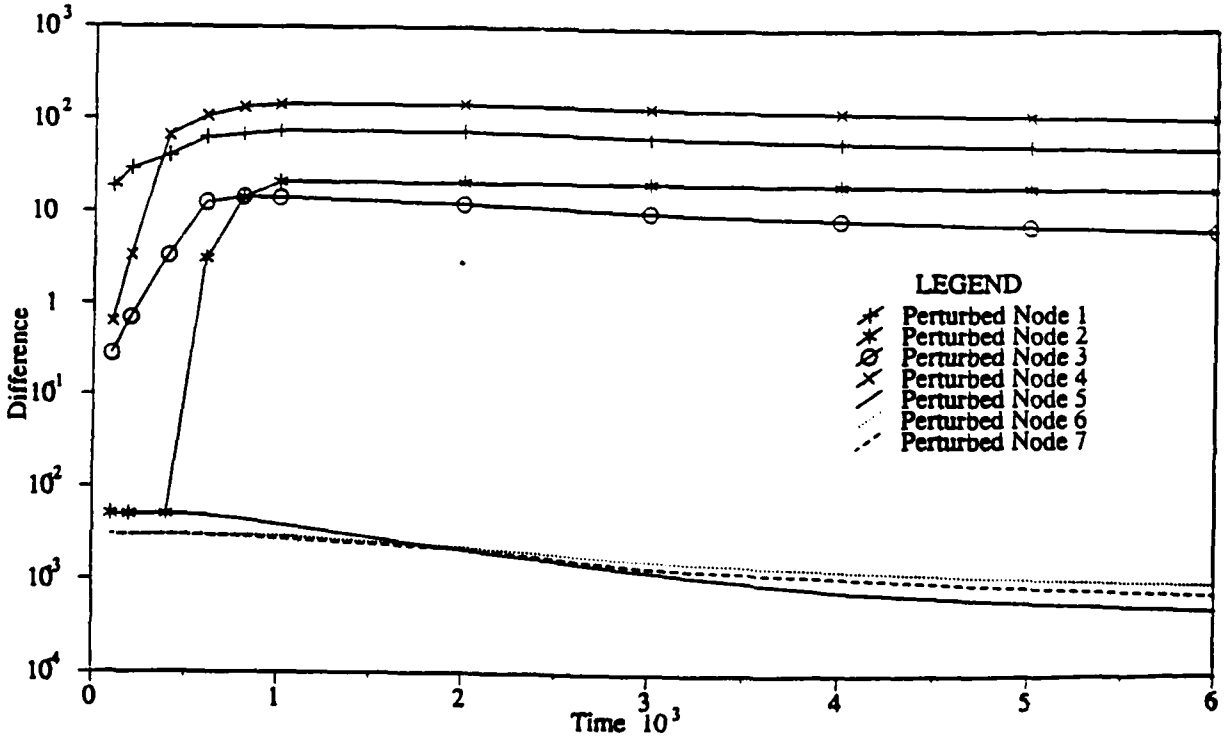

Figure 4-5: Difference Relief for One-Node Perturbed Elevation Fields

Some other trajectories do not diverge exponentially from the base trajectory during the whole network expansion period as can be seen in Figure 4-5. In these cases $d_{12}(t)$ decreases rapidly even if there was a small initial expansion. The interesting fact is that the final networks are identical in the bounded case while on the exponentially divergent cases the resulting networks are completely different. In terms of the phase space, the base trajectory attracts some of the perturbed trajectories. The relationship between exponential divergence and different final network is one-to-one. Final networks are presented in Figure 4-6

There are some features common to the chaotic behavior of the Meinhardt and the WBR systems. The analytical formulation of the Meinhardt model permits the ellucidation of the way in which perturbations grow and dominate the solution (see [47]). Fluctuations in the channel formation function near the branch will propagate in an unstable manner, and fluctuations away from the differentiation process are reduced. However, if the differentiation boundary passes at a later time through the zone where traces of the original fluctuations still exist, then they also propagate unstably. In the WBR model, elevation perturbations affect both flow directions and channel formation function values (the latter through the slope factor in the channel formation function equation).These variations enter into the model equations and eventually dominate the solution. Notice also that perturbations at nodes away from the differentiation process do not grow at all.

This unstable propagation of fluctuations raises the issue of whether the numerical solution of the WBR model is really a true catchment evolution. Given that numerical errors grow unstably, the numerical solution may not be a true trajectory. A possibility is that the numerical solution bounces around different real trajectories of the dynamical system. However, recent research by Yorke, Grebogi and coworkers [12] in simple systems seems to indicate that there is always a true solution near a numerical one in chaotic dynamical systems. Even though further research is still necessary, these preliminary steps

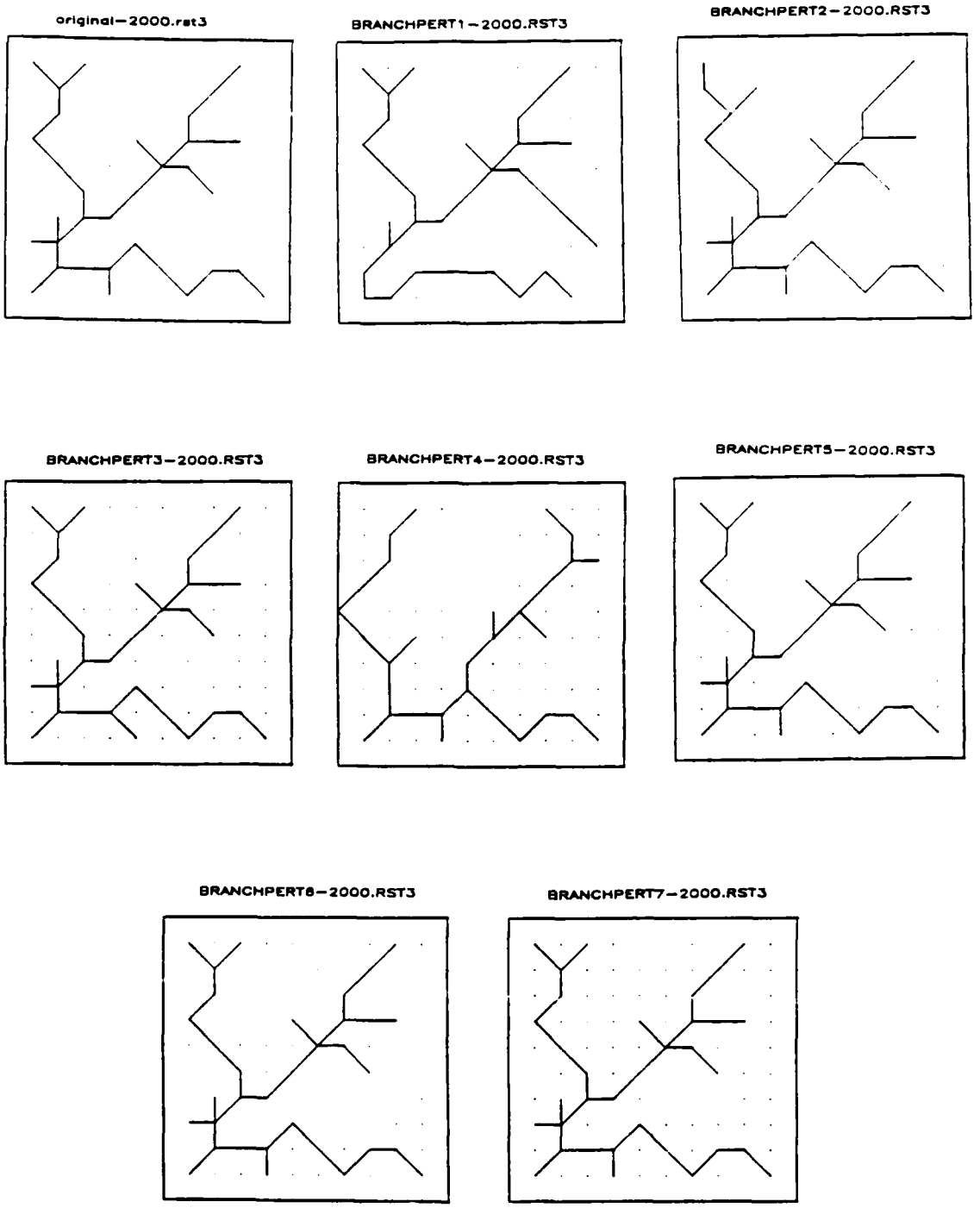

Figure 4-6: Final Networks for One-Node Perturbed Elevation Fields

give confidence on the good behavior of numerical solutions of chaotic dynamical solutions. Of course, long-term predictability is not possible in these systems if the precision is finite.

4.5 Expansion of a Ball in the Phase Space of Elevation Fields

In Section 4.4 $\mathbf{Z}_2$ was constructed by changing the elevation at one node in $\mathbf{Z}_1$. Another possibility is to change the elevations at every node, i.e. to take a completely different initial elevation field drawn from the same distribution to which $\mathbf{Z}_1$ belongs. Given that the coefficient of variation of the uniform distribution of node elevations is small, the relief difference $d_{12}(0)$ will be also small. Thinking in terms of the n*m-D phase space, perturbations at one node correspond to movement along one of the axes while perturbations corresponding to new random elevation fields are represented by points positioned away from the origin into the space. Various trajectories corresponding to different initial random fields were compared in time with the evolution of $\mathbf{Z}_b$. These initial elevation fields can be viewed as a ball in the phase space. The deformation of this small ball was followed. The goal was to examine the possibility of exponential growth of the ball as in Figure 4-3 in section 4.2 . If exponential growth occurs, the SIC property is shown not to be restricted to single node perturbations and the sum of the Lyapunov exponents can be studied.

Figure 4-7 shows three measures of the ball's evolution: the maximum and the minimum values of the set of the relief differences, and the maximum distance between trajectories. All three measures provide insight into the ball expansion process. The second measure proves that it is not a small group of trajectories that is diverging from $\mathbf{Z}_1$ but that effectively all of them are moving away exponentially fast. The last measure gives an idea of the largest principal axis size (its exponential rate is equivalent to the largest Lyapunov exponent, see [27]).

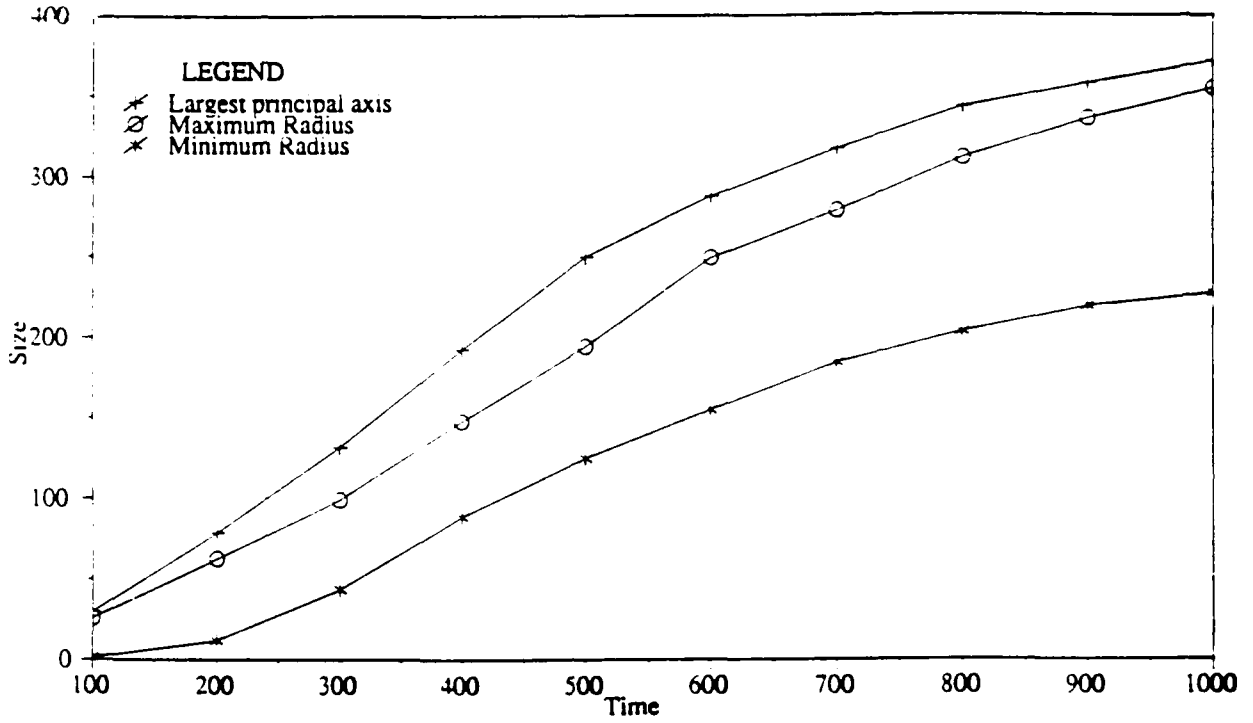

Figure 4-7: Three Measures of the Expansion of a Volume of Nearby Initial Random Fields in Phase Space

Even though a very large number of points is required to determine with precision the value of the sum of the Lyapunov exponents based on the volume expansion of the ball of initial conditions, Figure 4-7 gives adequate certainty about the positive sign of the largest Lyapunov exponent and therefore the chaotic nature of the WBR system.

4.6 Another Test Related to the SIC Hypothesis

Another test, based on ideas by Wolf et al. [48] is to examine not only the evolution of trajectories corresponding to initial points near the base elevation field, but also to look at evolutions that begin near the base trajectory at later times, as was shown in Figure 4-2. This method has a clear advantage: given that the size of the domain under consideration in the phase space is finite, then exponential divergence cannot continue forever (as can be seen in Figure 4-5). That is the reason why in chaotic dynamical systems both time and space averages have to be taken in order to calculate Lyapunov exponents.

For this reason perturbations of the base elevation field were performed at different times and their trajectories were compared to the base field evolution. Results appear in Figure 4-8. In this figure the perturbations that begin at different timesteps have been translated to coincide with the origin. Times in the legend indicate the step at which the elevation field is perturbed. Notice that SIC and chaotic behavior is present only while the network is still growing. The network grows up to nondimensional time 2000; perturbations initiated after this point decay in time.

Once the network captures the catchment and provides rigidity to the elevation field, perturbations decrease with time. The WBR system exhibits what is called transient chaos. The largest Lyapunov exponent can be calculated using the different perturbations and Equation (4.2).

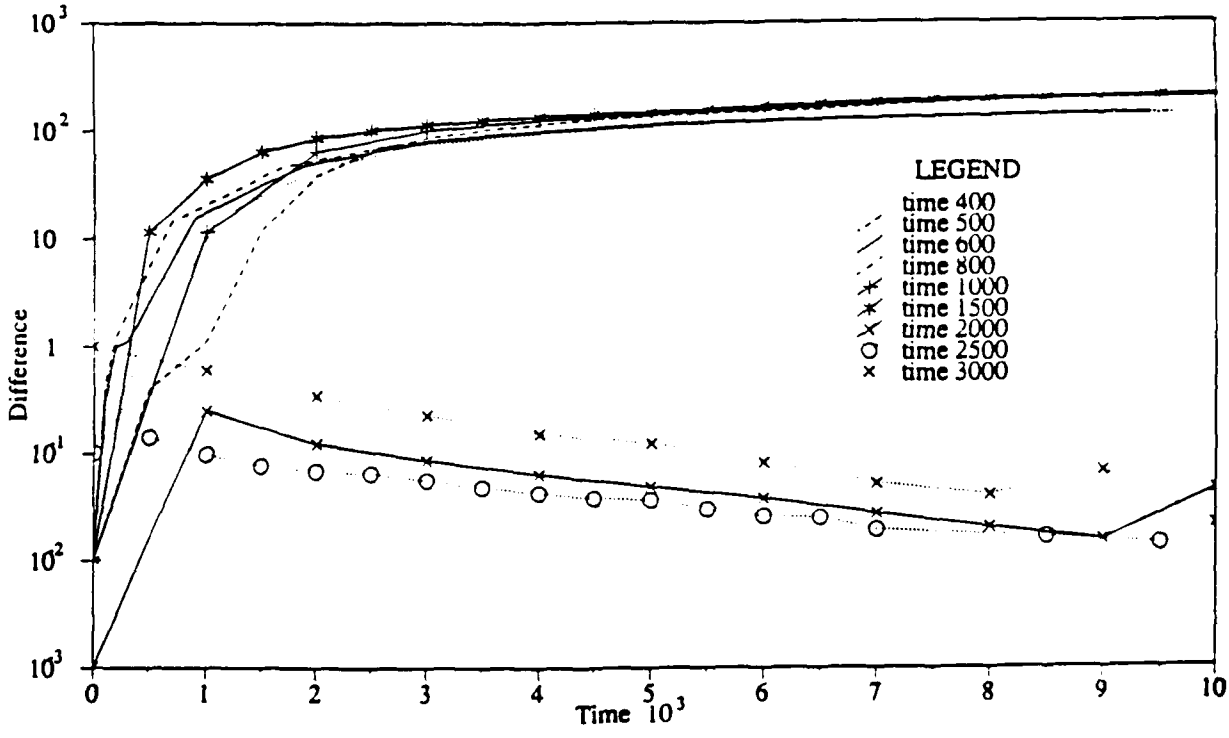

Figure 4-8: Relief Difference of Nearby Points Along the Base Trajectory

4.7 One-Node Perturbation Thresholds

By performing various experiments like the ones described in Section 4.4 it was found that there was a perturbation size threshold that has to be exceeded in order to have exponential divergence of trajectories in the system. This is to due to the one-to-one relation between the exponential divergence of trajectories and the change of network form, as well as the existence of an channel formation function threshold that has to be surpassed in order to trigger channelization. Of course, the fact that only eight possible flow directions are considered at each node also influences the perturbation threshold.

In classical chaotic studies the SIC property is always thought of in terms of infinitesimal perturbations. The WBR model behaves differently on this respect. Consider the base elevation field Z_b and choose a node. If perturbations are made to the elevation at that node, the perturbed fields are located along one of the axes of the phase space. The evolution of the relief difference for perturbations performed this way over Z_b at different nodes are shown in figures 4-9 and 4-10.

Notice that if the perturbation is small enough, even though the separation grows exponentially for some time, the distance between trajectories stops growing; it decreases even before the network finishes the capture process. There exists a threshold value, dependent on the elevation at neighboring nodes and on the parameter values but it is certainly small. Above this threshold the perturbed trajectory continues its exponential separation. These are the two different behaviors observed in Figures 4-9 and 4-10. In the experiments the original node elevation was 10.10428. if the elevation at that node in Z_2 were larger than 10.10850 or smaller than 10.10258 then the exponential separation occurs during the whole network expansion period. The jump at these two values occurs, not surprisingly with the change in network form. Regions in the catchment begin to evolve in a different manner and the trajectories in phase space diverge from each other. Thinking in

terms of the phase space, a cylinder of very small size exists around the base trajectory in which nearby trajectories behave differently from those outside the cylinder.

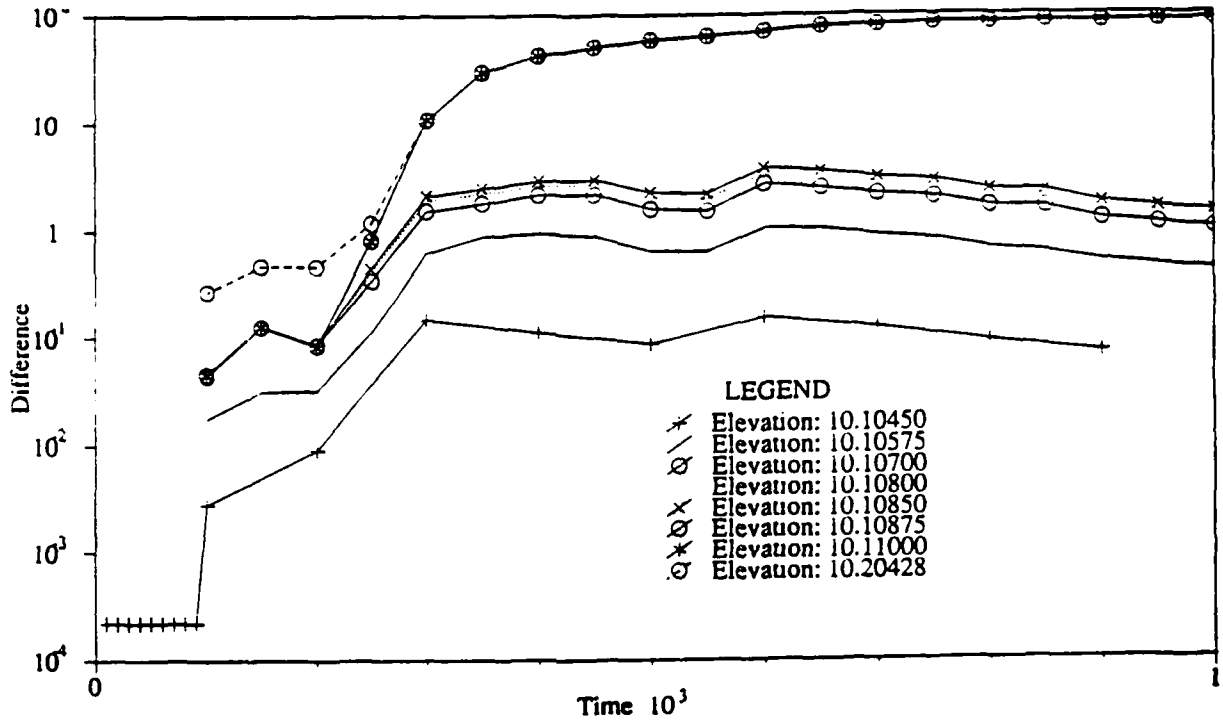

Figure 4-9: Perturbation Threshold One-Node Perturbations.
Upward Perturbations
Original Node Elevation 10.10428

The figures referred to earlier show a discontinuous jump between two regimes that vary continuously with the size of the elevation perturbation. Figure 4-11 coresponds to the slopes of least-squares lines fitted to the portion of the curves in the time interval [300,1000] in the semilog plane. The results shown in Figure 4-11 are based on both Figures 4-9 and 4-10. It can be observed that near the original node elevation (i.e. inside the cylinder in phase space) slopes are negative and the base trajectory attracts neighbor trajectories.

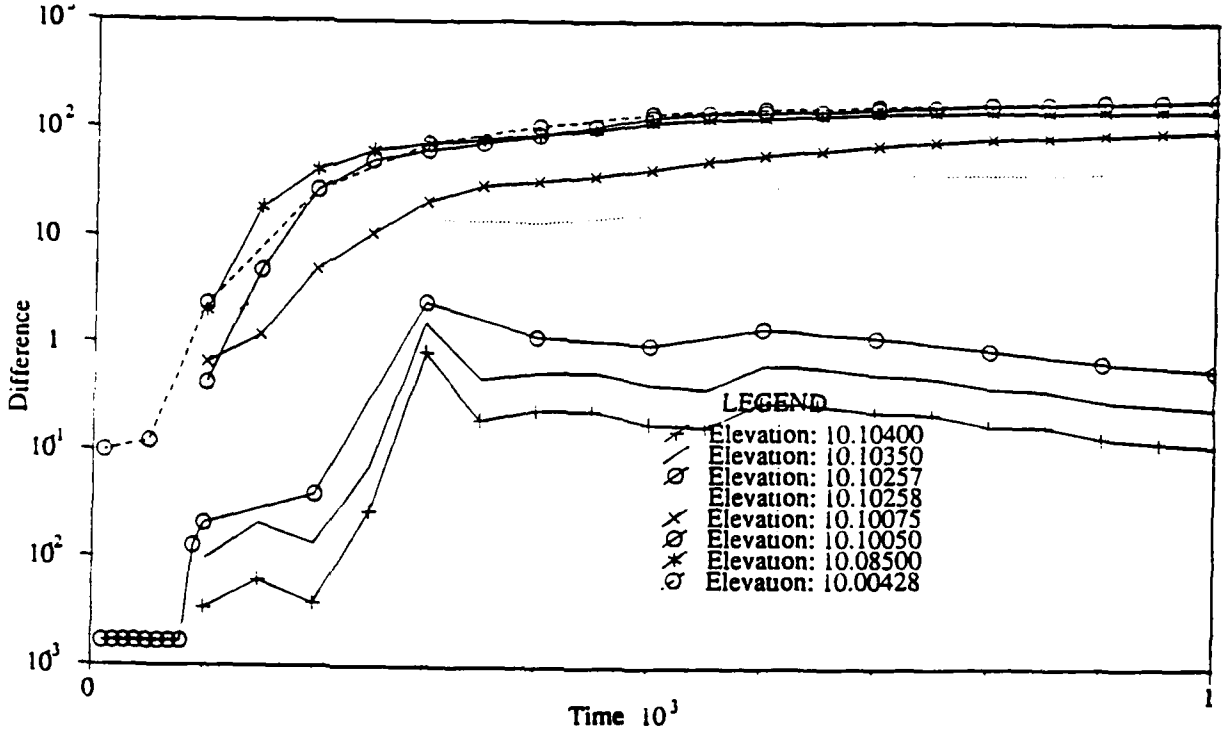

Figure 4-10: Perturbation Threshold One-Node Perturbations.
Downward Perturbations
Original Node Elevation 10.10428

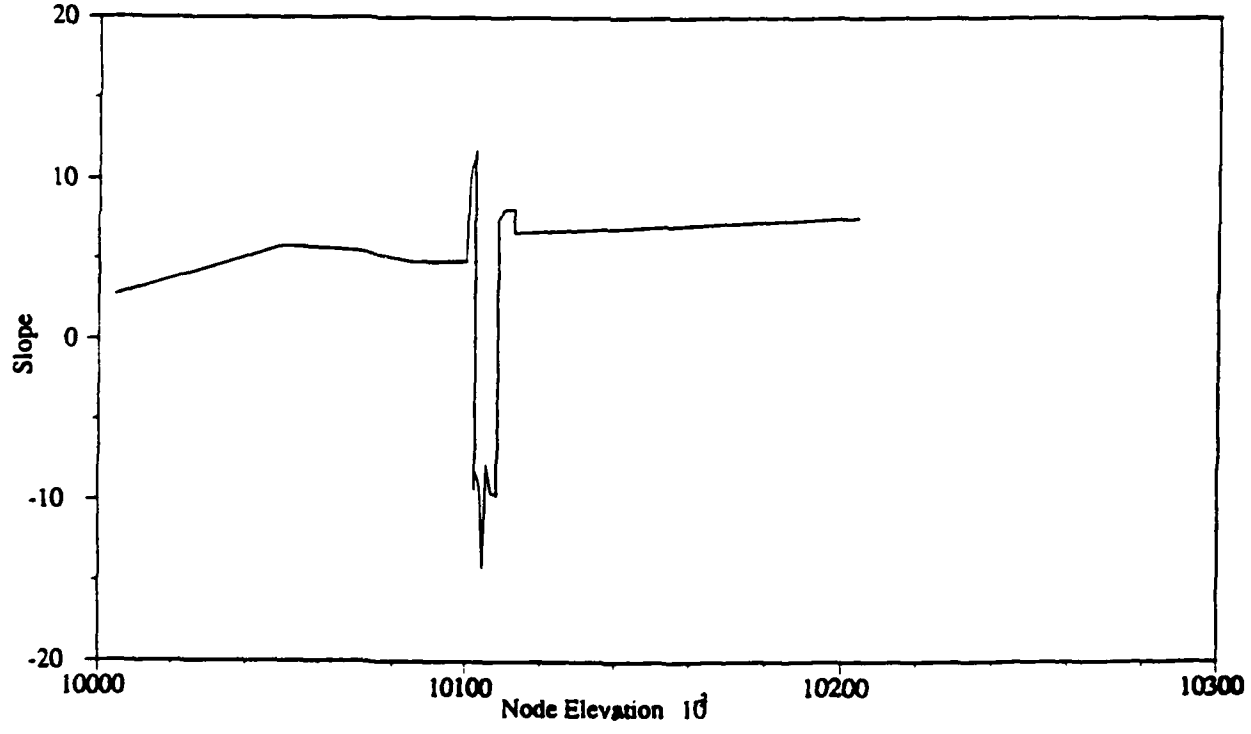

Figure 4-11: Slopes of Relief Difference Curves
Original Node Elevation 10.10428

4.8 Parameter Dependence of SIC

A number of parameters can be varied in the WBR model, and when this occurs the chaotic behavior of the system changes as well. The most important parameters to be studied are the exponents of the flow and slope terms in the sediment transport and channel formation function equations (m_1,n_1,m_5, and n_5 respectively), the channel formation function threshold ($1/c_1$), the coefficient β_3 used in the relation flow-area (a rainfall measure), the coefficient β_1 in the sediment transport formula and the relation between channel and hillslope sediment transport (O_t).

In the next set of experiments the evolutions of a base elevation field Z_b and a perturbed one Z_2 are again followed. The initial elevation field $Z_2(0)$ was chosen as in Section 4.5. This time, however, the fields under observation are kept constant and the parameter values are varied. This procedure will show the dependence of the divergence of the trajectories with respect to the parameter values. The following graphs show the exponential trajectory divergence of the same two random initial elevation fields for different parameter values. In each case a semilog graph corresponding to the long-term behavior, a semilog graph that covers the network growth period, and an arithmetic graph coresponding to that same period are presented. The first graph illustrates the behavior of the system during the dying period of the catchment, the second graph shows the whole period of network growth and the third graph presents in detail the most intense period of network expansion.

An increasing trend of the exponential rate of separation with increasing values of m_1 is observed in Figures 4-12 to 4-14. This effect appears simultaneously with an increase in drainage density in the final networks: the perturbation information is communicated over the whole catchment by the network. Without network there is no spatial communication of elevation differences and no exponential divergence exists. The same effect is observed in

the channel formation function threshold case (Figures 4-15 to 4-17). As c_1 increases, the drainage density increases because the channel formation function threshold is reduced and the exponential rate of divergence increases. A change of behavior occurs around c_1=0.0007 in this experiment because the network begins to lose its branched structure and a "blob" is formed instead.

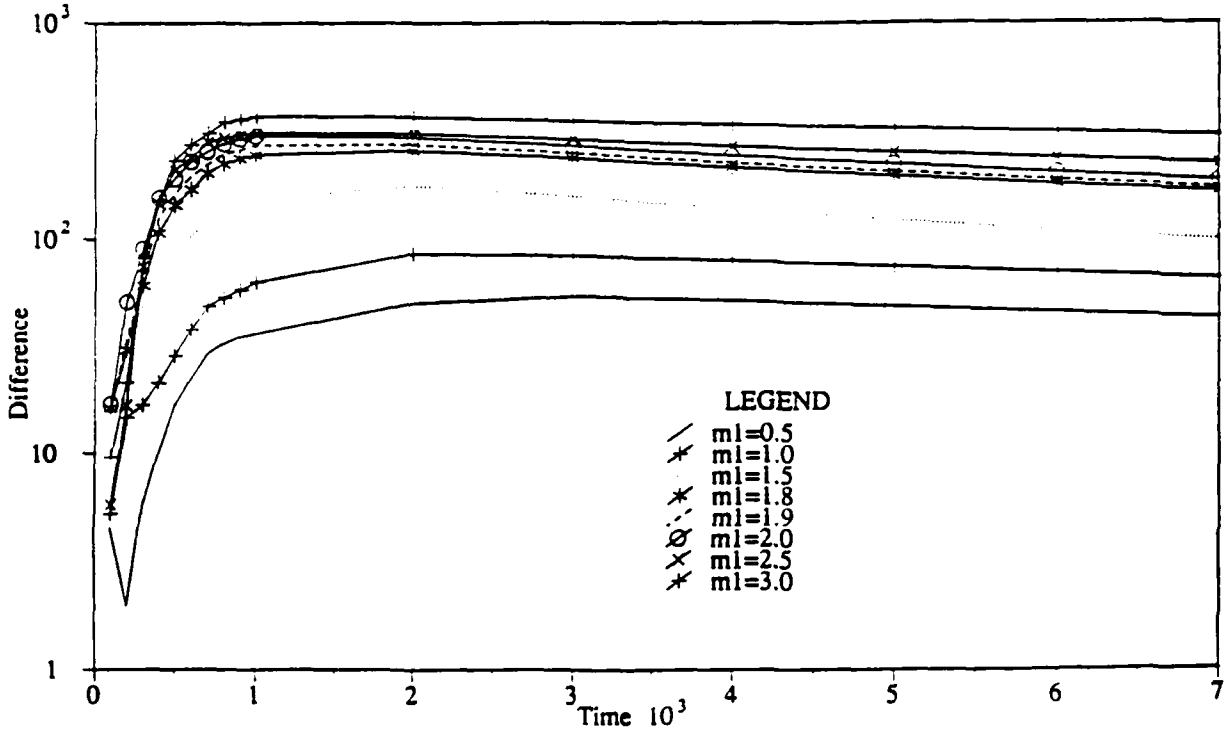

Figure 4-12: Relief Difference Under m_1 Variations

The variation with n_1 is in the opposite direction. In Figures 4-18 to 4-20, as n_1 increases, sharp peaks and steep slopes tend to be flattened out faster because the sediment transport is larger everything else being the same, so the separation rate between trajectories is smaller. The variations with β_3 shown in Figures 4-33 to 4-35 correspond to the relation between Lyapunov exponents and rainfall. In this case the drainage density is also a key factor in explaining the behavior observed. Figures 4-24 to 4-26 correspond to O_t variations. Notice how the relief difference decreases at long time in a manner directly correlated to the size of O_t.

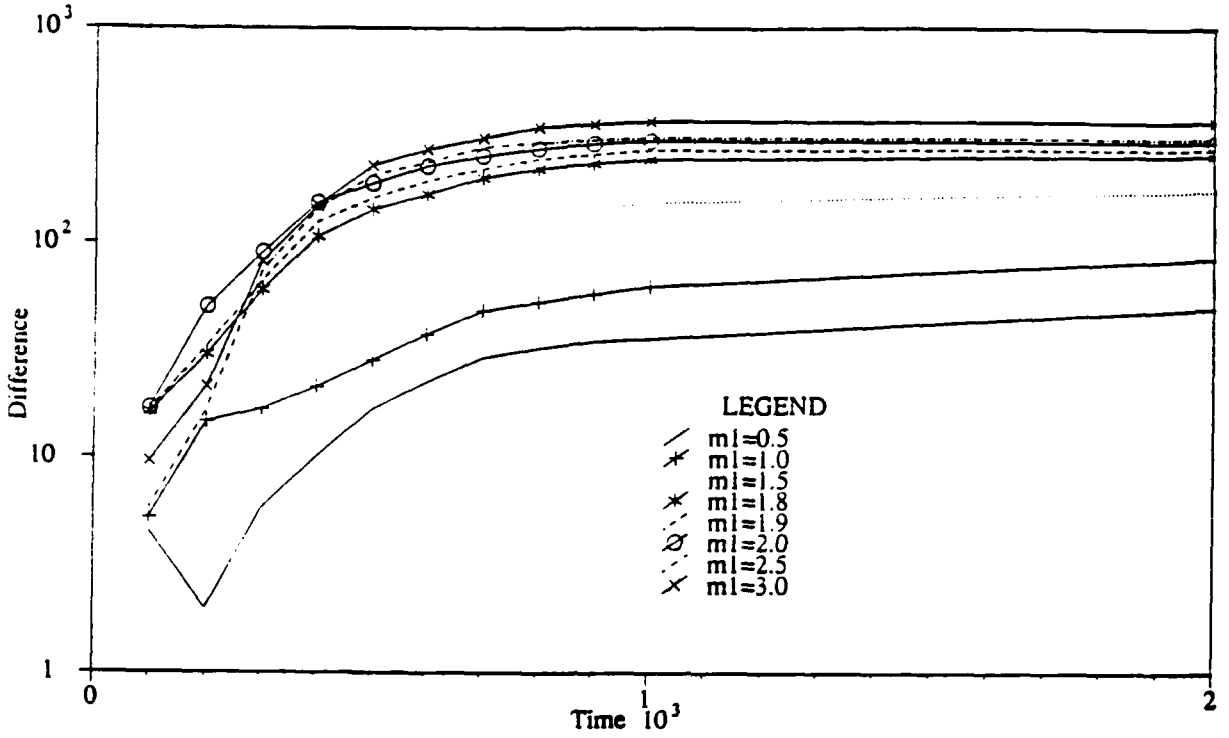

Figure 4-13: Relief Difference Under m_1 Variations During Network Growth

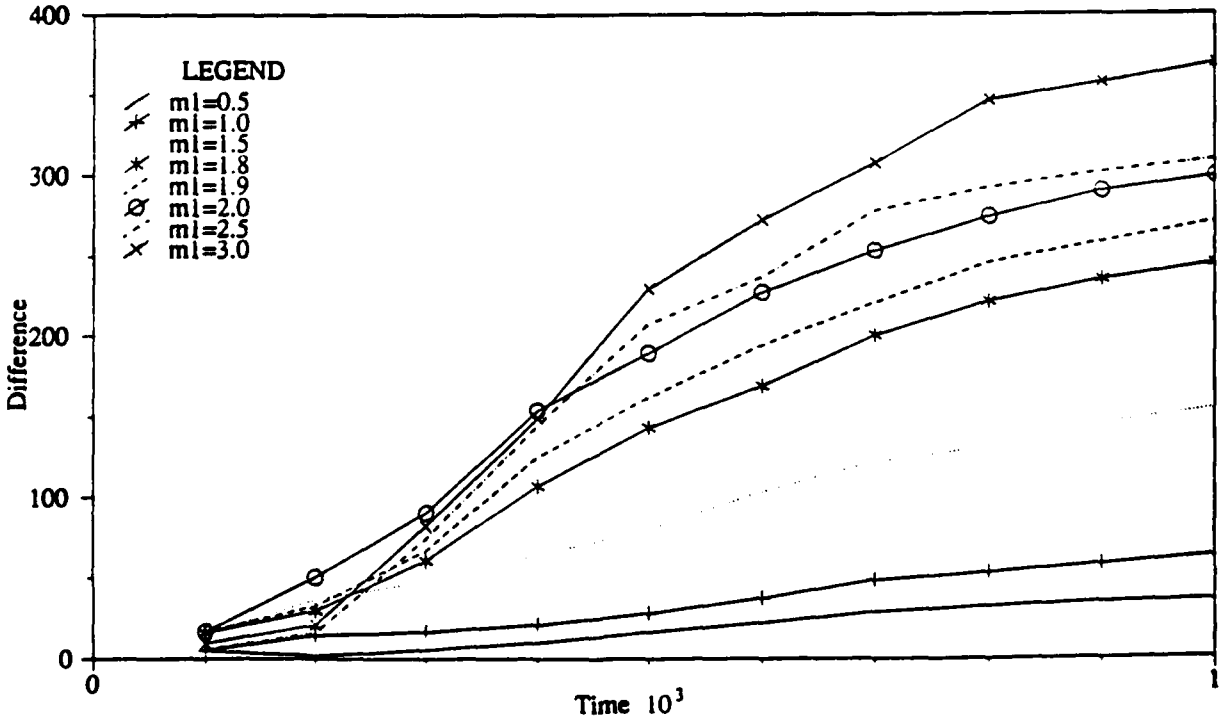

Figure 4-14: Relief Difference Under m_1 Variations.
Arithmetic Scale

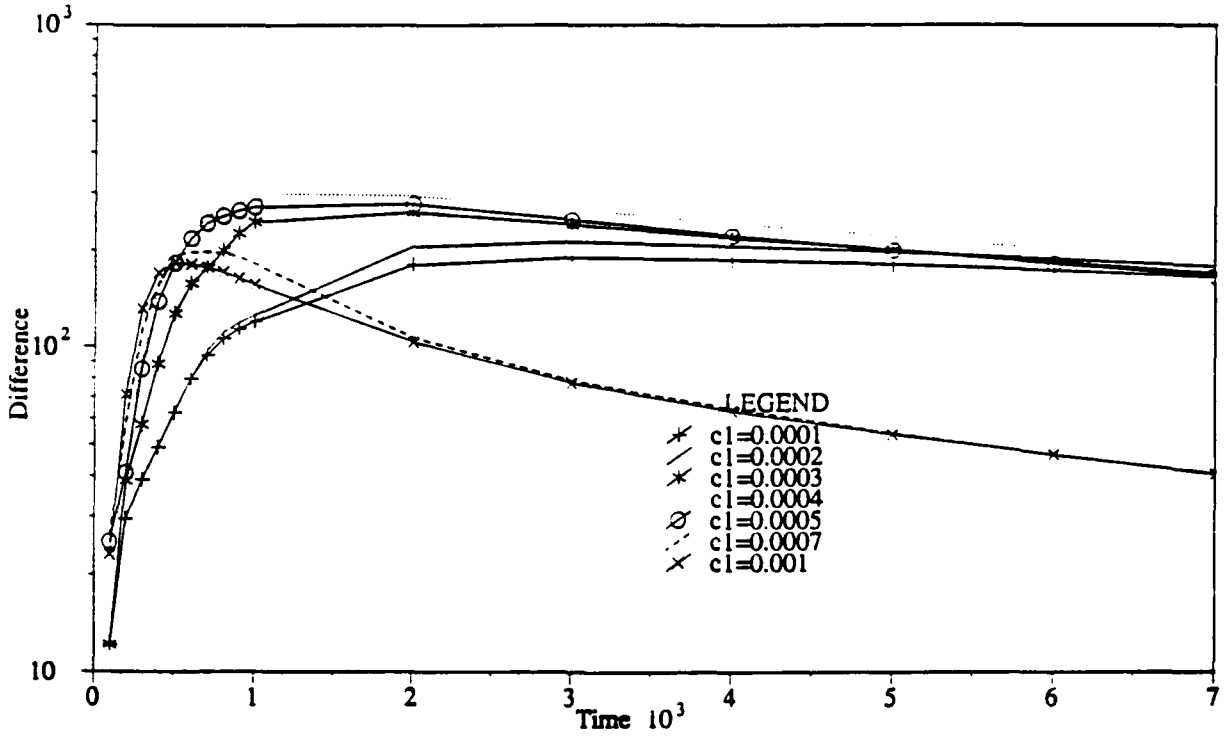

Figure 4-15: Relief Difference Under c_1 Variations

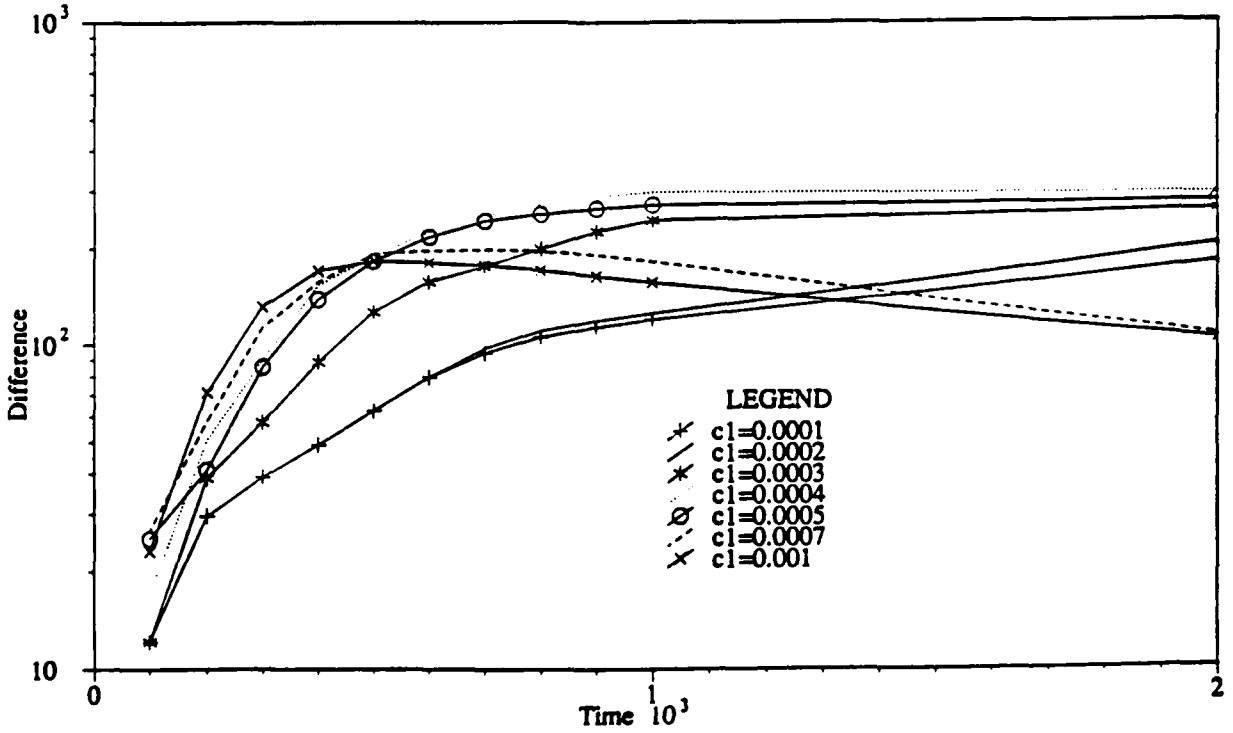

Figure 4-16: Relief Difference Under c_1 Variations During Network Growth

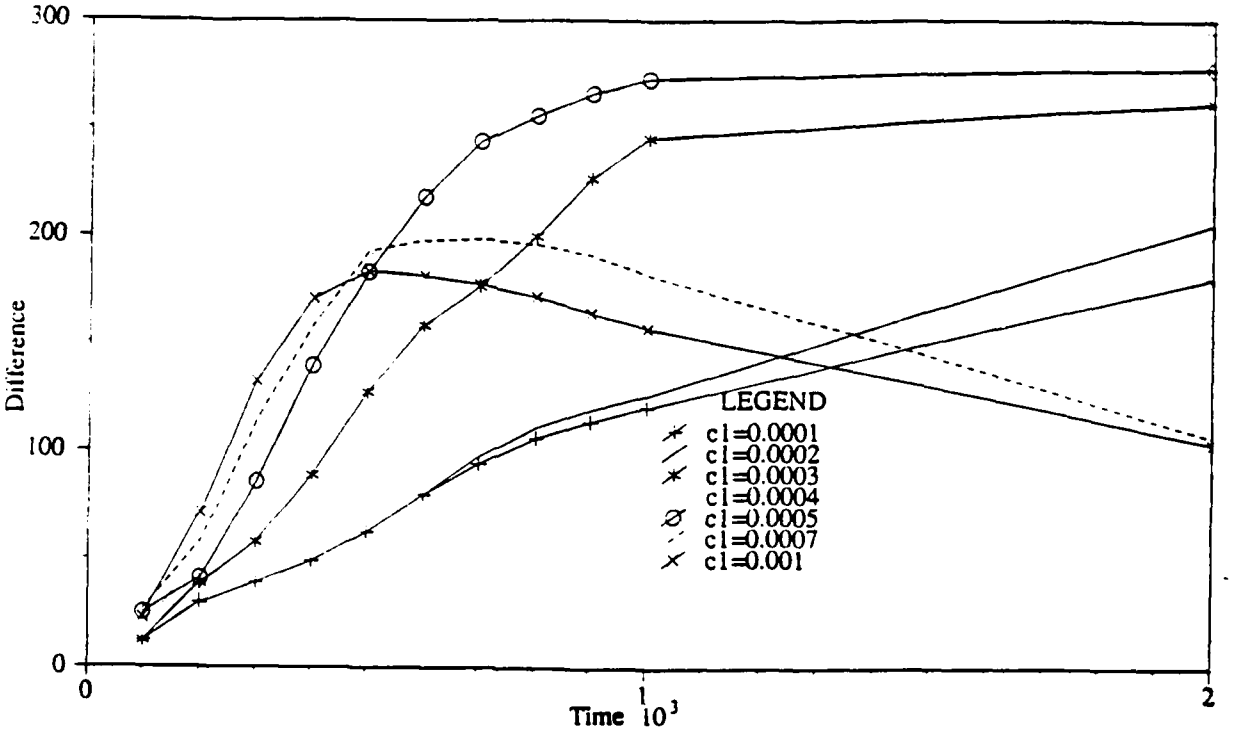

Figure 4-17: Relief Difference Under c_1 Variations.
Arithmetic Scale

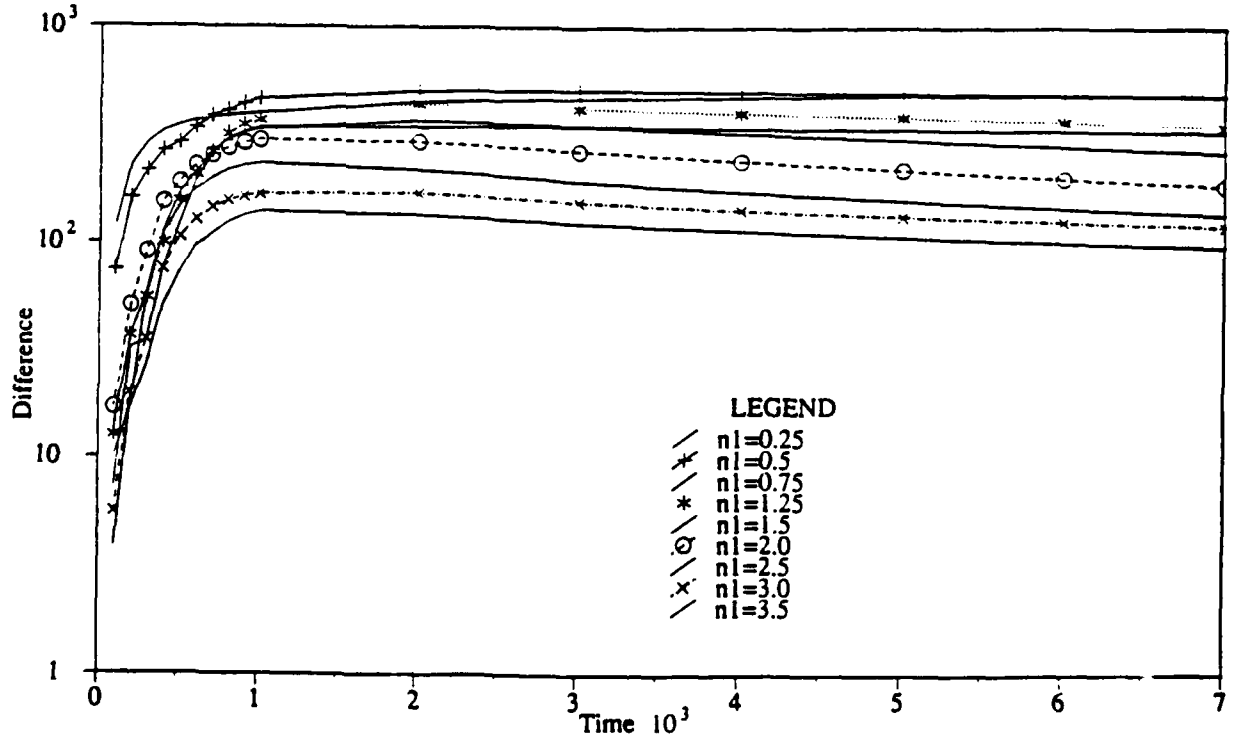

Figure 4-18: Relief Difference Under n_1 Variations

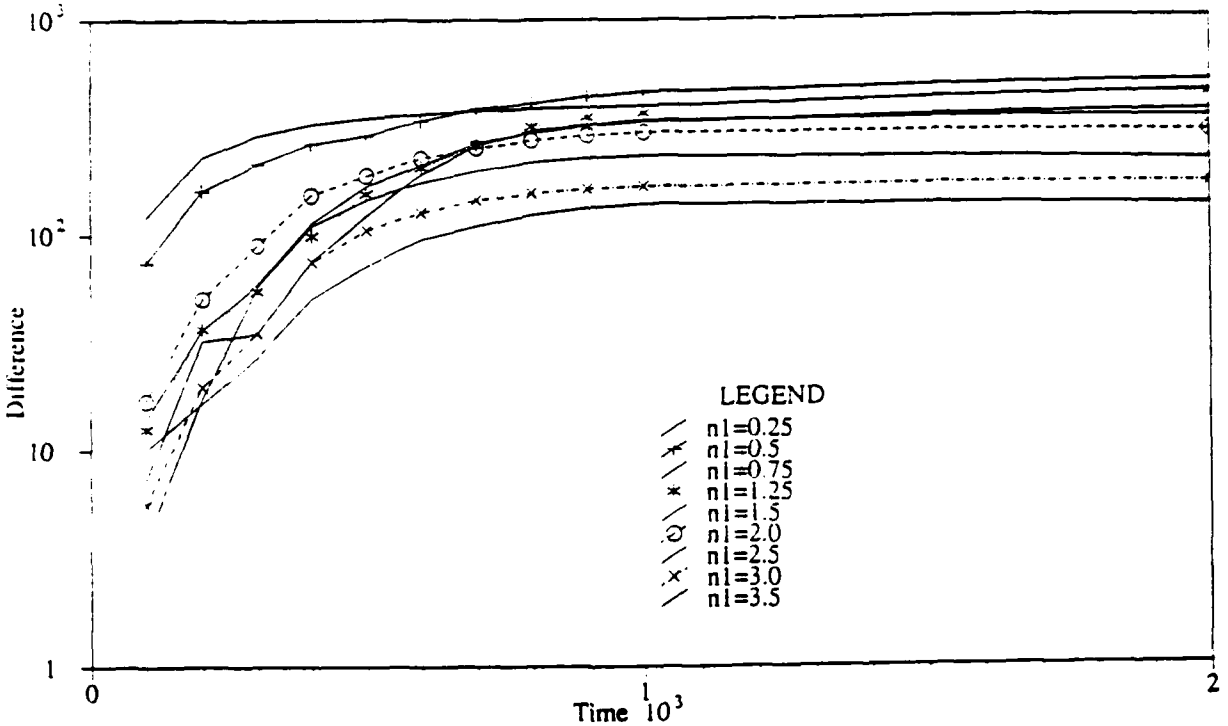

Figure 4-19: Relief Difference Under n_1 Variations During Network Growth

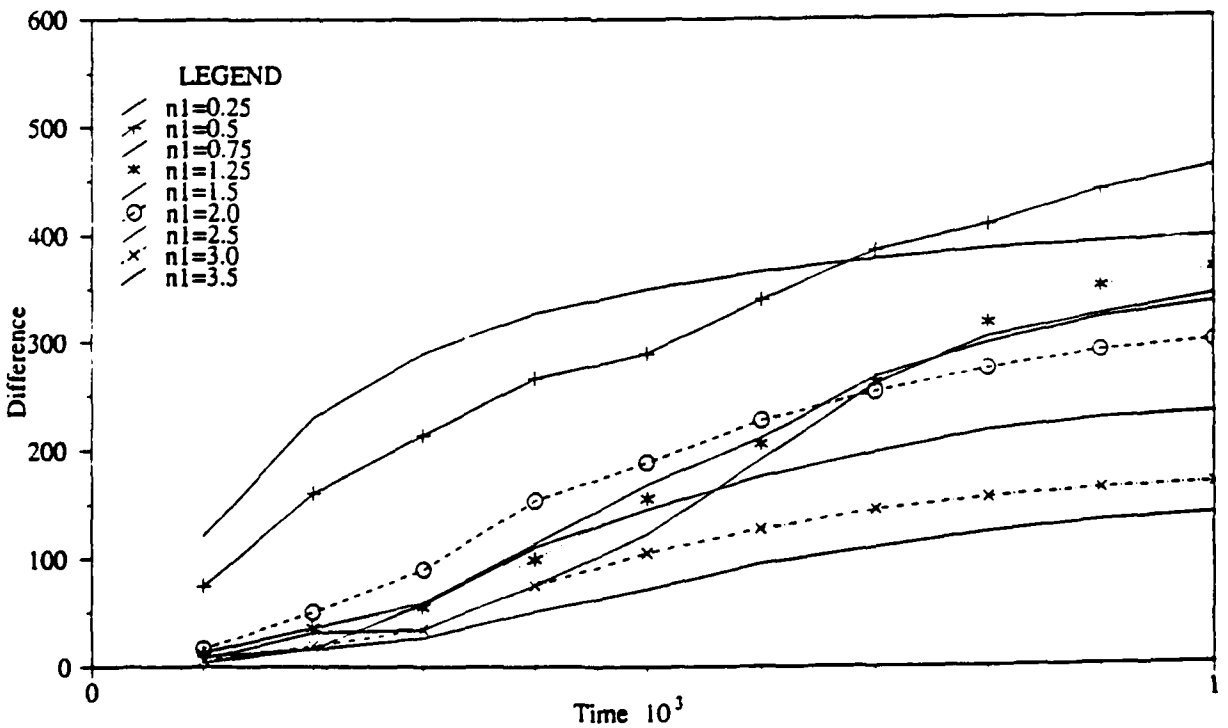

Figure 4-20: Relief Difference Under n_1 Variations.
Arithmetic Scale

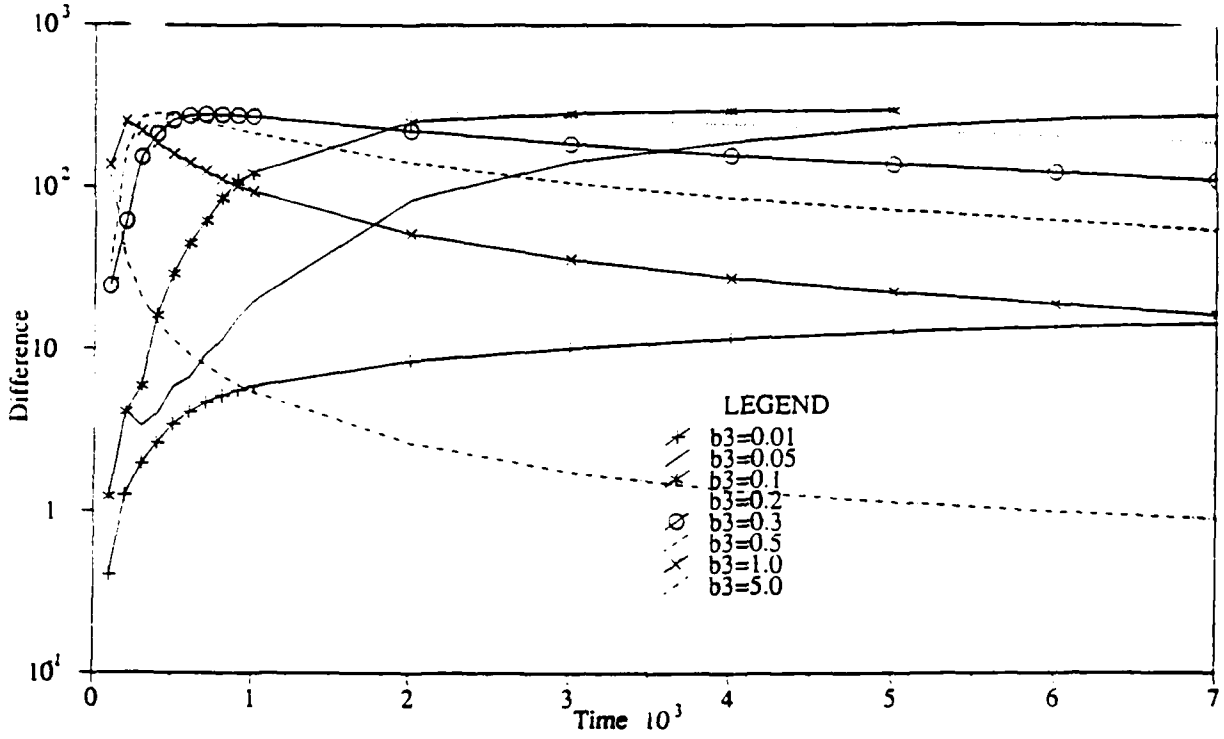

Figure 4-21: Relief Difference Under β_3 Variations

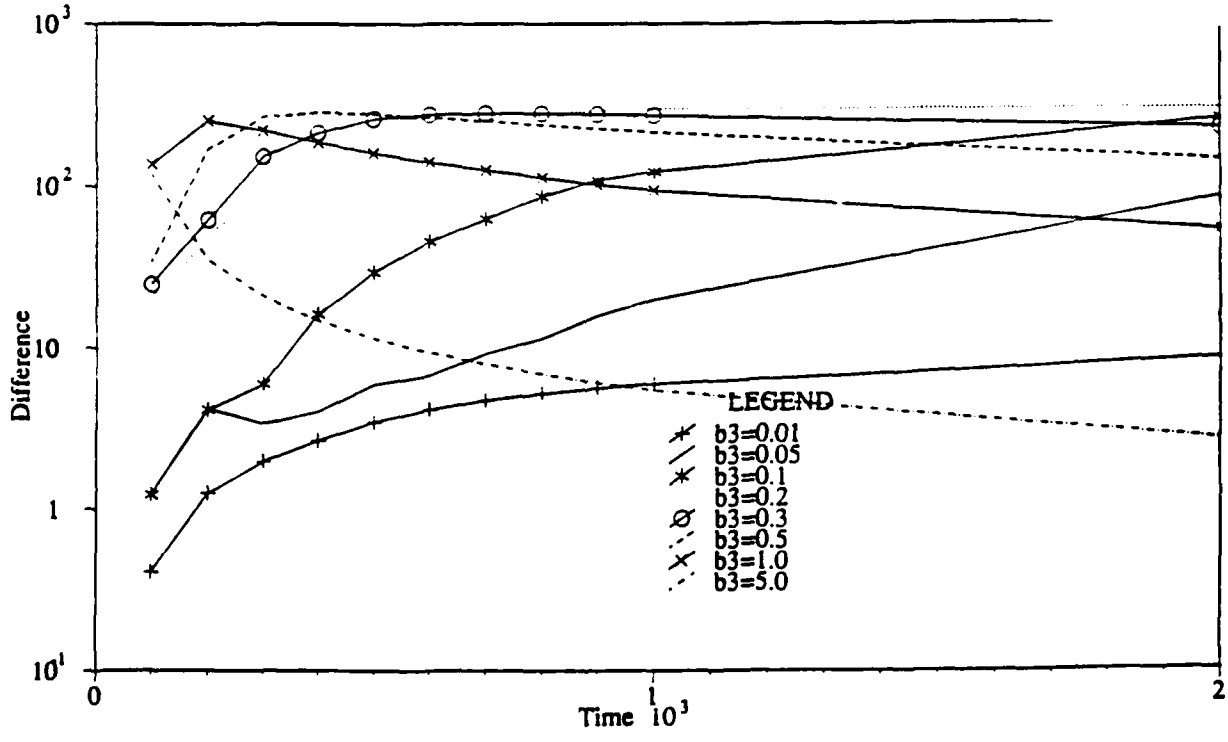

Figure 4-22: Relief Difference Under β_3 Variations During Network Growth

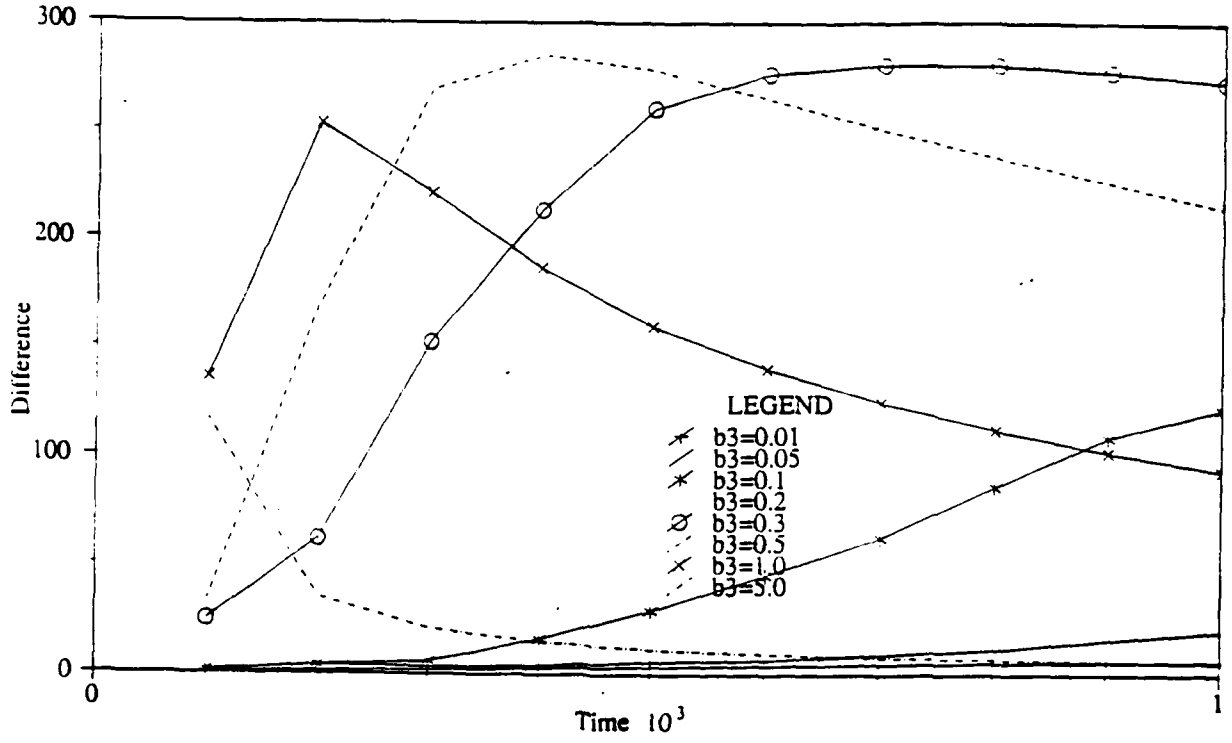

Figure 4-23: Relief Difference Under β_3 Variations.
Arithmetic Scale

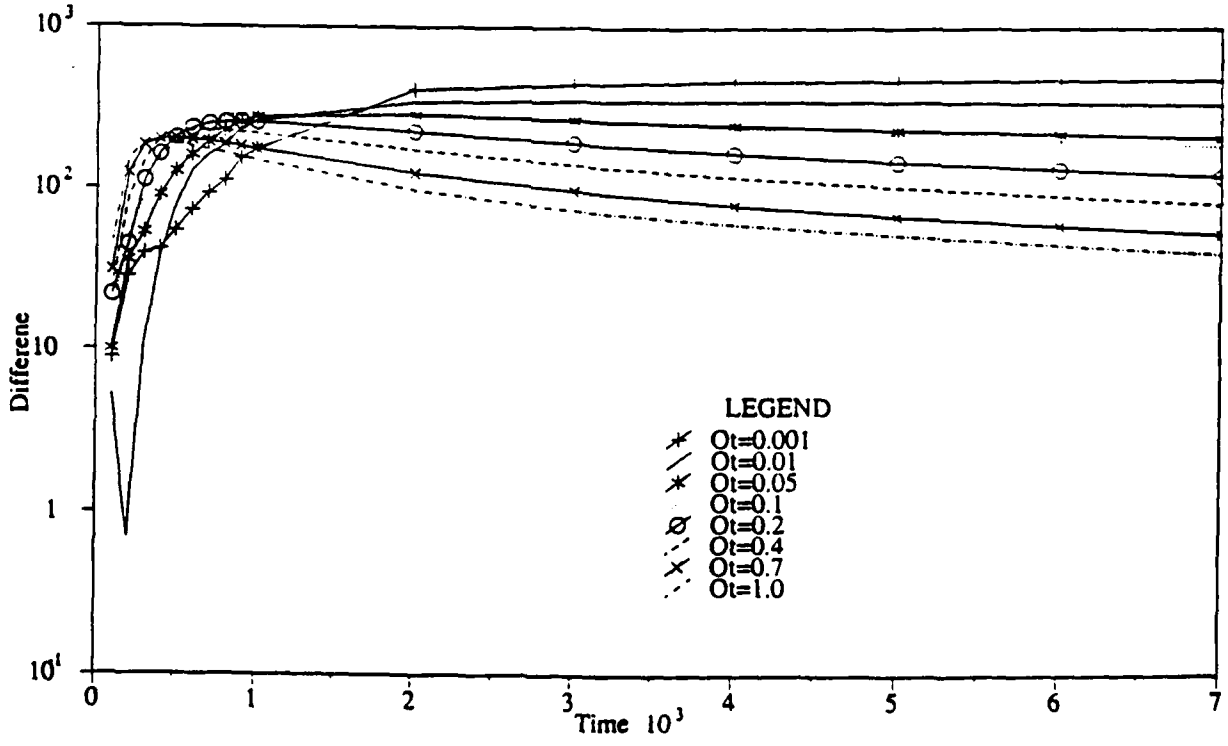

Figure 4-24: Relief Difference Under O_t Variations

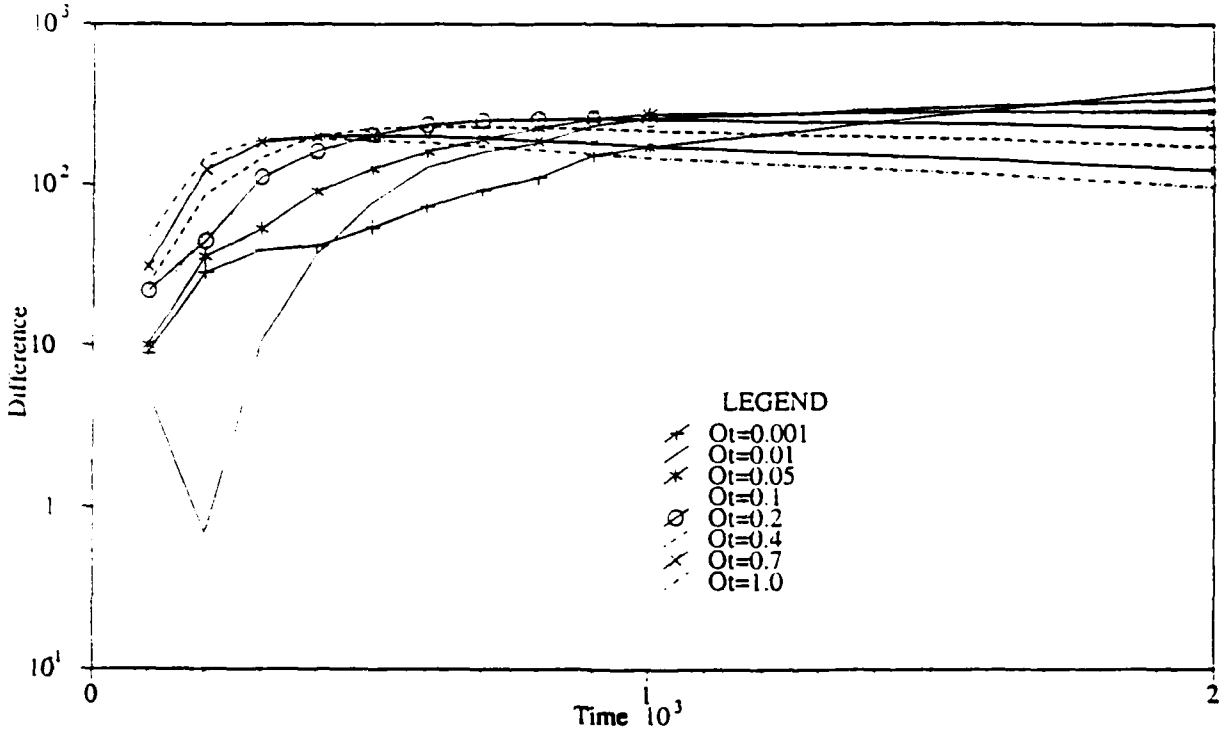

Figure 4-25: Relief Difference Under O_t Variations During Network Growth

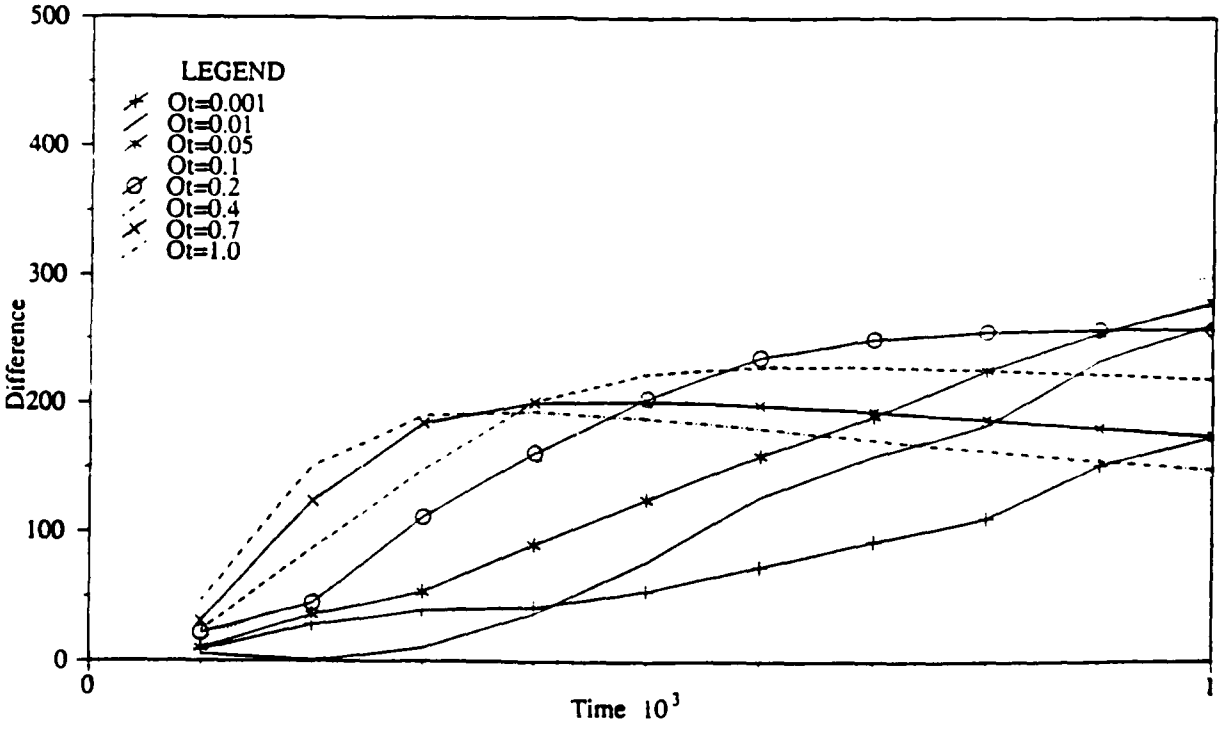

Figure 4-26: Relief Difference Under O_t Variations.
Arithmetic Scale

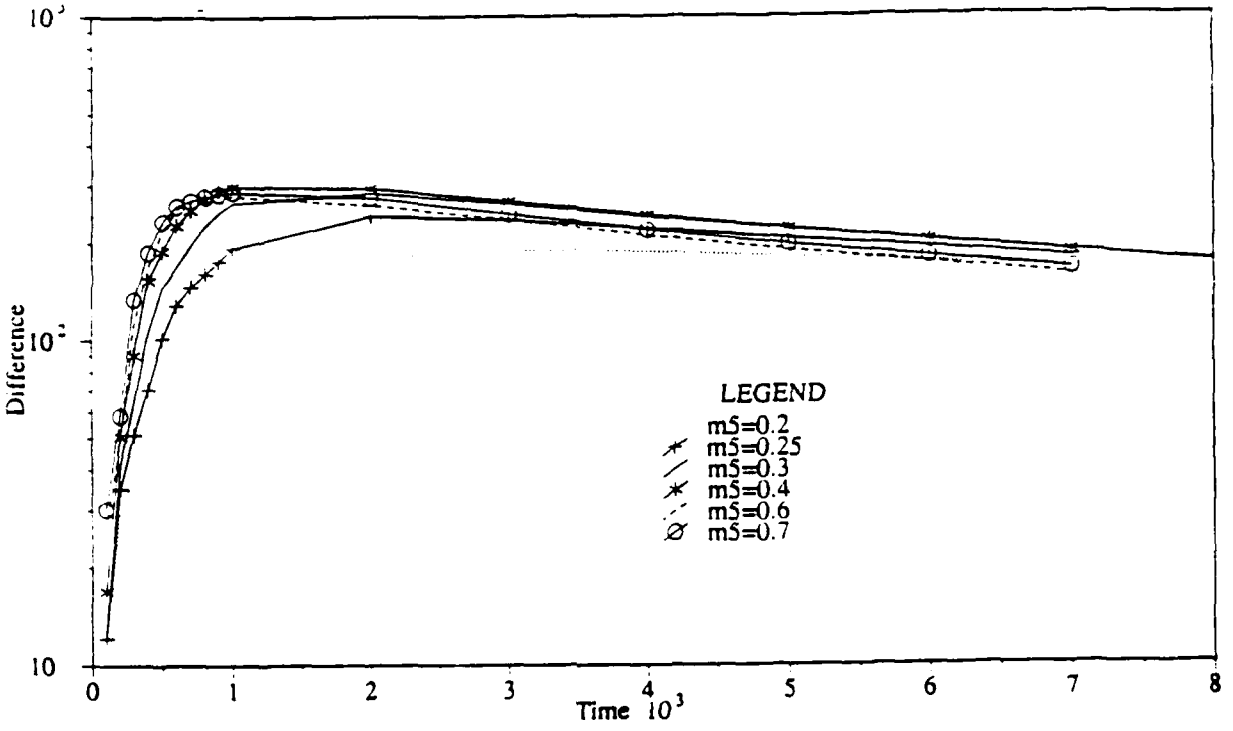

Figure 4-27: Relief Difference Under m_5 Variations

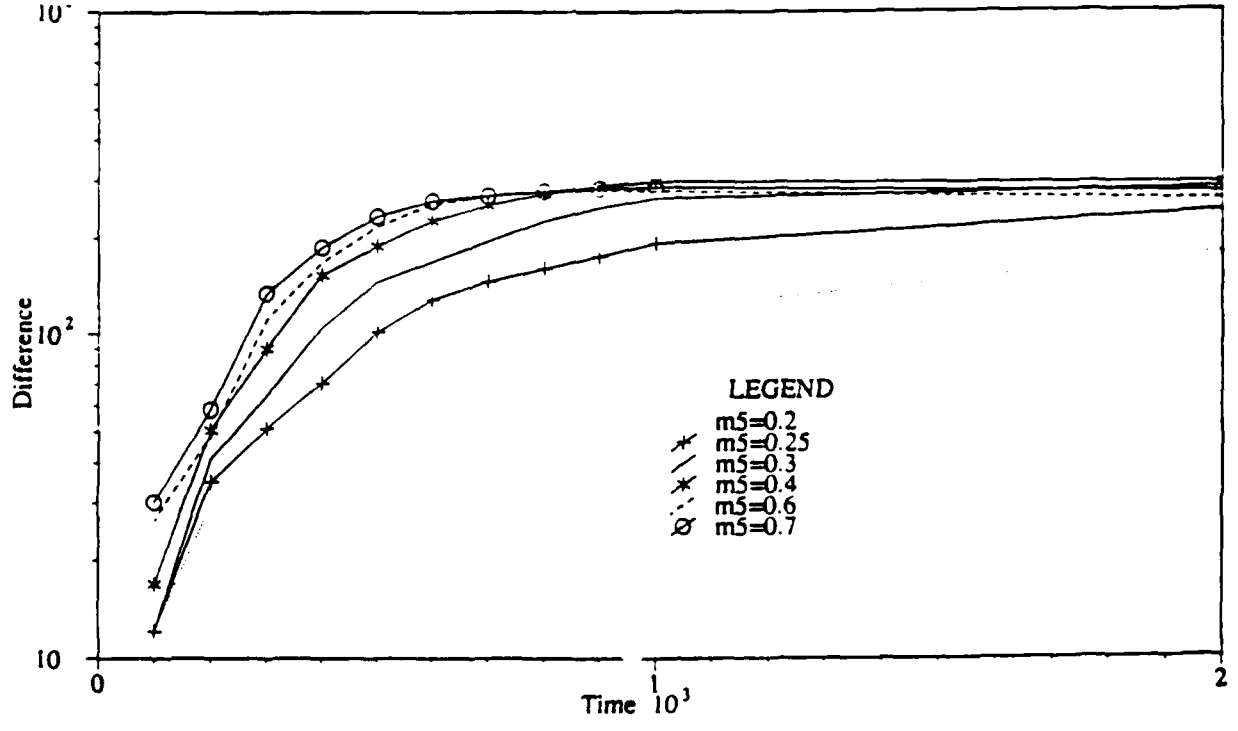

Figure 4-28: Relief Difference Under m_5 Variations During Network Growth

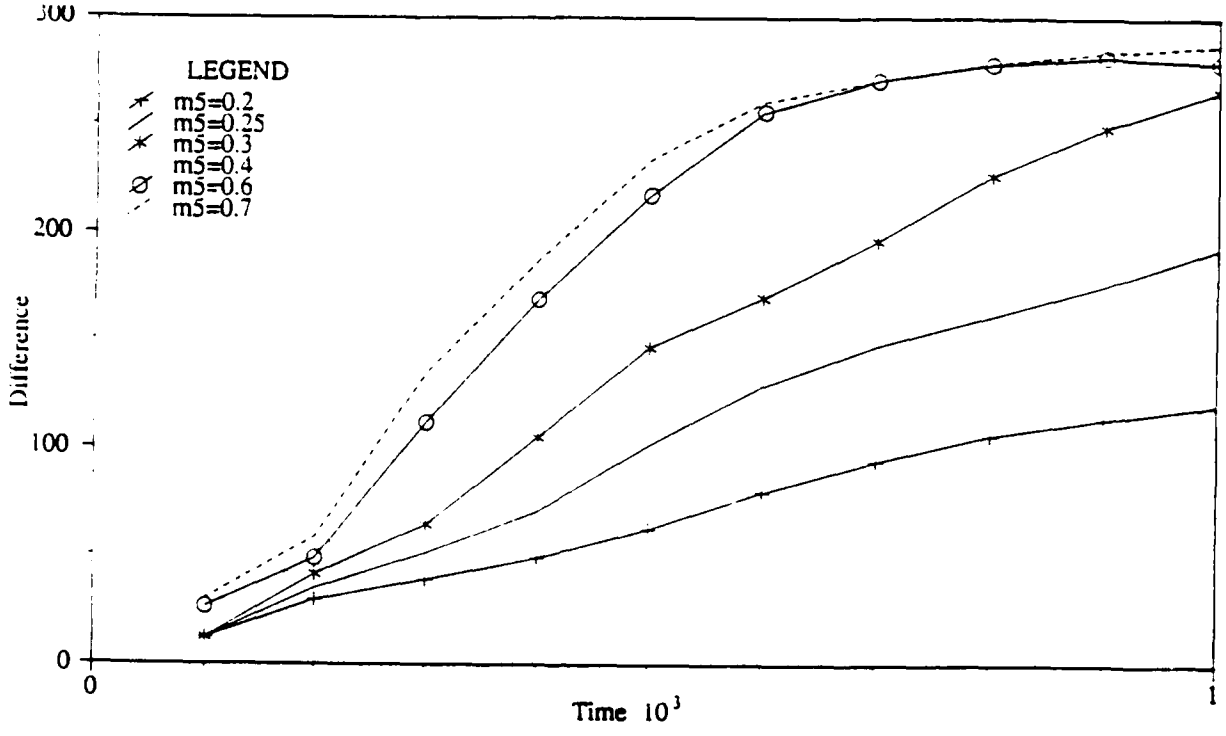

Figure 4-29: Relief Difference Under m_5 Variations.
Arithmetic Scale

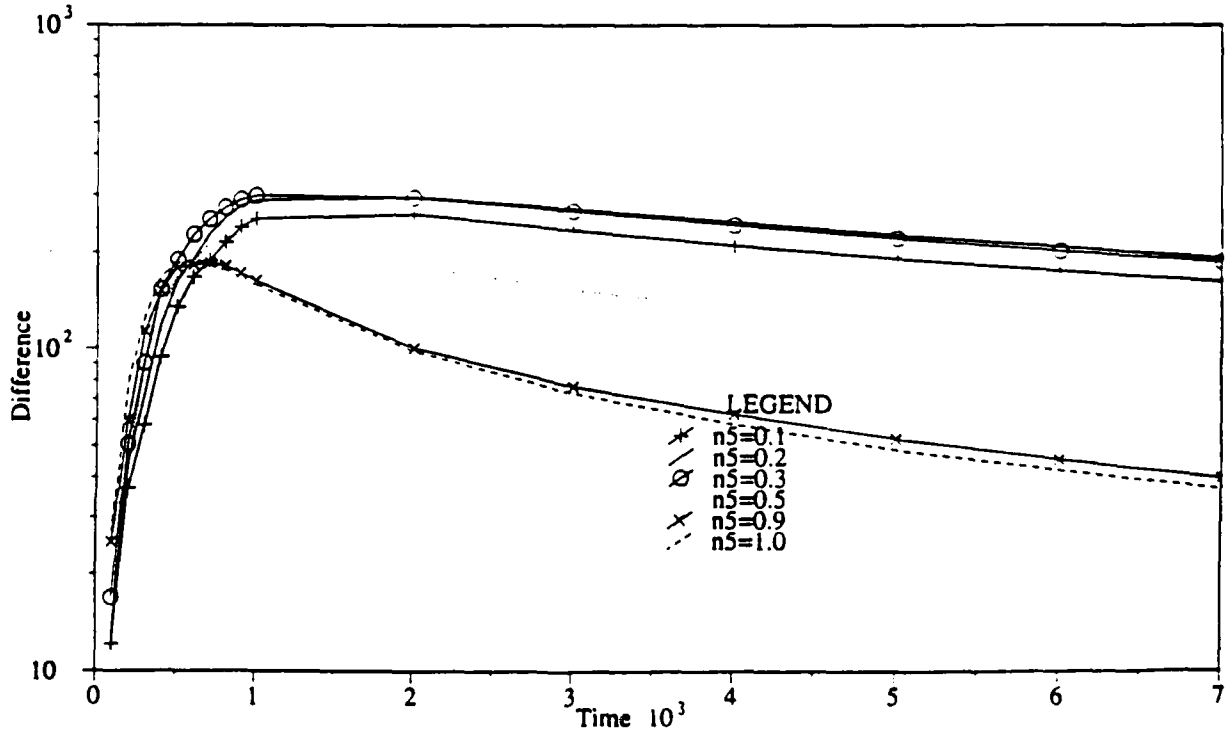

Figure 4-30: Relief Difference Under n_5 Variations

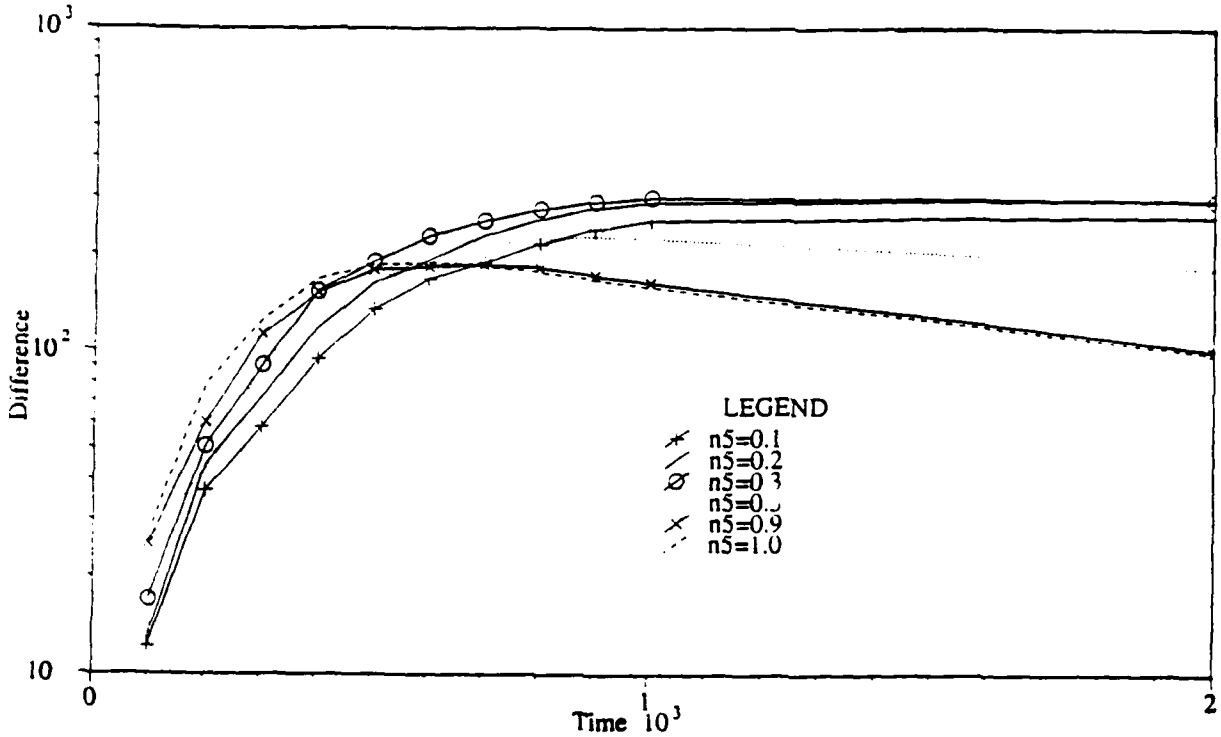

Figure 4-31: Relief Difference Under n_5 Variations During Network Growth

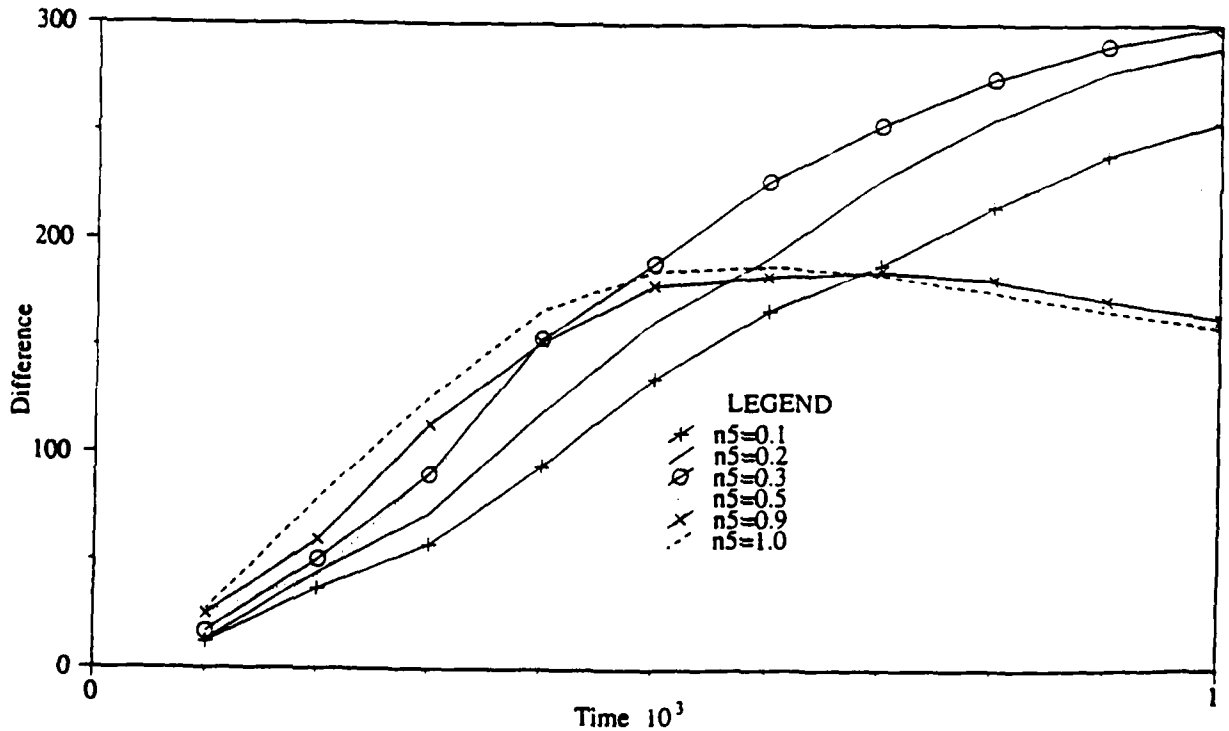

Figure 4-32: Relief Difference Under n_5 Variations.
Arithmetic Scale

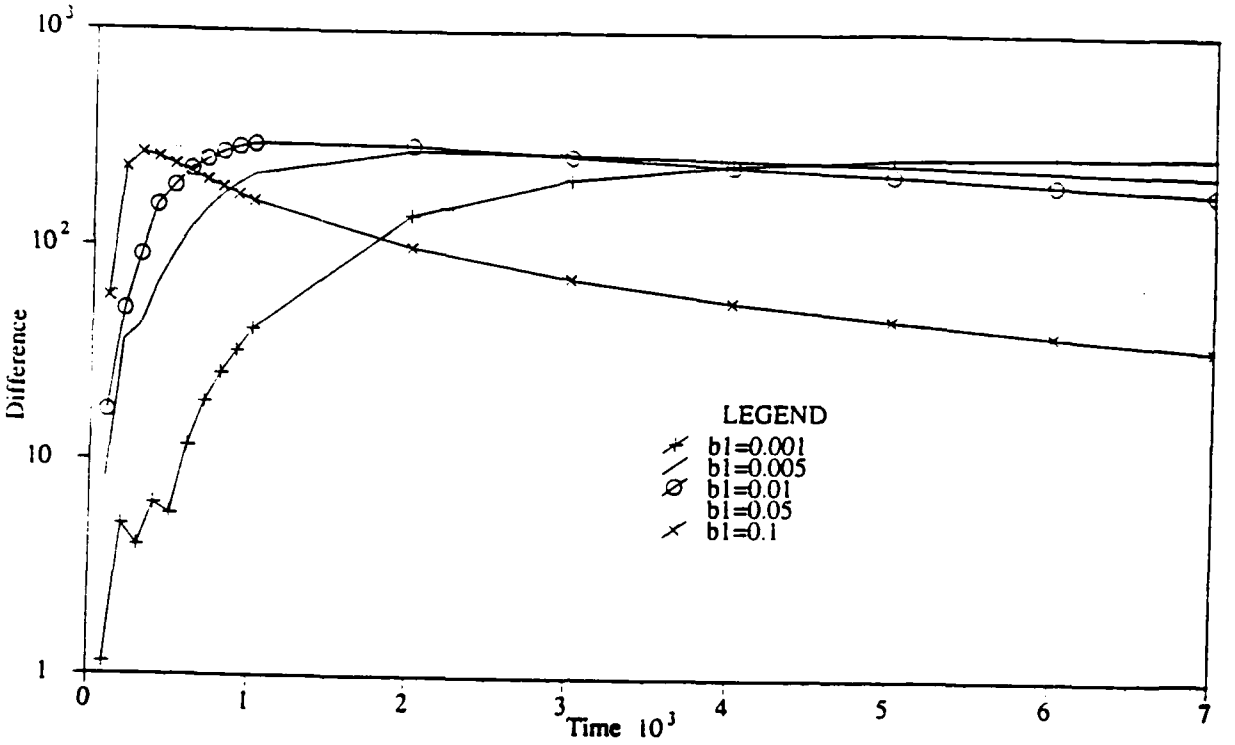

Figure 4-33: Relief Difference Under β_1 Variations

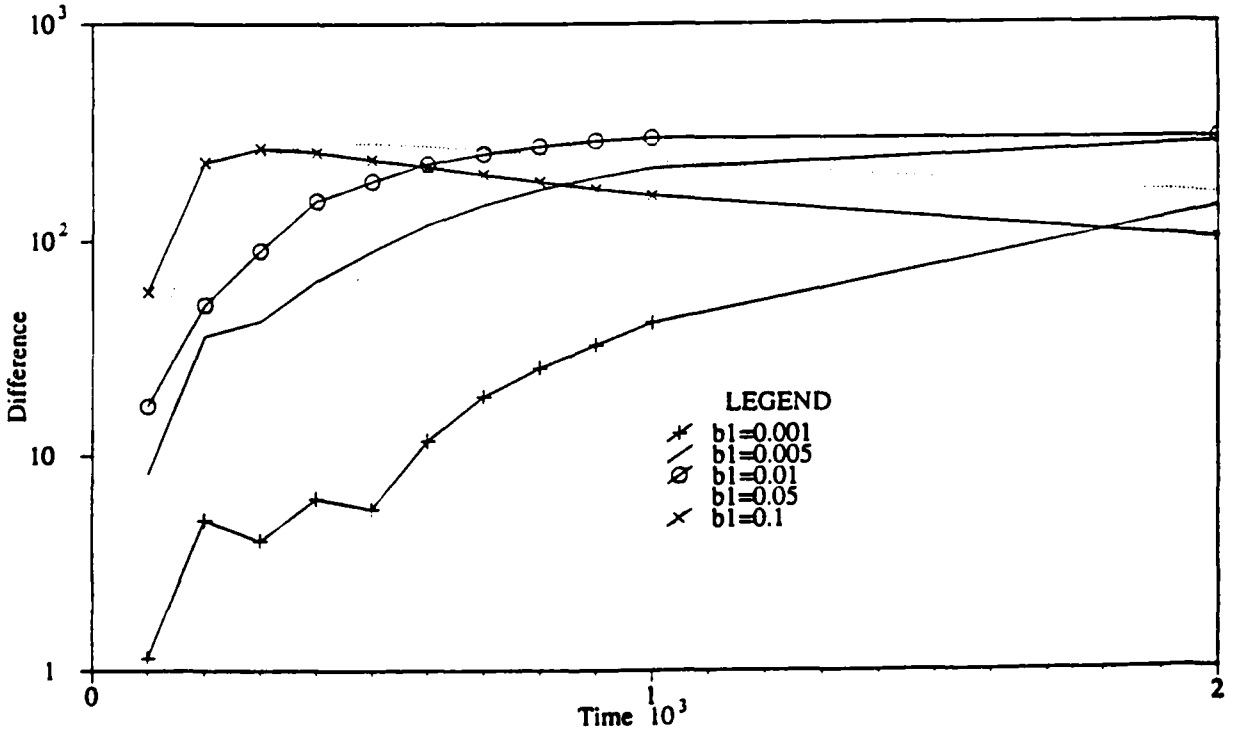

Figure 4-34: Relief Difference Under β_1 Variations During Network Growth

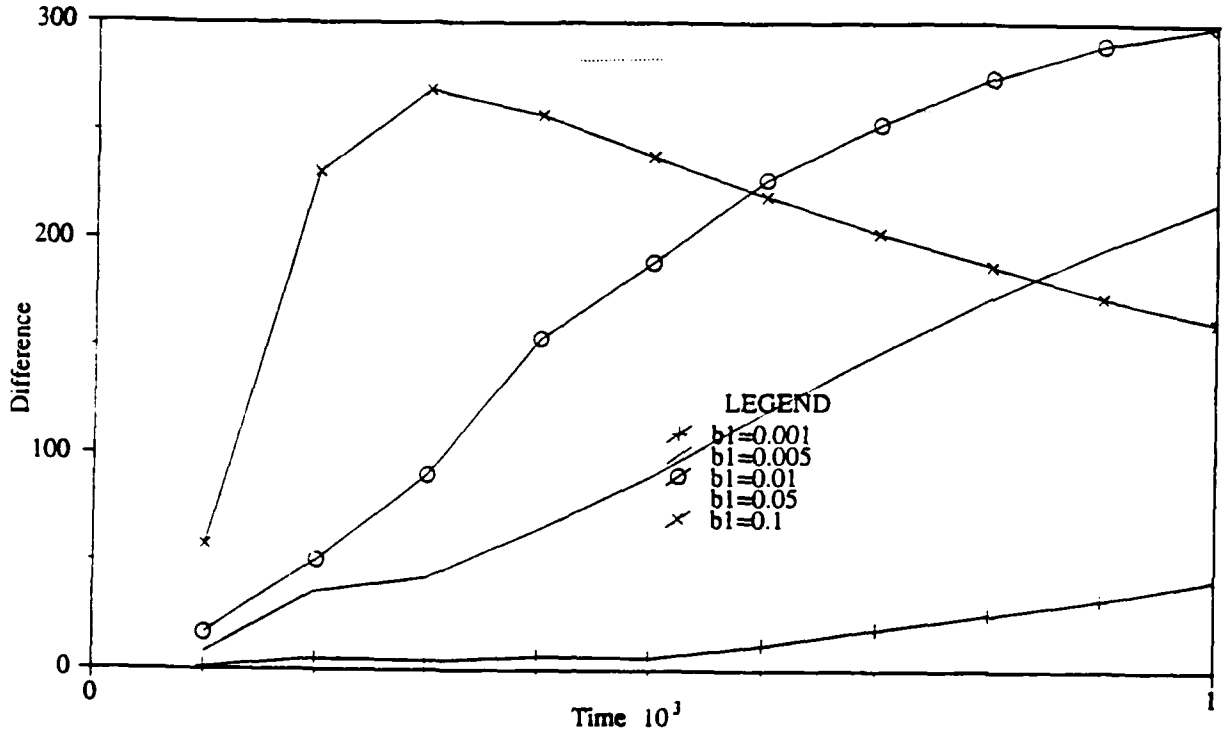

Figure 4-35: Relief Difference Under β_1 Variations.
Arithmetic Scale

Dependence on m_5 (Figures 4-27 to 4-29) as well as on n_5 (Figures 4-30 to 4-32) is very similar to the dependence on m_1 and n_1 respectively. Finally, the variation in the multiplicative factor β_1 of the sediment transport equation is shown in Figures 4-33 to 4-35. Of course, some of the parameter values may be out of the physically valid range but this analysis provides additional insight on the behavior of the model as a dynamical system in itself.

4.9 Final Remarks

The sensitivity to initial conditions and the chaotic behavior of systems are properties that are going to be studied in much more detail in future years because of their implications in predictability. In this chapter it has been shown how this property produces completely different networks out of processes with identical parameter values but with

small differences in the initial elevation fields. The intrinsic temporal and spatial variability of the results imply the necessity of a statistical analysis of the networks. Furthermore, the implications of the SIC property on long-term predictability have to be taken into account if the WBR model is to be used in future years for field predictions.

The Lyapunov exponents were shown to have a positive sign in the system using different tests that have been developed in the literature under a variety of conditions. The fact that the signs are positive proves the existence of transient chaos in the evolution of the system. However, calculations of the exact values of the Lyapunov exponents require a very large number of experiments or a stronger theory on spatially extended systems which has not been developed yet. The exact values of these exponents will provide a bound for long-term predictions using this model and this may be one of the most important applications of the understanding of the chaotic behavior of the system.

Chapter 5

Conclusions

5.1 Summary of Results

This work consists of two sections. Both sections study different aspects of the channel network and catchment evolution model developed by Willgoose, Bras and Rodriguez-Iturbe [47], henceforth called the WBR model. This model uses a sediment transport continuity equation to model elevations, and concepts of erosion engineering to define a channel formation function that triggers the growth of channels. The overland flow production mechanism used in the WBR model is the Hortonian. One of the most interesting features of the WBR model is the way hillslopes and channels interact through the different sediment transport processes. The purpose of the first section of this work is to study the effect of the overland flow production mechanism at hillslopes on the overall behavior of the system. This first part changes the Hortonian runoff of the WBR model to the subsurface saturation mechanism. In the Hortonian case overland flow is assumed to be generated uniformly over the whole area whereas in the subsurface saturation mechanism only saturated areas contribute to the overland flow.

After a review of previous work, a modified version of the WBR model, including the subsurface saturation runoff mechanism, is presented in Chapter 3. A series of simulations were shown and their geomorphological characteristics studied. All the measures under consideration (e.g. Strahler's bifurcation, length, slope and area ratios) were within reasonable limits. The modified model still presented the inherent variability in network's growth that appeared in the WBR model and which is the subject of study of Chapter 4. The influence of diffusive sediment transport processes (e.g. rockslide and rainsplash) was found to be more important in the modified model than in the original one.

The influence of these processes was shown to be particularly important in the time evolution of the hypsometric curve. Finally, various geomorphological characteristics (e.g. area-slope renormalization, link length distribution, etc.) were studied in the simulated catchments and their behavior was found to be similar to field data.

A non-dimensional form of the modified model, similar to the original non-dimensional WBR model, was developed and a new non-dimensional number introduced to describe the threshold value that distinguishes between saturated and unsaturated hillslope nodes. The purpose of these non-dimensional numbers is to provide a way to meaningfully compare catchments at different scales.

A second modification to the WBR model was developed in which the probabilistic nature of rainfall was taken into account. In the first modification the rainfall at the mean flood was used to determine which nodes were saturated and which were not. In the second case, rainfalls above the mean that saturate and erode nodes previously considered as unsaturated were included in the model. Differences were found in the evolution of the hypsometric curves. Other geomorphological measures were not very different.

An important conclusion is the robustness of the WBR model in relation to overland flow distribution. Even though some properties of the behavior change, the overall characteristics of the catchment evolutions are very similar.

The second part of this work studies the sensitivity to initial conditions in the WBR model and is presented in Chapter 4. Using the relief difference, a measure of the difference between elevation fields, the sensitivity of the model to small variations in the initial elevation field was studied. This sensitivity is a manifestation of the underlying transient chaos present in the system. A variety of experiments, based on various tests described in the chaos literature, were used to analyze the behavior of the model under different parameter values. Analytical calculations to prove the existence of chaos are very difficult to develop in the WBR model because of the way contributing areas, a fundamental term in

almost every expression of the model, are calculated. Nevertheless, the series of experiments shown in Chapter 4 demonstrates how the inherent variability of the resulting model networks is related to extreme sensitivity to initial conditions.

5.2 Further Research

Both the analysis of the WBR model in [47] and in this work have begun to look at a channel network evolution model that keeps the number of parameters as small as possible. Based on these analyses a number of possibilities are open for further research. This research can proceed in three directions: modification and improvement of the numerical algorithm that solves the model; extensions of the model to include different geomorphological and hydrological hypotheses about the evolution of the basin; and field measurements that verify and provide a path for new theoretical work. Ideally, these three branches should be developed in parallel.

First of all, underlying any proposed avenue of further research there exists the problem of improving the numerical simulation scheme. The original code is time intensive and the modified version is even more so. This is because of the overland flow calculation that has to take into account the saturation deficits at unsaturated nodes. Reducing the computer time will allow larger size domains to be studied, which are necessary to develop some of the ideas that will be described in this section.

There are some interesting extensions and modifications to the WBR model. For example, the study of the effect of geomorphological controls different from the tectonic input used in the WBR model. Soil layering, horizontal variation of soil properties and limits in sediment transport produced by the amount of material available for erosion, are three possible problems to study. More realistic evolutions would probably arise from these simulations.

The tectonic input term that was used both in this work and in [47] was constant in time and space. The effect of a history of discrete uplift events (e.g. produced by earthquakes) instead of a continuous process, is also a possibility to be studied. Also, the issue of erosion-deposition and its relationship with geomorphological configurations like deltas may be a point to examine carefully with the model.

The boundary conditions used in all the simulations correspond to idealized walls around the domain and a corner that was defined as outlet. Different boundary conditions would allow the study of the competition for water and space between neighboring watersheds and the behavior of their boundaries.

Another avenue of theoretical research comes from the inclusion of the probabilistic distribution of flood rainfalls. In Section 3.11 the influence of this distribution on the overland flow production was studied. Notice that the indicator function makes a clear and permanent distinction between channel and hillslope nodes. However, a node defined as a hillslope using the mean flood rainfall could erode as a channel under larger rainfall events. The inclusion of this effect would smooth out the transition between channel and hillslope nodes (Willgoose, personal communication). At this point sediment transport field data linked to floods as well as to the advance and retreat of channel heads are necessary.

As Morisawa states in [26], vegetation plays an important role in the network expansion process. After disruptive tectonic events like earthquakes, where vegetation is sometimes destroyed, the protection of the soil decreases and the variation in elevations make the network evolve. As time passes and vegetation regenerates, the characteristics of the process change and a temporal variation of the parameters of the model could mimic this effect.

As described in Chapter 3, even though the overland flow production mechanism is different between the WBR model and the modified version developed in this work, there are some features that are common to both models. Therefore, different simulation tools

may help to increase the simulation speed at the cost of losing certain details of the evolution but preserving some features of the model's evolution. Cellular automata, for example, which involve discretization not only in time but also in the variables of interest (elevation in this case), could be useful in large-scale simulations. These simulations with large domain sizes could be used in studies that compare fractal properties of the surface or the network generated by the model with those measured in the field. Notice that the tests to measure fractal properties usually require large amounts of data implying very large simulation domains.

Finally, notice that the analysis presented in Chapter 3 was based on certain assumptions on the subsurface saturation mechanism which should be looked at carefully. Processes like pipeflow and macropore bypassing and their effect on the geomorphological evolution of the basin may also be important in certain situations.

The third avenue of research corresponds to the problem of field verification of the model. Given that the timescales of network evolution are usually very large, field measurements of the whole process at large scales will be limited except for a few special cases. For example, settings like mines, volcanic eruptions or recently deforested zones in tropical regions with high precipitation and easily erodable soils may be used for field sites. Field experiments should try to measure characteristics that enable the calculation of both the nondimensional numbers defined in Section 3.8 and the exponents of sediment transport. Laboratory experiments like the ones performed in the 70's in the rainfall erosion experiment facility at Colorado State University have been compared against simulations of the WBR model, see [47]. Additional experiments that take into account the problem of scales in the diffusive sediment transport processes (like rockslide and rainsplash) can be performed. The linkage with real field data will permit, in the long term, the study and prediction of effects that change in land use, change in topographical characteristics of a basin (mines, earthquakes, etc.), or even change in climate will have on the geomorphology of the basin. The implications of Chapter 4 should be taken into account at this point.

It is important to notice that even though the first studies of the WBR model have been concentrated specifically on geomorphological issues, the hydrological importance of the model should not be ignored. In the long term, more research could be directed towards the understanding of the possible links between the model parameters and the hydrologic response of the basin. This would allow conclusions about the evolution of the hydrological response as the geomorphology of the basins changes with time.

Finally, in a more abstract setting, work with this model could also add some mathematical insight into the interesting basin evolution problem. In general terms the problem can be stated as:

$$\frac{\partial z}{\partial t} = -\nabla \cdot \underline{n} F \qquad (5.1)$$

where z is elevation, $\underline{n}$ is the unit vector in the steepest slope direction, and F is the sediment transport flux which is usually assumed to be a function of area and slope. Notice that the WBR model is analogous to this problem when some assumptions about the form of F are added. As stated in Chapter 4, the mapping that assigns the contributing area to each point according to elevation gradients has not been studied in detail and is not easy to handle. Up to now, only perturbation analyses of the system's behavior have been performed in [40]. A mathematical analysis of the evolution of the process, which is not only non-linear but also spatially variable, is yet to be developed. The WBR model could be a useful tool for this purpose.

Appendix A

Parameter Values of Simulations

SIMULATION	TS	TA	TD	TSC	O_t
		10^{-3}	10^{-8}	10^{3}	
BR643SATU10	6.59	17.97	0.0	0.92	0.1
SATU21	6.59	22.47	0.0	0.92	0.1
SATU29	32.95	17.97	0.0	0.92	0.1
SATU31	6.59	17.97	0.0	0.92	0.01
SATU32	6.59	17.97	2.0	0.92	0.1
SATU34	6.59	17.97	0.0	0.92	0.1
SATU35	6.59	17.97	0.0	0.92	0.1
SATU36	6.59	17.97	0.0	0.92	0.1
SATU37	6.59	17.97	0.0	0.92	0.1
SATU38	6.59	17.97	0.0	4.60	0.1
SATU39	6.59	17.97	0.0	0.28	0.1
SATU40	6.59	13.48	0.0	0.92	0.1
SATU42	6.59	7.07	0.0	0.92	0.1
SATU43	6.59	22.47	0.0	1.84	0.1
SATU44	6.59	13.48	0.0	0.42	0.1
SATU45	6.59	22.47	0.0	2.80	0.01

Table A-I: Parameters of Simulations

All the simulations had m_1=2, n_1=2, m_5=0.4, n_5=0.3, **TT**=1x10^{-6}, **TC**=1, except SATU42 that had m_5=0.275. All the simulations had $\overline{\beta}_6$=1.0 except SATU31 with 0.1, SATU37 with 10. and SATU45 with 0.5.

References

[1] Abrahams, A.D.
Channel Networks: A Geomorphological Perspective.
Water Resources Research (20(2)):161-168, 1984.

[2] Beven, K.
On Subsurface Stormflow: An Analysis of Response Function.
Hydrological Sciences-Journal-des Sciences Hydrologiques (4):505-521, 1982.

[3] Berge,P., Pomeau, Y., Vidal, C.
Order Within Chaos.
John Wiley & Sons, 1984.

[4] Beven, K.J.
Runoff Production and Flood Frequency in Catchments of Order n: An Alternative Approach.
Scale Problems in Hydrology.
D. Reidel Publishing Company, 1986, pages 107-131.

[5] Beven, K.J. and Kirkby, M.J.
A Physically Based, Variable Contributing Area Model of Basin Hydrology.
Hydrological Sciences-Bulletin-des Sciences Hydrologiques (24):43-69, 1979.

[6] Beven, K.J. and Wood, E.F.
Catchment Geomorphology and the Dynamics of Runoff Contributing Areas.
Journal of Hydrology (65):139-158, 1983.

[7] Cayley, A.
On Analytical Forms Called Trees.
Philosophical Magazine (18):374-378, 1859.

[8] Dunne, T.
Field Studies of Hillslope Flow Processes.
Hillslope Hydrology.
Wiley, 1978, pages 227-294.

[9] Flint, J. J.
Stream Gradient as a Function of Order, Magnitude and Discharge.
Water Resources Research (10(5)):969-973, 1974.

[10] Gupta, V.K., Waymire, E. and Wang, C.T.
A representation of an instantaneous unit hydograph from geomorphology.
Water Resources Research (16(5)):855-862, 1980.

[11] Gupta, V.K. and Waymire, E.
Statistical Self-similarity in River Networks parameterized by Elevation.
Water Resources Research (25(3)):463-476, 1989.

[12] Hammel, S.M., Yorke, J. and Grebogi, C.
Numerical Orbits of Chaotic Processes Represent True Orbits.
Bulletin (New Series) of the American Mathematical Society (19(2)):465-469, 1988.

[13] Horton, R.E.
Drainage Basin Characteristics.
Eos Transactions AGU (13):350-361, 1932.

[14] Horton, R. E.
Erosional Development of Streams and their Drainage Basins.
Bulletin of the Geological Society of America (56):275-370, 1945.

[15] Howard, A.D.
Simulation of Stream Networks by Headward Growth and Branching.
Geographical Analysis (3):29-50, 1971.

[16] Kaneko, K.
Pattern Dynamics in SpatioTemporal Chaos.
Physica D (34D):1-41, 1989.

[17] Kaneko, K.
Spatiotemporal Chaps in One and Two-Dimensional Coupled Map Lattices.
Physica D (37D):60-82, 1989.

[18] Kirkby, M.J.
Hillslope Process-response Models Based on the Continuity Equation.
Institute of British Geographers Special Publication. Number 3:*Slopes: Form and Process.*
Institute of British Geographers, 1971, pages 15-30.

[19] Kirkby, M.J.
Modelling Some Influences of Soil Erosion, Landslides and Valley Gradient on Drainage Density and Hollow Development.
Catena Supplement. Number 10:*Geomorphological Models.*
Catena Verlag, 1987, pages 1-14.

[20] Kirkby, M.
Hillslope Runoff Processes and Models.
Journal of Hydrology (100):315-339, 1988.

[21] Leopold, L.B. and Langbein, W.B.
The Concept of Entropy in Landscape Evolution.
Technical Report 500-A, USGS: U.S. Geological Survey Professional papers, 1962.

[22] Luke, J.C.
Special Solutions for Nonlinear Erosion Problems.
Journal of Geophysical Research (79(26)):4035-4040, 1974.

[23] Mayer-Kress, G. and Kaneko, K.
Spatiotemporal Chaos and Noise.
Journal of Statistical Physics (54(5-6)):1489-1501, 1989.

[24] Meinhardt, H.A.
Morphogenesis of Lines and Nets.
Differentiation (6):117-123, 1976.

[25] Meinhardt, H.A.
Model of Biological Pattern Formation.
Academic Press, 1982.

[26] Morisawa, M.
Development of Drainage Systems on an Upraised Lake Floor.
American Journal of Science (262):340-354, 1964.

[27] Moon, Francis.
Chaotic Vibrations.
John Wiley & Sons, 1987.

[28] Montgomery, D.R. and Dietrich, W.E.
Where do Channels Begin?
Nature (336):232-234, 1988.

[29] Mesa, O.J.
Analysis of Channel Networks Parametrized by Elevation.
PhD thesis, Unniversity of Mississippi, 1986.

[30] O'Loughlin.
Prediction of Surface Saturation Zones in Natural Catchments by Topographic Analysis.
Water Resources Research (22(5)):794-804, 1986.

[31] Rodriguez-Iturbe, I. and Valdes, J.B.
The Geomorphologic Structure of Hydrologic Response.
Water Resources Research (15(6)):1409-1420, 1979.

[32] Shreve, R.L.
Statistical Law of Stream Numbers.
Journal of Geology (74):17-37, 1966.

[33] Shreve, R.L.
Infinite Topologically Random Channel Networks.
Journal of Geology (75):178-186, 1967.

[34] Shreve, R.L.
Stream Lengths and Basin Areas in Topologically Random Channel networks.
Journal of Geology (77):397-414, 1969.

[35] Sivapalan, M. and Wood, E.F.
On Hydrologic Similarity 3. A dimensionless Flood frequency Model Using a Generalized Geomorphologic Unit Hydograph and Partial Area Runoff Generation.
Water Resources Research (26(1)):43-58, 1990.

[36] Smart, J.S.
Statistical properties of Stream Lengths.
Water Resources Research (4):1001-1014, 1968.

[37] Smart, J.S.
Distribution of Interior Link Lengths in Natural Channel Networks.
Water Resources Research (5(6)):1337-1342, 1969.

[38] Smart, J.S.
Quantitative Characterization of Channel network Structure.
Water Resources Research (8(6)):1487-1496, 1972.

[39] Smart, J.S.
Link Lengths and Channel Network Topology.
Earth Surface Processes and Landforms (6):87-98, 1981.

[40] Smith, T.R. and Bretherton, F.P.
Stability and the Conservation of Mass in Drainage Basin Evolution.
Water Resources Research (8(6)):1506-1529, 1972.

[41] Strahler, A.N.
Hypsometric (Area-Altitude) Analysis of Erosional Topography.
Bulletin of the Geological Society of America (63):1117-1142, 1952.

[42] Tarboton, D.G., Bras, R.L. and Rodriguez-Iturbe, I.
The Fractal Nature of River Networks.
Water Resources Research (24(8)):1317-1322, 1988.

[43] Tarboton, D.G., Bras, R.L. and Rodriguez-Iturbe, I.
Scaling and Elevation in River Networks.
Water Resources Research (25(9)):2037-2051, 1989.

[44] Tarboton, D.
The Analysis of River Basins and Channel Networks Using Digital Terrain data.
Technical Report 326, Ralph M. Parsons Laboratory, Massachusetts Institute of Technology, 1989.

[45] Tokunaga, E.
Consideration of the Composition of Drainage Networks and their Evolution.
Technical Report Geographical Report No. 13, Tokyo Metropolitan University, 1978.

[46] van der Tak, L.
Part I: Stream Length Distributions, Hillslope Effects and Other Refinements of the geomorphologic IUH. Part II: Topologically Random Channel networks and Horton's Laws: the Howard Network Simulation Model Revisited.
Master's thesis, Massachusetts Institute of technology, May, 1988.

[47] Willgoose, G.R., Bras, R.L. and Rodriguez-Iturbe, I.
A Physically Based Channel Network and Catchment Evolution Model.
Technical Report 322, Ralph M. Parsons Laboratory, Massachusetts Institute of Technology, 1989.

[48] Wolf, A., Swift, J., Swinney, H., Vastano, J.
Determining Lyapunov Exponents from a Time Series.
Physica D (16D):285-317, 1986.